

COUPLED TRANSPORT, FRACTIONATION AND STABILIZATION OF
DISSOLVED ORGANIC MATTER AND RARE EARTH ELEMENTS IN THE
CRITICAL ZONE

by

Angélica Vázquez-Ortega

A Dissertation Submitted to the Faculty of the
DEPARTMENT OF SOIL, WATER AND ENVIRONMENTAL SCIENCE
In Partial Fulfillment of the Requirements
For the Degree of
DOCTOR OF PHILOSOPHY
WITH A MAJOR IN SOIL WATER AND ENVIRONMENTAL SCIENCES
In the Graduate College
THE UNIVERSITY OF ARIZONA

2013

THE UNIVERSITY OF ARIZONA
GRADUATE COLLEGE

As members of the Dissertation Committee, we certify that we have read the dissertation prepared by Angélica Vázquez-Ortega, titled COUPLED TRANSPORT, FRACTIONATION AND STABILIZATION OF DISSOLVED ORGANIC MATTER AND RARE EARTH ELEMENTS IN THE CRITICAL ZONE and recommend that it be accepted as fulfilling the dissertation requirement for the Degree of Doctor of Philosophy.

_____ Date: July 26, 2013
Dr. Jon Chorover

_____ Date: July 26, 2013
Dr. Craig Rasmussen

_____ Date: July 26, 2013
Dr. Jennifer McIntosh

_____ Date: July 26, 2013
Dr. Julia Perdrial

Final approval and acceptance of this dissertation is contingent upon the candidate's submission of the final copies of the dissertation to the Graduate College.

I hereby certify that I have read this dissertation prepared under my direction and recommend that it be accepted as fulfilling the dissertation requirement.

_____ Date: July 26, 2013
Dissertation Director: Dr. Jon Chorover

STATEMENT BY AUTHOR

This document has been submitted in partial fulfillment of requirements for an advanced degree at the University of Arizona and is deposited in the University Library to be made available to borrowers under rules of the Library.

Brief quotations from this document are allowable without special permission, provided that accurate acknowledgment of source is made. Request for permission for extended quotation from or reproduction of this manuscript in whole or in part may be granted by the head of the major department of the Dean of the Graduate College when in his or her judgment the proposed use of the material is in the interest of scholarship. In all other instances, however, permission must be obtained from the author.

SIGNED: Angélica Vázquez-Ortega

ACKNOWLEDGEMENTS

I would like to acknowledge my dissertation advisor, Dr. Jon Chorover for his guidance and valuable suggestions and Mary Kay Amistadi and Juliana Gil for her technical support. Also, I would like to extend my thanks to my committee members Craig Rasmussen, Jennifer McIntosh, and Julia Perdrial for their academic support and suggestions. Finally, I want to share this extraordinary achievement with my adorable family, Carlos Soto, Adrián Soto, and Paola Soto.

TABLE OF CONTENTS

LIST OF FIGURES.....	6
ABSTRACT.....	7
CHAPTER 1: INTRODUCTION.....	9
CHAPTER 2: PRESENT STUDY.....	22
REFERENCES.....	29
APPENDIX A: FRACTIONATION OF DISSOLVED ORGANIC MATTER BY (OXY)HYDROXIDE-COATED QUARTZ SANDS: COMPETITIVE SORBATE DISPLACEMENT DURING REACTIVE TRANSPORT	35
APPENDIX B: RARE EARTH ELEMENTS AS REACTIVE TRACERS OF BIOGEOCHEMICAL WEATHERING IN FORESTED RHYOLITIC TERRAIN	77
APPENDIX C: REDISTRIBUTION OF RARE EARTH ELEMENTS AND YTTRIUM (REY) IN TOPOGRAPHICALLY DISTINCT, RHYOLITE-DERIVED PEDONS ...	139
APPENDIX D: <i>ELECTRONIC ANNEX FOR</i> FRACTIONATION OF DISSOLVED ORGANIC MATTER BY (OXY)HYDROXIDE-COATED QUARTZ SANDS: COMPETITIVE SORBATE DISPLACEMENT DURING REACTIVE TRANSPORT.....	188
APPENDIX E: <i>ELECTRONIC ANNEX FOR</i> RARE EARTH ELEMENTS AS REACTIVE TRACERS OF BIOGEOCHEMICAL WEATHERING IN FORESTED RHYOLITIC TERRAIN	191
APPENDIX F: <i>ELECTRONIC ANNEX FOR</i> REDISTRIBUTION OF RARE EARTH ELEMENTS AND YTTRIUM (REY) IN TOPOGRAPHICALLY DISTINCT, RHYOLITE-DERIVED PEDONS	199

LIST OF FIGURES:

Figure 1 Conceptual model of organo-mineral interactions in soils from Kleber et al. (2007).

Figure 2 Complexation of REE with fulvic acids as a function of pH. Figure from Pourret et al. (2007).

ABSTRACT

It is important to understand the processes that influence the critical zone (CZ) evolution to ensure its sustainability. This thesis reports on laboratory and field experiments designed to measure the behavior of biogenic and lithogenic chemical species and their interaction in the CZ from column to pedon to catchment scales. We postulated that interactions between organic matter and rock-derived metals drive coupled processes of carbon stabilization and chemical weathering and denudation in the Jemez River Basin Critical Zone Observatory (JRB-CZO). First, we observed that secondary mineral coatings (Al and Fe (oxy)hydroxides) on primary silicate surfaces play a major role in sequestering aromatic and “humified” dissolved organic matter (DOM) into sorbate form, significantly retarding their subsurface transport. Further, reinfusion to OM-reacted-porous-media of a different DOM source resulted in exchange reactions consistent with a zonal model of OM adsorption at mineral surfaces.

This dissertation also aimed to examine the influence of water and DOM fluxes on the CZ weathering processes. Rare earth elements (REE) were selected because of their coherent trends in reactivity toward organic ligands common to soils. Specifically, trends in REE fractionation were explored for their utility to inform on biogeochemical weathering processes in forested terrain in the JRB-CZO. Mineral weathering mechanisms are expected to differentially influence REE release, fractionation, and transport and the relative importance of such processes should be reflected in REE signatures of bulk soil, pore and surface waters. Our studies showed: (1) REE depletion trends with depth in bulk soils are correlated with topographically-induced variation in

water and dissolved organic carbon (DOC) flux (reflected in negative correlations between total water and C fluxes) and solid phase REE concentrations measured at the same depths; (2) REE and DOC concentrations in stream waters were strongly correlated during snowmelt periods of high discharge, consistent with REE complexation and mobilization in association with organic ligands during shallow subsurface flow; (3) preferential sequestration of Eu occurs during formation of secondary Mn(IV)-oxides, explaining patterns of Eu enrichment in bulk soils; and (4) the incremental increase in positive Ce-anomalies with depth in bulk soils are apparently controlled by adsorption/co-precipitation with secondary Fe-(oxy)hydroxide minerals.

CHAPTER 1: INTRODUCTION

This research is part of a multi-disciplinary collaborative project in which researchers with expertise in across a range of earth science fields are working together to better understand the processes that govern critical zone (CZ) evolution. The CZ is defined as that portion of the earth's near surface that extends from the top of the vegetation canopy to the bottom of the groundwater system (NRC, 2001). The research reported herein primarily seeks to understand the influence and links between water and reduced organic carbon (OC) fluxes on CZ subsurface biogeochemical processes. Specifically, the overarching goal of this dissertation is to better understand the fractionation and transport of dissolved organic matter (DOM) and rare earth elements plus yttrium (REY) in the Jemez River Basin Critical Zone Observatory (JRB-CZO). The JRB-CZO is a natural laboratory that enables us to monitor biogeochemical processes in soil and natural waters that ultimately influence OC and REY fractionation and stabilization. Elucidating OC stabilizing mechanisms are essential to understand C flux feedbacks to climate change and in the decision making for land-use management (Six et al., 2002; Goh, 2004; von Luetzow et al., 2006; von Lutzow et al., 2008).

Net ecosystem exchange calculations (net C movement between the atmosphere and the ecosystem under investigation) in our study site reported in Perdrial et al. (in prep) indicated a net C accumulation by the terrestrial ecosystem. The soil C pool ranges from 80,000 to 160,000 kg C h⁻¹. This large soil C pool can be susceptible to climatic changes which in turn can induce high release of CO₂ to the atmosphere increasing global warming. Among the various processes involved in DOM stabilization, adsorption at Al

and Fe (oxy)hydroxide surfaces is a very important factor (Eusterhues et al., 2003; Eusterhues et al., 2005). The neo-formation of Al and Fe (oxy)hydroxide minerals (e.g. gibbsite and goethite, respectively) is ubiquitous in soils and these reactive mineral surfaces have the potential to sequester aromatic and “humified” DOM. **Appendix A** aims to investigate the role of Al- and Fe-(oxy)hydroxide coatings in the stabilization of DOM derived from grassland and mixed conifer organic horizons during progressive surface loading via saturated column experiments.

Also, the current work sought to assess whether REY trends in rock, water and soil could be applied to resolve aspects of biogeochemical weathering resulting from snowmelt events in seasonally-snow covered nested catchments (main focus of **Appendix B**). Prior studies have shown the potential for REY to serve as reactive tracers of surficial weathering processes (e.g., Leybourne and Johannesson, 2008; Shiller, 2010). Systematic variation in metal-ligand chemical reactivity makes the REY useful for studying biological impacts on weathering in the CZ because of the documented variation in their tendency to form stable complexes with organic (carboxyl- and phenolic-OH) and inorganic (e.g., hydroxylated surfaces of Fe, Mn and Al oxide) ligands (Davranche et al., 2005; Pourret et al., 2007; Pourret and Martinez, 2009; Davranche et al., 2004). Hence their mobilization (i.e., chemical denudation) from a weathering soil profile and into stream drainage waters is strongly controlled by localized incongruent weathering reactions and organic carbon flux (Dupre et al., 1999; Gruau et al., 2004; Pourret et al., 2010).

This dissertation contains a summary chapter entitled “Present Study” in which the three manuscripts that will be submitted for publication are briefly described, including main objectives, relevant methods, and findings. Appendices A, B, and C correspond to three manuscripts that will be submitted to peer review journals which were formatted according to the journal guidances. Supplemental information that will be submitted with each manuscript is included in Appendices C, D, and F. A review of the most relevant literature will follow in sections I and II as part of the introduction.

I. Transport and Stabilization of DOM

A. SOM and DOM Definition

The definition of soil organic matter (SOM) according to the functional concept (quoted from (Trumbore, 1997 and Kleber and Johnson, pp. 77-142) states that: “SOM is defined as the non-living component of organic matter in soil. There is a general agreement that SOM contains at least three identifiable C pools: root exudates and rapidly decomposed components of fresh plant litter (“active” pool); stabilized organic matter that persists in soils over several years (“passive” pool); and a poorly defined “slow” C pool that has turnover times in the range of years to centuries”.

Dissolved organic matter (DOM) is defined operationally as the fraction of organic matter that passes through a 0.45 μm filter. It is postulated that DOM can be originated from recent deposited litter and from stable organic matter (also known as humus) (Kalbitz et al., 2000).

Several studies (Gu et al., 1994; Gu et al., 1995; Kaiser and Guggenberger, 2000; Guo and Chorover, 2006) have reported that soils adsorb very weakly the hydrophilic DOM fraction (readily decompose by the biodegradation point of view), whereas the more hydrophobic fraction (dominantly comprising lignin-derived phenols with varying degrees of substituent carboxylation) can form stable covalent bonds via ligand exchange at surface hydroxyl groups of Fe and Al (oxy)hydroxides. The hydrophilic DOM or more labile fraction (“active” pool) can be transported via lateral or vertical flow within the soil profile and it is readily available to microorganisms as a source of energy. In contrast, the hydrophobic fraction transport (“passive” or “slow” pool) will be retarded and less bioavailable.

Column experiments were performed to test the hypotheses related to the impacts of (oxy)hydroxide coatings on retardation of DOM during reactive transport and the impacts of progressive sorbate OM coating on such retardation effects. The use of UV-Vis and fluorescence spectroscopy techniques will provide insights on the type of DOM that is preferentially retained or eluded from the mineral media.

B. Mechanisms involved in DOM Transport and Stabilization

Dissolved organic matter is a reactive pool (trace metals undergo sorption/desorption processes) that has been implicated in soil formation, mineral weathering, and nutrient and pollutant transport, among other processes occurring in the CZ (Kalbitz et al., 2000 and references within). DOM sorptive stabilization

by soil minerals can promote mineral dissolution releasing metals into natural waters (Oliva et al., 1999). Proposed mechanisms of DOM sorption to mineral surfaces are anion exchange, ligand exchange-surface complexation, cation bridging, hydrogen bonding, van der Waals forces, and physical adsorption (Kalbitz et al., 2000; Scheel et al., 2007). Reactive mineral surfaces such as Al and Fe-(oxy)hydroxides exhibit a strong binding complexation with different functional groups in DOM (Kaiser and Guggenberger, 2000; Kalbitz et al., 2000). Several studies have reported that DOM with high molar absorptivity, high molecular weight, and low hydrophilicity are preferentially removed from the DOM solution by soils (Kaiser and Guggenberger, 2000; Kaiser and Zech, 1997; Chorover and Amistadi, 2001; Banaitis et al., 2006; Hunt et al., 2007). The hydrophobic DOM fraction has been reported to form stronger bonds with Al and Fe-(oxy)hydroxide minerals than the hydrophilic fraction (Kaiser and Zech, 1997).

C. Conceptual Model of Organo-mineral Interactions in Soils

Soil organic matter contains non-humic (protein, carbohydrates, lipids) and humic substances. Humic substances (HS) are biogenic heterogeneous organic substances that are recalcitrant in nature (stable OM from biodegradation point of view). Traditionally, HS genesis is primarily explained by the polyphenol theory which involves the formation of quinones (Sparks, pp. 79-113). However, a newer model proposed by Kleber et al. (2007) aims to provide insights concerning the molecular structure of SOM. The conceptual model of

organo-mineral interactions in soils assumes that humic substances consists at the molecular level of small and chemically diverse organic molecules linked by hydrophobic, cation-bridging, and hydrogen bond interactions which are capable of self-organizing (pseudo-micellar) behavior in aqueous solution (Sutton and Sposito, 2005) and, therefore, at the mineral-water interface. Thus, the model postulates the distribution of sorbed DOM among three distinct zones: (i) the mineral contact zone, (ii) intermediate hydrophobic zone, and (ii) peripheral kinetic zone Figure 1. The contact zone is where organic moieties are anchored for relatively long time scales to the surface via electrostatic, covalent, and (to a lesser extent) hydrophobic interactions. The hydrophobic zone is mainly characterized by hydrophobic interactions and moderate DOM exchange rate. Finally, the kinetic zone is characterized by cation bridging and hydrogen bonding interactions, further accumulation of OM, and a high DOM exchange rate (Kleber et al., 2007). **Appendix A** aims to present empirical evidence to support the hypothetical zonal model of organo-mineral interactions.

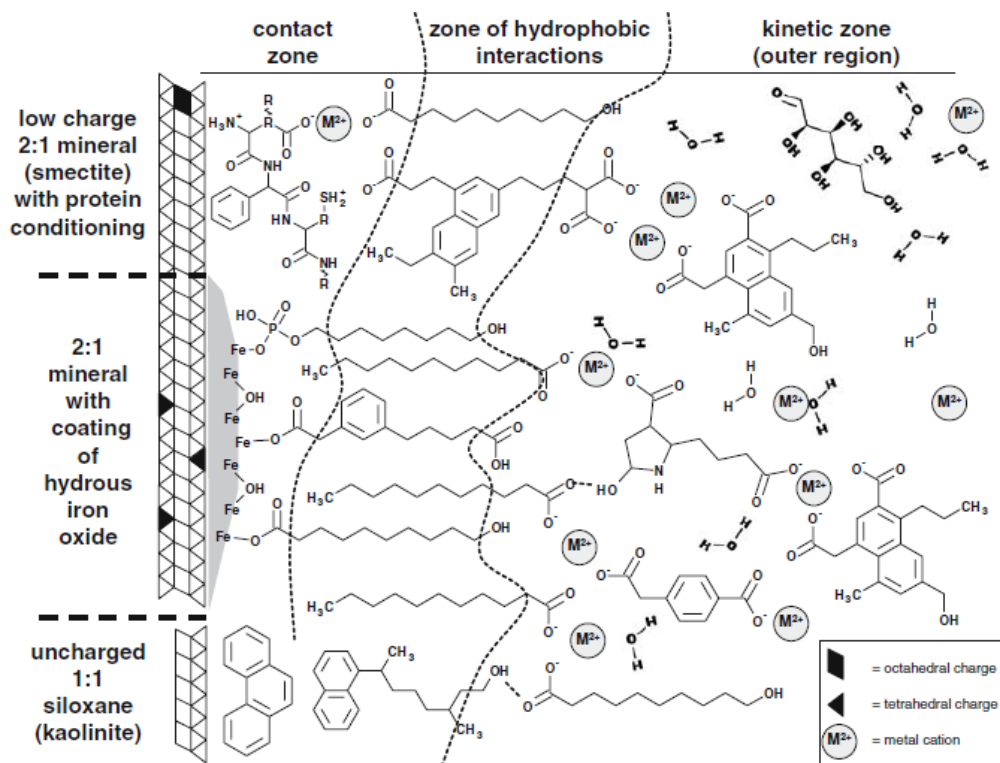


Figure 1 Conceptual model of organo-mineral interactions in soils from Kleber et al. (2007).

II. Transport and Stabilization of REY

A. General Information about REY

Rare earth elements (REE) can be separated into light (L), middle (M) and heavy (H) groups, respectively (LREE: La to Nd, MREE: Sm to Tb, and HREE: Dy to Lu). Because yttrium (Y, atomic number 39) has a similar outer electron shell structure it is often included as a pseudo-lanthanide with an ionic radius nearly identical to that of holmium (Ho) and consequently similar chemical behavior (a.k.a. “geochemical twins”) (Bau et al., 1995; Bau, 1999; Thompson et al., in press). Small predictable variations in chemical properties (ionic radius and

atomic mass) with increasing atomic number make the lanthanide series useful probes of biogeochemical weathering processes in the CZ.

The rare earth elements and yttrium (REY) have been used as reactive tracers to elucidate soil biogeochemical weathering processes such as mineral dissolution, argilluviation, redox processes, DOM complexation, and biological cycling among others (Aubert et al., 2001; Braun et al., 1990; Cullers et al., 1975; Nezat et al., 2007; Laveuf et al., 2008; Laveuf and Cornu, 2009; Laveuf et al., 2012; Stille et al., 2006; Goyne et al., 2010; Ma et al., 2011). Dissolution of phosphate minerals such as apatite and monazite have been implicated in controlling REY concentrations in the soil profile (Aubert et al., 2001). By using the MREE-enrichment and the Eu-anomaly, argilluviation has been traced in soils in which the eluviated horizon display enrichment in MREE and Eu (Cullers et al., 1975). Redox processes have been implicated in the preferential immobilization of Ce during pedogenesis, in which Ce is mainly associated with Fe- and Mn-(oxy)hydroxides (Laveuf et al., 2012). Concentrations of REY in natural terrestrial waters, for example, have been shown to correlate strongly with DOC concentration, suggesting biological mediation of REY chemical denudation (Johannesson et al., 2004; Tang and Johannesson, 2003). Stille et al. (2006) reported that plants in the Strengbach chatchement (mainly beech trees) were preferentially uptaking LREE.

B. Normalization and Anomalies

The REY patterns are typically plotted as a function of their increasing atomic number with the exception of yttrium which is placed next to holmium. Plots of REY concentrations across the lanthanide series are typically normalized to a reference geological media in order to account for differences in their natural abundance, thereby enabling assessment of their fractionation. References used in REY normalization include, but are not limited to, i) parent material, ii) soil horizons from the system under investigation or iii) published values such as the upper continental crustal (UCC) mean or chondritic samples (Taylor and McLennan, 1981; Anders and Grevesse, 1989). Normalized REY values less than (greater than) unity indicate depletion (enrichment) relative to the selected reference. Preferential enrichment or depletion of individual REY can be assessed by concentration ratios obtained relative to neighboring elements, with “anomalous” results exceeding threshold values. The distinctive chemical properties that lead to series wide trends in incorporation into (or exclusion from) secondary minerals and/or complexes with natural organic matter make them appropriate for studies of biogeochemical weathering and subsequent solute denudation from the soil profile as well (Elderfield et al., 1990; Sholkovitz, 1992; Johannesson et al., 1997).

C. *Impacts of Biogeochemical processes on REY Mobilization*

Presence of organic matter, Fe, Mn-(oxy)hydroxides and redox conditions have been reported to influence REY fractionation and transport in the CZ soils (Pourret et al., 2007; Laveuf and Cornu, 2009; Goyne et al., 2010; Laveuf et al., 2012).

1. *Impact of Organic Matter on REY Mobilization*

Organic matter has been reported to display a high capability to complex, adsorb or chelate positively charged REY (Laveuf and Cornu, 2009). Organic complexes (bio-ligands) favor the fractionation of MREE and HREE because of their smaller ionic radii they tend to form strong stable complexes with carboxyl groups and phenolic hydroxyl groups in DOM (Pourret et al., 2007; Pourret and Martinez, 2009; Tang and Johannesson, 2010). Complexation of REE with fulvic acids evidenced a MREE downward concavity (MREE enrichment) at low pH values (Pourret et al., 2007) (Figure 2). Colloidal OM seems to play an important role on REY mobilization in the CZ soils as it was observed in the research discussed in **Appendix C**. Briefly, a large mass fraction of REY was associated with the colloidal pool (which comprises organic and Al- and Fe-(oxy)hydroxides colloids). The colloidal pool was dispersed from the CZ soils during a sequential extraction procedure.

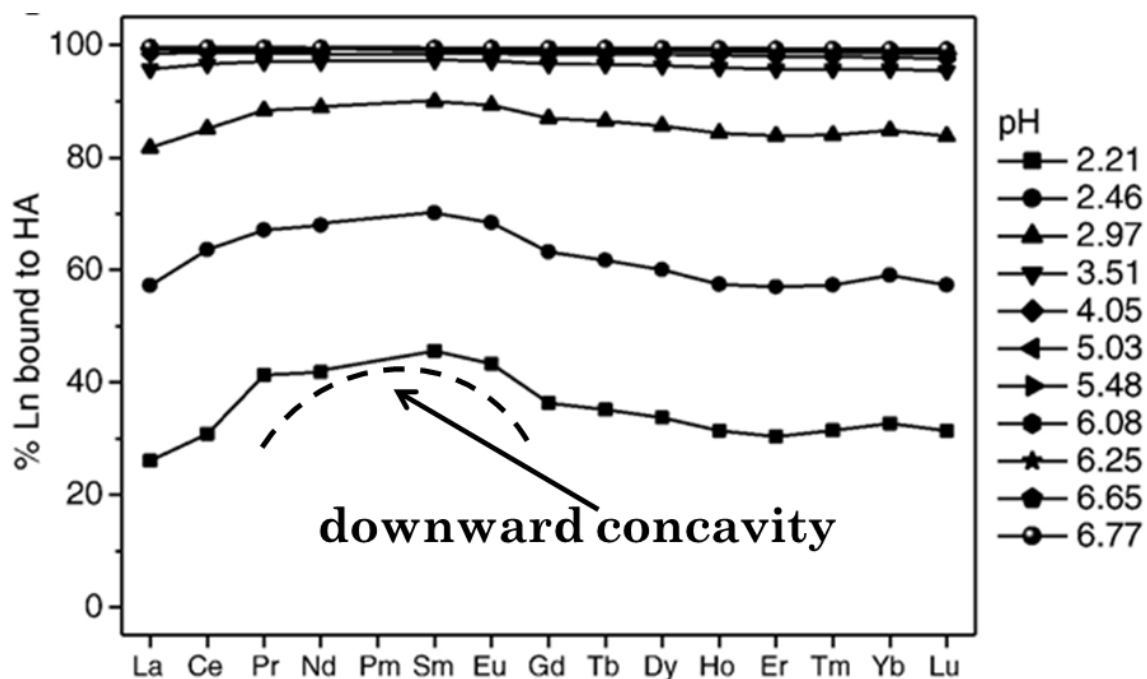


Figure 2 Complexation of REE with fulvic acids as a function of pH. Figure from Pourret et al. (2007).

2. Impact of Fe-, Mn-oxides on REY Mobilization

Iron and manganese oxides, in particular, scavenge REY through one or a combination of co-precipitation, adsorption (surface complex formation and/or ion exchange), and lattice diffusion processes (Bau, 1999; Ohta and Kawabe, 2001; Bau and Koschinsky, 2009; Davranche et al., 2011). Amorphous Fe- and Mn-oxides are postulated to be more enriched in REY than crystalline oxides because as the minerals undergo solid-state transformation and ripening, REY may be expelled from the increasingly constrained crystal structure. **Appendix C** highlights the significant role that these minerals play in trace metal retention in the CZ soils.

3. Impact of Redox processes on REY Mobilization

Redox conditions can influence REY fractionation and sorption/desorption processes in the CZ soils, (Elderfield, 1988; Moffett, 1994; Bau and Koschinsky, 2009; Davranche, et al, 2011). Europium and cerium are redox sensitive elements, but the reduction of Eu requires strong reducing conditions hardly encountered in near surface low pressure-temperature systems (Panahi et al., 2000; Laveuf and Cornu, 2009). Europium reduction predominates in magmatic systems; therefore, Eu is not a suitable tracer for redox processes in soils. The oxidation of Ce(III) to Ce(IV) however occurs at Eh values around than 300mV (De Carlo and Wen, 1998), which are encountered under natural soil conditions. The oxidation of Ce induces changes in ionic charge and radius which induces the decoupling of Ce(IV) from the rest of the lanthanide group, thereby generating positive Ce anomalies in soils (Feng, 2010; Laveuf et al., 2012). Under sub-oxic conditions, microbially-catalyzed dissolution of Fe(III)- and Mn(IV)-oxides occurs in preference to that of cerianite, enabling a positive Ce-anomaly to persist despite reductive dissolution and soil profile loss of Fe- and Mn-oxides (Laveuf and Cornu, 2009). The anomalous behavior of Ce in soil and aqueous solutions can be used to trace redox conditions in natural systems which is the focus of the study presented in **Appendix B**.

This study aims to provide useful and relevant information to better understand the biogeochemical processes that are involved in the critical zone evolution. Sequestration of DOM by soil mineral components helps in the formation and stabilization of soil aggregates. Organic matter influences water retention and provides energy to fungi, bacteria and soil animals (Brady and Weil, pp 94-133). Organic and Al- and Fe-(oxy)hydroxide colloids play a significant role as mobile nano-particulate sorbents for trace metals (possibly nutrients and contaminants). Lateral and vertical water fluxes will transport these colloidal-metal complexes into groundwater and surface water systems which ultimately will be used by aquatic organisms. In order to properly manage and ensure the sustainability of the CZ resources, it is fundamental to comprehend the biogeochemical processes that ensure the CZ optimal functionality.

CHAPTER 2: PRESENT STUDY

The present study is divided into three manuscripts that are included in this dissertation as Appendices A, B, and C. A summary of each manuscript will follow.

2.2 **Summary of Paper 1: FRACTIONATION OF DISSOLVED ORGANIC MATTER BY (OXY)HYDROXIDE-COATED QUARTZ SANDS: COMPETITIVE SORBATE DISPLACEMENT DURING REACTIVE TRANSPORT**

The objectives of the manuscript presented in **Appendix A** are: 1) to investigate the role of oxy-hydroxides minerals in the stabilization of DOM from a mixed conifer forest floor during progressive surface loading via saturated column experiments, 2) to use fluorescence spectroscopy as a tool to monitor effluent DOM solutions and thereby infer sorption-desorption and fractionation during reactive transport, and 3) to present empirical evidence to support a hypothetical zonal model of organo-mineral interactions.

In order to investigate the role of oxy-hydroxides minerals in stabilization of DOM, organic (O) horizons were collected in September, 2010 from a grassland (G) and a mixed conifer forest (F) vegetations. The O horizons were located within an instrumented zero order basin (ZOB) of the La Jara catchment, Valles Caldera National Preserve (Jemez Springs, NM). Columns packed with quartz sand (Qtz), Fe-hydroxide-coated quartz sand (Fe-Qtz), and Al-hydroxide-coated quartz sand (Al-Qtz) were irrigated with extracted DOM solutions. Al and Fe (oxy)hydroxide surfaces have been implicated in DOM stabilization (Eusterhues et al., 2003; Eusterhues et al., 2005). Although Al and Fe oxides often represent a small total mass fraction of soil mineral mass, they exert a disproportionate effect on interfacial reactions because of their nucleation and lateral growth on the surfaces of other minerals, including less DOM-

reactive tectosilicates such as feldspars and quartz (Coston et al., 1995). Each Qtz, Al-Qtz, or Fe-Qtz column experiment was run in duplicate and comprised two phases: (1) initial irrigation of fresh mineral media with grassland (G) DOM and (2) re-irrigation of the OM-coated mineral surfaces with the mixed conifer forest (F) DOM solution. Effluent solutions were monitored throughout the experiment for pH, total organic carbon (TOC), aromaticity and fluorescence spectroscopic characteristics.

During initial irrigation of fresh mineral media with G-DOM (Phase 1), the magnitude of DOM sorption followed this trend: Al-Qtz > Fe-Qtz > Qtz. Effluent solutions showed diminished molar absorptivity (ϵ) and fluorescence humification index (HIX) values, indicating preferential uptake of high molar mass aromatic constituents during reactive transport. At initiation of Phase 2, as a result of the earlier infusion of G-DOM, the Al-Qtz and Fe-Qtz columns contained 244 ± 3 and 190 ± 13 mg kg⁻¹ (C basis) of grassland sorbate organic matter (G-SOM) (calculated at 30 PV assuming pseudo-steady state conditions). Introduction of F-DOM (Phase 2) to G-SOM-coated surfaces revealed competitive desorption of G-SOM from the organo-mineral interface. During all treatments, high HIX values were observed in Phase 2 effluent solutions, indicating remobilization of G-SOM by displacement and/or aqueous complexation. Fluorescence emission suggested that fulvic and humic acid-like compounds were eluted from the organo-mineral interface, providing evidence for kinetic DOM exchange reactions.

These results indicate that weathering process favoring the neo-formation of gibbsite and goethite in natural soils will also favor high OM adsorption and further stabilization. The role of soils as a sink for OM is in part is due to the presence of Al, Fe-

(oxy)hydroxide minerals in the natural soil system. Soils in the CZ can serve as sinks of C (uptaking CO₂ and minimizing global warming) and understanding the mechanisms of OC stabilization will ensure the proper management and sustainability of the CZ.

2.3 **Summary of Paper 2: RARE EARTH ELEMENTS AS REACTIVE TRACERS OF BIOGEOCHEMICAL WEATHERING IN THE JEMEZ RIVER BASIN CRITICAL ZONE OBSERVATORY**

The principal objectives of the manuscript presented in **Appendix B** are: (i) to explore whether REE patterns of distinct catchment sources are reflected in their contributions to stream water REE effluxes, including changes with time and spatial scales; (ii) to reveal biogeochemical processes influencing catchment REE fractionation during snowmelt events. Most annual (bio)chemical denudation of REE occurred during the snowmelt-derived DOC pulse.

Rare earth elements were evaluated as potential tracers to elucidate biogeochemical weathering processes occurring during snowmelt at different scales, ranging from zero order basin (ZOB), to catchment (La Jara) and finally to watershed (East Fork Jemez River) scales. The study includes time series of REE patterns in precipitation, soil pore water, ground water, and stream water, and relates these data to REE composition of soil, rock and atmospheric dust. The potential biogeochemical processes influencing REY fractionation and mobilization in the study are: 1) weathering of primary minerals, 2) colloidal transport, 3) REY-DOM complexation, 4) REY adsorption by silicate clay and Fe-(oxy)hydroxide minerals, 5) dust deposition, and 6) redox conditions.

Concentrations of REY in natural terrestrial waters exhibited a strong correlation with dissolved organic carbon concentrations. Pronounced positive Eu-anomalies were observed in the soil matrix, soil solutions, and stream waters. Processes contributing to the positive Eu-anomaly include dust deposition, preferential dissolution of plagioclase

feldspars, and hydrothermal alteration of the parent materials. An incremental increase in cerium was observed in the soils and this enrichment was attributed to Ce adsorption onto the surface of Fe-Mn-oxides.

Since REE mobility can be affected by the same processes that influence trace metals (Cu, Cr, Co, Ni, Pb, U, Th) mobility in solution (Grybos et al., 2007); REE have been postulated to be a very useful tool that allow us to learn more about the biogeochemical weathering processes occurring in natural systems that affect trace metal sorption/desorption and transport. In this study site, for instance, REE fractionation patterns in stream waters exhibited an increase from La to Lu (a.k.a. the lanthanide contraction), indicating the prevalence formation of organo-REE complexes (Tang and Johannesson, 2010). Also, a strong positive correlation between DOC and $\sum\text{REE}$ was observed in stream waters, suggesting a strong role for biological mediation of REE chemical denudation. This study also highlights the role of Fe and Al-(oxy)hydroxides colloids as mobile nano-particulate sorbents for REE (possibly other trace metals). Finally, the use of Ce-anomalies proved to be useful in describing redox fluctuations during the snowmelt period at pedon scale.

2.4 **Summary of Paper 3: REDISTRIBUTION OF RARE EARTH ELEMENTS AND YTTRIUM (REY) IN TOPOGRAPHICALLY DISTINCT, RHYOLITE-DERIVED PEDONS**

The objectives of the work presented in **Appendix C** are: (i) to investigate the influence of water and reduced carbon flux regimes on REY depletion patterns at the pedon scale induced by different landscape positions; (ii) to further elucidate the biogeochemical processes influencing Eu and Ce anomalous behaviors in the soil matrix (discussed in **Appendix B**); and (iii) to investigate if yttrium (Y) and holmium (Ho) reflect differential incorporation in pedogenic Fe-(oxy)hydroxide precipitates (determined from Y/Ho ratios).

In order to elucidate which mineral and organic phases are controlling the transport and fate of REY in temperate soils, soil samples (planar and convergent hillslope soil profiles) from La Jara ZOB were collected and subjected to a sequential chemical extraction. The sequential chemical extraction scheme resulted in six chemically distinct fractions, namely, water soluble, exchangeable and carbonate bound (Step 1), reductive dissolution of Mn-oxides, i.e., birnessite (Step 2), dispersion of organo-metal colloids (Step 3), reductive dissolution of short range order (SRO) Fe-oxides, i.e., ferrihydrite, (Step 4), reductive dissolution of long range order (LRO) Fe-oxides, i.e., goethite (Step 5), and the final residues (mainly silicates). Major elements, rare earth elements and yttrium were analyzed using inductively coupled plasma mass spectrometry.

Distinct REY depletion trends with depth were correlated with topographically-induced variation in water and dissolved organic carbon fluxes. The planar hillslope

location displayed depletion trends (high depletion in upper horizons) in the solid phase for the light, medium and heavy rare earth elements (LREE, MREE and HREE). An opposite trend was observed in the convergent site (high depletion in bottom horizons). The sequestration of Eu by Mn(IV)-oxides was proposed to explain the large enrichment of Eu in the soil matrix as revealed by pronounced positive Eu-anomalies after the reductive dissolution of Mn(IV)-oxides. Positive Ce-anomalies in the solid phase of the ZOB soils were highly correlated with Fe-(oxy)hydroxides as revealed by positive Ce-anomalies after the reductive dissolution of SRO Fe-oxides and LRO Fe-oxides.

The use of REE as reactive tracers of biogeochemical weathering processes informed us about the following relevant processes occurring in the CZ soils. A MREE downward concavity pattern was revealed in the organo-metal colloid pool, suggesting the formation of stable REE and humic substance complexes. The organo-metal colloid pool strongly influenced trace metal mobilization in the convergent site which was characterized by high water and reduced OC fluxes at depth. This study also highlights the significant role of Mn- and Fe-(oxy)hydroxides pools as sorbents for REE (possibly other trace metals).

REFERENCES

- Aubert D., Stille P. and Probst A. (2001) REE fractionation during granite weathering and removal by waters and suspended loads: Sr and Nd isotopic evidence. *Geochim. Cosmochim. Acta* **65**, 387-406.
- Anders, E. and Grevesse, N. (1989) Abundances of the elements - meteoritic and solar. *Geochim. Cosmochim. Acta*, **53**, 197-214.
- Banaitis M. R., Waldrip-Dail H., Diehl M. S., Holmes B. C., Hunt J. F., Lynch R. P. and Ohno T. (2006) Investigating sorption-driven dissolved organic matter fractionation by multidimensional fluorescence spectroscopy and PARAFAC. *J. Colloid Interface Sci.* **304**, 271-276.
- Bau, M. (1999) Scavenging of dissolved yttrium and rare earths by precipitating iron oxyhydroxide: experimental evidence for Ce oxidation, Y-Ho fractionation, and lanthanide tetrad effect. *Geochim. Cosmochim. Acta* **63**, 67-77.
- Bau, M., Dulski, P. and Moller, P. (1995) Yttrium and holmium in south-pacific seawater - vertical-distribution and possible fractionation mechanisms. *Chem Erde-Geochem.* **55**, 1-16.
- Bau M. and Koschinsky A. (2009) Oxidative scavenging of cerium on hydrous Fe oxide: Evidence from the distribution of rare earth elements and yttrium between Fe oxides and Mn oxides in hydrogenetic ferromanganese crusts. *Geochem. J.* **43**, 37-47.
- Brady, N. C., & Weil, R. R. (2004). Elements of the nature and properties of soils. New Jersey: Pearson Education Ltd. pp 93-133.
- Braun J., Pagel M., Muller J., Bilong P., Michard A. and Guillet B. (1990) Cerium anomalies in lateritic profiles. *Geochim. Cosmochim. Acta* **54**, 781-795.
- Chorover J. and Amistadi M. K. (2001) Reaction of forest floor organic matter at goethite, birnessite and smectite surfaces. *Geochim. Cosmochim. Acta* **65**, 95-109.
- Coston J., Fuller C. and Dacis J. (1995) Pb²⁺ and Zn²⁺ adsorption by a natural aluminum-bearing and iron-bearing surface coating on an aquifer sand. *Geochim. Cosmochim. Acta* **59**, 3535-3547.
- Cullers R., Chaudhuri S., Arnold B., Lee M. and Wolf C. (1975) Rare-earth distributions in clay-minerals and in clay-sized fraction of Lower Permian Havensville and Eskridge shales of Kansas and Oklahoma. *Geochim. Cosmochim. Acta* **39**, 1691-1703.

- Davranche M., Pourret O., Gruau G. and Dia A. (2004) Impact of humate complexation on the adsorption of REE onto Fe oxyhydroxide. *J. Colloid Interface Sci.* **277**, 271-279.
- Davranche M., Pourret O., Gruau G., Dia A. and Le Coz-Bouhnik M. (2005) Adsorption of REE(III)-humate complexes onto MnO₂: Experimental evidence for cerium anomaly and lanthanide tetrad effect suppression. *Geochim. Cosmochim. Acta* **69**, 4825-4835.
- Davranche M., Grybos M., Gruau G., Pedrot M., Dia A. and Marsac R. (2011) Rare earth element patterns: a tool for identifying trace metal sources during wetland soil reduction. *Chem. Geol.* **284**, 127-137.
- De Carlo E., and Wen X. (1998) The influence of redox reactions on the uptake of dissolved Ce by suspended Fe and Mn oxide particles. *Aquatic Geochemistry* **3**, 357-389.
- Dupre B., Viers J., Dandurand J., Polve M., Benezeth P., Vervier P. and Braun J. (1999) Major and trace elements associated with colloids in organic-rich river waters: ultrafiltration of natural and spiked solutions. *Chem. Geol.* **160**, 63-80.
- Elderfield H. (1988) The oceanic chemistry of the rare-earth elements. *Philos. Trans. R. Soc. A-Math. Phys. Eng. Sci.* **325**, 105-126.
- Elderfield D H., Upstillgoddard R. and Sholkovitz E. (1990) The rare-earth elements in rivers, estuaries, and coastal seas and their significance to the composition of ocean waters. *Geochim. Cosmochim. Acta* **54**, 971-991.
- Eusterhues K., Rumpel C. and Kogel-Knabner I. (2005) Organo-mineral associations in sandy acid forest soils: importance of specific surface area, iron oxides and micropores. *Eur. J. Soil Sci.* **56**, 753-763.
- Eusterhues K., Rumpel C., Kleber M. and Kogel-Knabner I. (2003) Stabilisation of soil organic matter by interactions with minerals as revealed by mineral dissolution and oxidative degradation. *Org. Geochem.* **34**, 1591-1600.
- Feng, J. (2010) Behaviour of rare earth elements and yttrium in ferromanganese concretions, gibbsite spots, and the surrounding terra rossa over dolomite during chemical weathering. *Chem. Geol.*, **271**, 112-132.
- Goh K. (2004) Carbon sequestration and stabilization in soils: implications for soil productivity and climate change. *Soil Sci. Plant Nutr.* **50**, 467-476.

- Goyne K. W., Brantley S. L. and Chorover J. (2010) Rare earth element release from phosphate minerals in the presence of organic acids. *Chem. Geol.* **278**, 1-14.
- Gruau G., Dia A., Olivie-Lauqueta G., Davranche M. and Pinay G. (2004) Controls on the distribution of rare earth elements in shallow groundwaters. *Water Res.* **38**, 3576-3586.
- Grybos M., Davranche M., Gruau G., Petitjean P. (2007) Is trace metal release in wetland soils controlled by organic matter mobility or Fe-oxyhydroxides reduction? *Journal of Colloid and Interface Science* **314**, 490-501.
- Hunt J. F., Ohno T., He Z., Honeycutt C. W. and Dail D. B. (2007) Influence of decomposition on chemical properties of plant- and manure-derived dissolved organic matter and sorption to goethite. *J. Environ. Qual.* **36**, 135-143.
- Tang J. and Johannesson K. H. (2010) Ligand extraction of rare earth elements from aquifer sediments: implications for rare earth element complexation with organic matter in natural waters. *Geochim. Cosmochim. Acta* **74**, 6690; 6690-6705/6705; 6705.
- Johannesson K., Stetzenbach K. and Hodge V. (1997) Rare earth elements as geochemical tracers of regional groundwater mixing. *Geochim. Cosmochim. Acta* **61**, 3605-3618.
- Johannesson K., Tang J., Daniels J., Bounds W. and Burdige D. (2004) Rare earth element concentrations and speciation in organic-rich blackwaters of the Great Dismal Swamp, Virginia, USA. *Chem. Geol.* **209**, 271-294.
- Kaiser K. and Guggenberger G. (2000) The role of DOM sorption to mineral surfaces in the preservation of organic matter in soils. *Org. Geochem.* **31**, 711-725.
- Kaiser K. and Zech W. (1997) Competitive sorption of dissolved organic matter fractions to soils and related mineral phases. *Soil Sci. Soc. Am. J.* **61**, 64-69.
- Kalbitz K., Solinger S., Park J. H., Michalzik B. and Matzner E. (2000) Controls on the dynamics of dissolved organic matter in soils: A review. *Soil Sci.* **165**, 277-304.
- Kleber M., Sollins P. and Sutton R. (2007) A conceptual model of organo-mineral interactions in soils: self-assembly of organic molecular fragments into zonal structures on mineral surfaces. *Biogeochemistry* **85**, 9-24.
- Kleber M. and Johnson M. G. Chapter 3 - Advances in understanding the molecular structure of soil organic matter: implications for interactions in the environment. In *Advances in Agronomy* (Anonymous). Academic Press, pp. 77-142.

- Laveuf C. and Cornu S. (2009) A review on the potentiality of rare earth elements to trace pedogenetic processes. *Geoderma* **154**, 1-12.
- Laveuf C., Cornu S., Guilherme L. R. G., Guerin A. and Juillot F. (2012) The impact of redox conditions on the rare earth element signature of redoximorphic features in a soil sequence developed from limestone. *Geoderma* **170**, 25-38.
- Laveuf C., Cornu S. and Juillot F. (2008) Rare earth elements as tracers of pedogenetic processes. *C. R. Geosci.* **340**, 523-532.
- Leybourne M. I. and Johannesson K. H. (2008) Rare earth elements (REE) and yttrium in stream waters, stream sediments, and Fe-Mn oxyhydroxides: fractionation, speciation, and controls over REE plus Y patterns in the surface environment RID B-2541-2009. *Geochim. Cosmochim. Acta* **72**, 5962-5983.
- Ma, L., Jin, L. and Brantley, S.L. (2011) How mineralogy and slope aspect affect REE release and fractionation during shale weathering in the Susquehanna/Shale Hills Critical Zone Observatory. *Chem. Geol.* **290**, 31-49.
- Moffett J. (1994) A radiotracer study of cerium and manganese uptake onto suspended particles in Chesapeake Bay. *Geochim. Cosmochim. Acta* **58**, 695-703.
- NRC (2001) Basic research opportunities in earth sciences. National Academies Press. Washington, DC, National Research Council.
- Nezat C. A., Blum J. D., Yanai R. D. and Hamburg S. P. (2007) A sequential extraction to determine the distribution of apatite in granitoid soil mineral pools with application to weathering at the Hubbard Brook Experimental Forest, NH, USA. *Appl. Geochem.* **22**, 2406-2421.
- Ohta, A. and Kawabe, I. (2001) REE(III) adsorption onto Mn dioxide (δ -MnO₂) and Fe oxyhydroxide: Ce(III) oxidation by δ -MnO₂. *Geochim. Cosmochim. Acta*, **65**, 695-703.
- Oliva P., Viers J., Dupre B., Fortune J., Martin F., Braun J., Nahon D. and Robain H. (1999) The effect of organic matter on chemical weathering: Study of a small tropical watershed: Nsimi-Zoetele site, Cameroon. *Geochim. Cosmochim. Acta* **63**, 4013-4035.
- Panahi A., Young G. and Rainbird R. (2000) Behavior of major and trace elements (including REE) during Paleoproterozoic pedogenesis and diagenetic alteration of an Archean granite near Ville Marie, Quebec, Canada. *Geochim. Cosmochim. Acta* **64**, 2199-2220.

- Perdrial J.N., Stielstra C., Lybrand R., Swetnam T., Mitra B., Huckel D., Harpold A., J. McIntosh T. Meixner, Vázquez-Ortega A., Condon K., Brooks P., Chorover J.. (In prep) The impact of climate change on the carbon budget of forested headwater catchments: a CZO synthesis project.
- Pourret O., Davranche M., Gruau G. and Dia A. (2007) Rare earth elements complexation with humic acid. *Chem. Geol.* **243**, 128-141.
- Pourret O. and Martinez R. E. (2009) Modeling lanthanide series binding sites on humic acid. *J. Colloid Interface Sci.* **330**, 45-50.
- Pourret O., Gruau G., Dia A., Davranche M. and Molenat J. (2010) Colloidal control on the distribution of rare earth elements in shallow groundwaters. *Aquat. Geochem.* **16**, 31-59.
- Rasmussen C., Troch P. A., Chorover J., Brooks P., Pelletier J. and Huxman T. E. (2011) An open system framework for integrating critical zone structure and function. *Biogeochemistry* 102, 15-29.
- Scheel T., Dorfler C. and Kalbitz K. (2007) Precipitation of dissolved organic matter by aluminum stabilizes carbon in acidic forest soils. *Soil Sci. Soc. Am. J.* **71**, 64-74.
- Shiller A. M. (2010) Dissolved rare earth elements in a seasonally snow-covered, alpine/subalpine watershed, Loch Vale, Colorado. *Geochim. Cosmochim. Acta* **74**, 2040-2052.
- Sholkovitz E. (1992) Chemical evolution of rare-earth elements - fractionation between colloidal and solution phases of filtered river water. *Earth Planet. Sci. Lett.* **114**, 77-84.
- Six J., Conant R., Paul E. and Paustian K (2002) Stabilization mechanisms of soil organic matter: Implications for C-saturation of soils. *Plant Soil* **241**, 155-176.
- Stille P., Steinmann M., Pierret M. -, Gauthier-Lafaye F., Chabaux F., Viville D., Pourcelot L., Matera V., Aouad G. and Aubert D. (2006) The impact of vegetation on REE fractionation in stream waters of a small forested catchment (the Strengbach case). *Geochim. Cosmochim. Acta* **70**, 3217-3230.
- Sutton, R. and G. Sposito. 2005. Molecular structure in soil humic substances: the new view. *Environ. Sci. Technol.* **39**, 9009-9015.
- Tang J, Johannesson K. (2003) Speciation of rare earth elements in natural terrestrial waters: assessing the role of dissolved organic matter from the modeling approach. *Geochimica et Cosmochimica Acta* **67**: 2321-39.

- Taylor S. and McLennan S. (1981) The composition and evolution of the continental-crust - rare-earth element evidence from sedimentary-rocks. *Philos. Trans. R. Soc. Lond. Ser. A-Math. Phys. Eng. Sci.* **301**, 381-399.
- Thompson A., Amistadi M.K., Chadwick O.A., and Chorover J. (In Press) Fractionation of yttrium and holmium during basaltic soil weathering. *Geochim. Cosmochim. Acta*
- Trumbore S. (1997) Potential responses of soil organic carbon to global environmental change. *Proc. Natl. Acad. Sci. U. S. A.* **94**, 8284-8291.
- von Luetzow M., Koegel-Knabner I., Ekschmitt K., Matzner E., Guggenberger G., Marschner B. and Flessa H. (2006) Stabilization of organic matter in temperate soils: mechanisms and their relevance under different soil conditions - a review. *Eur. J. Soil Sci.* **57**, 426-445.
- von Lutzow M., Kogel-Knabner I., Ludwig B., Matzner E., Flessa H., Ekschmitt K., Guggenberger G., Marschner B. and Kalbitz K. (2008) Stabilization mechanisms of organic matter in four temperate soils: development and application of a conceptual model. *J. Plant Nutr. Soil Sci. -Z. Pflanzenernahr. Bodenkd.* **171**, 111-124.

APPENDIX A:**FRACTIONATION OF DISSOLVED ORGANIC MATTER BY
(OXY)HYDROXIDE-COATED QUARTZ SANDS: COMPETITIVE SORBATE
DISPLACEMENT DURING REACTIVE TRANSPORT**

Angélica Vázquez-Ortega^{a*}, Selene Hernandez-Ruiz^a, Mary Kay Amistadi^a, Craig Rasmussen^a, Jon Chorover^a

^aDepartment of Soil, Water & Environmental Science, University of Arizona, 1177 East Fourth Street, Tucson, Arizona 85721-0038, USA

*Corresponding author: avazquez@email.arizona.edu

To be submitted to special section in Vadose Zone Journal

ABSTRACT:

Sorptive retention of dissolved organic matter (DOM) at soil particle surfaces is a key control on carbon flux through the critical zone. Prior studies have shown that pristine Al and Fe (oxy)hydroxide surfaces are particularly reactive toward DOM sorptive stabilization. However, the impact of progressive and/or pre-existing organic surface coatings on further surficial uptake and exchange during prolonged or repeated DOM infusion episodes remains unclear, and is the focus of the current work. DOM solutions were extracted from organic horizons in (1) grass and (2) mixed conifer forest vegetation types in the Jemez River Basin Critical Zone Observatory (JRB-CZO). Extracted DOM solutions were used to sequentially irrigate replicated porous geomedia columns packed with either quartz sand (Qtz), Al-hydroxide-coated quartz sand (Al-Qtz), and Fe-hydroxide-coated quartz sand (Fe-Qtz). Use of the two (G and F) sources of DOM enabled investigation of how sorption, fractionation and exchange processes change with reactive transport through mineral surfaces becoming progressively coated with sorbate organic matter (SOM). Effluent solutions were characterized for DOC concentration, molar absorptivity, and fluorescence spectroscopy. During initial irrigation of fresh mineral media with grassland (G-)DOM (Phase 1), the magnitude of DOM sorption followed the trend: Al-Qtz > Fe-Qtz > Qtz. Effluent solutions showed diminished molar absorptivity (ϵ) and humification index (HIX) values, indicating preferential uptake of high molar mass aromatic constituents during reactive transport. Introduction of mixed conifer forest (F-)DOM (Phase 2) to grassland sorbate OM (G-SOM) coated surfaces revealed competitive desorption of G-SOM from the organo-mineral interface. During all

treatments, high HIX values were observed in Phase 2 effluent solutions, indicating re-mobilization of G-SOM by displacement and/or aqueous complexation. Fluorescence emission suggested that fulvic and humic acid-like compounds were eluted from the organo-mineral interface, providing evidence for kinetic DOM exchange reactions as postulated.

1 INTRODUCTION

The elucidation of biogeochemical mechanisms that stabilize carbon (C) in soils is important to understanding C flux feedbacks to climate change, including the impacts of land-use management (Six et al., 2002; Goh, 2004; von Luetzow et al., 2006; von Lutzow et al., 2008). Among the various processes involved in dissolved organic matter (DOM) stabilization, adsorption at Al and Fe (oxy)hydroxide surfaces is a very important factor (Eusterhues et al., 2003; Eusterhues et al., 2005). Although Al and Fe oxides often represent a small total mass fraction of soil mineral mass, they exert a disproportionate effect on interfacial reactions because of their nucleation and lateral growth on the surfaces of other minerals, including less DOM-reactive tectosilicates such as feldspars and quartz (Coston et al., 1995). However, the specific processes controlling OM complexation with oxide-coated surfaces and the mechanisms affecting exchange between DOM and soil organic matter (SOM) in the solid phase are not fully resolved. Proposed mechanisms controlling DOM sorption-desorption include anion exchange, ligand exchange-surface complexation, cation bridging, hydrogen bonding, van der Waals forces, and the hydrophobic effect (Eusterhues et al., 2005; von Luetzow et al., 2006; Scheel et al., 2007; von Lutzow et al., 2008).

Based on the heterogeneity and polyfunctionality of DOM molecular species, and the associated potential for intermolecular association (Sutton and Sposito, 2005; Lam and Simpson, 2008; Lattao et al., 2008; Simpson et al., 2012), Kleber et al. (2007) proposed a multi-faceted “zonal” model of OM sorption at mineral-water interfaces, similar to that proposed earlier by Wershaw (1993). The zonal model assumes a DOM molecular

structure consisting of small and chemically diverse organic molecules inter-linked by hydrophobic, cation-bridging, and hydrogen bonding interactions that are capable of self-organizing (pseudo-micellar) behavior in aqueous solution (Sutton and Sposito, 2005) and - by extension - at the mineral-water interface (Wwershaw, 1993; Kleber et al., 2007). The model postulates the distribution of sorbed DOM among three distinct zones: (i) mineral contact zone, (ii) intermediate hydrophobic zone, and (iii) peripheral kinetic zone. The contact zone is where organic moieties are anchored over relatively long time scales through polar moieties to the surface via electrostatic, covalent, and (to a lesser extent) hydrophobic interaction. The hydrophobic zone is characterized by hydrophobic interactions among apolar DOM moieties and moderate DOM exchange rate. Finally, the kinetic zone is postulated to be characterized by labile cation bridging and hydrogen bonding interactions, and a high DOM exchange rate. If kinetically labile domains exist at the particle-OM interface, they should be detectable in DOM reactive transport experiments that employ methods of detection that are sensitive to DOM molecular structure (e.g., UV-Vis and fluorescence excitation-emission spectroscopy) (Hunt and Ohno, 2007; Ohno et al., 2007; Ohno et al., 2008; Hernandez-Ruiz et al., 2012).

Organic matter exchange reactions at mineral-water interfaces may be prevalent in complex terrain affected by changes in hydrologic flow paths, and this likely affects the molecular composition of terrestrial DOM that is effluent to surface waters. For example, in catchments comprising grassland stands adjacent to mixed conifer forest on common hillslopes (as occurs in mountain environments throughout the western U.S.), such intermixing and exchange reactions are likely to be prevalent, especially during

saturated subsurface lateral flows, when the catchment subsurface is “connected” hydrologically (Harpold et al., WRR paper in press; Perdrial et al., Biogeochem. paper in review). To the extent that DOM derived from distinct vegetation types differs in molecular composition (Sanderman et al., 2008), competitive adsorption-desorption reactions are likely to ensue.

Hydroxylated surfaces of Al and Fe (oxy)hydroxides exhibit strong binding complexation with carboxyl and phenolic hydroxyl groups in DOM (Kaiser and Guggenberger, 2000; Chorover and Amistadi, 2001). In batch experiments, a steep Langmuir-type isotherm was observed for forest floor derived DOM adsorption to goethite (α -FeOOH) with a maximum retention of 10.5 g C kg⁻¹ (Chorover and Amistadi, 2001). Chi and Amy (2004) reported rapid DOM sorptive uptake to Fe-oxide coated quartz and also nonlinear isotherm shape (Langmuir curve). Previous experiments have demonstrated that the hydrophilic fraction in DOM is sorbed weakly in soils, whereas the more hydrophobic fraction (dominantly comprising lignin-derived phenols with varying degrees of substituent carboxylation) can form stable covalent bonds via ligand exchange at surface hydroxyl groups of Fe and Al (oxy)hydroxides (Gu et al., 1994; Gu et al., 1995; Kaiser and Guggenberger, 2000; Guo and Chorover, 2006). Hunt et al. (2007) observed an increase in sorption of both the hydrophilic and hydrophobic DOM fractions to goethite after microbial decomposition, with greater enhancement for the decomposed hydrophilic fraction.

Guo and Chorover (2003) studied the transport and fractionation of DOM in saturated columns comprising natural B horizon soil material. As a result of DOM

sorptive fractionation, the E2/E3 ratio (an index of humification) of the first effluent solutions was higher than those reported previously for natural DOM indicating removal of high molar mass constituents. In addition, sorption favored DOM fractions with high molar absorptivity, low phenolic and carboxylic acidity, and low hydrophilicity. Several studies have shown preferential adsorption of high molecular weight compounds onto the surface of Fe-oxides (Meier et al., 1999; Namjesnik-Dejanovic et al., 2000; Zhou et al., 2001). ^{13}C nuclear magnetic resonance (NMR) and diffuse reflectance infrared Fourier-transform (DRIFT) spectroscopies have shown that natural DOM rich in aromatic moieties and carboxyl groups (i.e., partially-oxidized lignin phenols) are preferentially sorbed by Al and Fe (oxy)hydroxide minerals (Kaiser et al., 1997; Chorover and Amistadi, 2001).

Sensitive, non-destructive techniques, such as UV-Vis and fluorescence spectroscopy, can be used to obtain information about DOM molecular structure (Hunt and Ohno, 2007; Ohno et al., 2007; Ohno et al., 2008; Hernandez-Ruiz et al., 2012). Fluorescence excitation-emission matrices (EEMs), in particular, contain information on spectrally-distinct DOM components (Banaitis et al., 2006) and are highly sensitive to DOM structure and sorptive fractionation reactions (Hunt and Ohno, 2007; Hunt et al., 2007). Such analyses are relatively rapid and can be performed on unperturbed natural waters from field sites or for a time-series of effluent solutions derived from reactive transport experiments.

The specific objectives were (1) to investigate the role of (oxy)hydroxide coatings in stabilization of DOM deriving from grassland and mixed conifer organic horizons during

progressive surface loading via saturated column experiments, (2) to use fluorescence spectroscopy as a tool to monitor effluent DOM solutions and thereby infer sorption-desorption and competitive fractionation during reactive transport, and (3) to present empirical evidence to support or refute the hypothetical zonal model of organo-mineral interactions.

2 MATERIALS AND METHODS

2.1 Sample Collection and DOM Extraction

Organic (O) horizons were collected in September, 2010 from grassland vegetation (G) and mixed conifer forest (F) stands established in adjacent locations within an instrumented zero order basin (ZOB) of the La Jara catchment, Valles Caldera National Preserve (Jemez Springs, NM). The study site was chosen because is representative of montane forested catchments common in western US. Samples were sealed in zip-lock bags and stored at 4°C. Upon arrival at the Environmental Biogeochemistry Laboratory at the University of Arizona, organic horizon materials were maintained in field moist conditions, sieved (< 2 mm), mixed, and stored at 4°C.

One hundred grams of field moist material and 500 grams of ultrapure (Barnstead) water were added to a 1 L bottle that was capped and placed on a reciprocal shaker at 100 rpm for 1 h. The gravimetric water contents (in g kg⁻¹, based on dry soil) for the O horizons in the grassland and mixed conifer vegetation were 676.9 and 1,350, respectively (giving a mass solid to solution ratio of 1:9 for the grassland and 1:13 for the forest). Solutions were transferred to 250 mL polypropylene copolymer (PPCO)

centrifuge bottles (for which DOC release during transfer time was measured to be negligible) and centrifuged at 10,000 rpm (15,182 RCF) for 30 min to remove sediment solids. The supernatant solution was transferred into 50 mL PPCO centrifuge tubes and centrifuged again at 18,500 rpm (44,003 RCF) for 20 min to remove polymerized material and clay fraction. Supernatants were filtered through a baked 0.7 micron glass fiber filter (GF/F) and 0.01 M NaN_3 was added to avoid subsequent microbial alteration. DOM solutions were stored at 4 °C for no more than 12 h prior to use in experiments.

2.2 Chemical Characterization of DOM Extracts

Several analytical methods were used to assess the chemical character of the extracted DOM solutions (Table 1). The pH was analyzed by probe (VWR symphony Model SP80PC), whereas non-purgeable organic carbon (TOC) was determined using high temperature oxidation followed by infrared detection of CO_2 (Shimadzu TOC-VCSH, Columbia, MD). DOM elemental composition was determined by inductively coupled plasma mass spectrometry (ICP-MS) (Perkin Elmer DRC II, Shelton, CT). Molar absorbances were determined by UV-VIS at 250, 280, 365, 465, and 665 nm (Shimadzu 2501PC UV-VIS spectrometer). Excitation-emission matrix (EEM) fluorescence spectra were obtained with the FluoroMax®-4 from HORIBA Jobin Yvon equipped with a 150-W Xe-arc lamp source. The EEM spectrum was acquired with excitation (Ex) from 200 to 450 and emission (Em) from 250 to 650 at 5 nm increments. Spectra were collected with Ex and Em slits at 5 nm and 2 nm band widths, respectively, and an integration time of 0.1 s. MATLAB R2010a was used to produce EEM contour plots. The fluorescence intensity of 0.003 M NaN_3 (after three fold dilution which

corresponds to the dilution applied to effluent samples) showed similar fluorescence intensity to nanopure water, concluding that NaN_3 has no detectable effect on spectroscopic results reported herein.

The humification index (HIX) was calculated from EEMs for all DOM breakthrough curves. The HIX, derived from intensity calculations pertaining to individual fluorescence excitation-emission spectra, has been used to determine the degree of DOM “recalcitrance” as a result of the degree of molecular complexity and condensation (Zsolnay et al., 1999; Kalbitz et al., 2003). The HIX is defined as sum of fluorescence intensity in the 435→480 nm region normalized by that of the 300→345 nm region, for a specific excitation wavelength of 255 nm:

$$\text{HIX} = (\sum I_{Em} 435 \rightarrow 480) / (\sum I_{Em} 300 \rightarrow 345) \quad (1)$$

2.3 Sorbent Preparation

2.3.1 Quartz Sand Coating Procedure

Quartz sand (ThermoFisher Scientific) was pre-cleaned in five steps in order to ensure a pristine media. Two hundred grams of sand were added to 1.0 kg of solution in a sealed bottle on reciprocating shaker (100 rpm). Between each step, the wash solutions were decanted, followed by a thorough rinse with ultrapure water until the solution was clear. The washing solutions and reaction time used for each step were (1) nitric acid (1.6 M, 2 h), (2) sodium hydroxide (0.5 M, 2 h), (3) hydrochloric acid (0.1 M, 24 h), (4) hydrochloric acid (pH 5, 24 h), and (5) sodium hydroxide (0.5 M, 2 h) to neutralize the acid. After five subsequent rinses with ultrapure water, the sand was spread to dry at 105° C for 24 h before being stored in an acid-washed container.

The procedure for coating the quartz sand with Al and Fe oxides was based on (Bolster et al., 2001; Park and Kim, 2010). For the Fe oxide-coated sand, 5.5 g of $\text{FeCl}_3 \cdot 6\text{H}_2\text{O}$ were dissolved in 100 mL ultrapure water. The solution was transferred to a round-bottom boiling flask and pH adjusted to 9.0 with 6 M NaOH. Quartz sand (200 g) was added to the solution and swirled to mix. The pH dropped to about 7, but was then readjusted to 9.0, the suspension was swirled, and the pH was checked again. Once the pH stabilized, the flask was placed onto a rotary evaporator pre-heated to 90°C and flushed with a blanket of N_2 at 80 rpm. The pH was checked at 5 min intervals and adjusted with dropwise additions of 1 M NaOH to maintain pH *ca.* 9, then returned to the evaporator. Heating continued for 90 min. The coated sand slurry was transferred to a Pyrex baking dish, rinsing the flask with a small amount of water to aid transfer, and then dried at 150 °C for 6 h, rinsed with ultrapure water, then dried again under the same conditions (rinse-bake-rinse-bake). For Al oxide-coated sand, the general procedure outlined above was followed, but using $\text{AlCl}_3 \cdot 6\text{H}_2\text{O}$ (4.4g) dissolved in 100 mL ultrapure water. The specific surface area of the quartz sand (Qtz), Al-hydroxide-coated quartz sand (Al-Qtz), and Fe-hydroxide-coated quartz sand (Fe-Qtz) are 0.029 ± 0.0006 , 1.28 ± 0.01 , and $1.31 \pm 0.01 \text{ m}^2 \text{ g}^{-1}$, respectively, based on BET analysis of N_2 adsorption data (Table 2). The (oxy)hydroxide surface coatings were loaded with 1.30 ± 0.02 and $2.97 \pm 0.46 \text{ g kg}^{-1}$ of total solid phase mass for Al and Fe respectively, determined after microwave digestion with 16 M HNO_3 .

2.3.2 Column Packing and Setup

Baked glass chromatography columns were packed with Qtz, Al-Qtz, and Fe-Qtz. A borosilicate fritted disc and glass wool with medium porosity were placed at the inlet and outlet of the column. A peristaltic pump (Masterflex L/S) was used to drive a constant upward column through-flow of 0.04 mL min^{-1} , which translates to a Darcy flux of 0.06 cm min^{-1} , slow enough to enable significant fluid-mineral interaction time. The upward solution flux was employed to diminish preferential flow.

2.4 DOM Reactive Transport Column Experiments

Each Qtz, Al-Qtz, or Fe-Qtz column experiment was run in duplicate and comprised two phases. The first phase involved initial irrigation of fresh mineral media with grassland (G) DOM. G- DOM solution was diluted with ultrapure water to give DOC concentration of 40 mg L^{-1} and pH 7.95. The DOC concentrations in pore waters in the study site ranged from 10 to 60 mg L^{-1} during the snowmelt season of WY 2011 (Vazquez-Ortega et al., in prep). During this phase, ca. 60 pore volumes (PV) were eluted. The effluent solution was collected every 150 min using a fraction collector (Foxy 200, Teledyne Isco Inc., Lincoln, Nebraska) for a total volume of 6 mL (equivalent to 1 PV) at each increment. At the end of phase 1, fluid flow was stopped, pore water was removed (air was pumped to remove the water) and the columns were dried in a vacuum chamber (67 kPa) for 7 d at room temperature. After the drying period, columns were reinstalled at the pump and phase 2 consisting in the re-irrigation of the OM-coated mineral surfaces with a mixed conifer forest (F) DOM solution with DOC concentration of 43 mg L^{-1} and pH 8, to model the OM sorbate exchange that might occur during

infusion of DOM from adjacent forest vegetation into grassland soils. This solution was applied at the same flow rate as phase 1 (0.04 mL min^{-1}) for collection of ca. 60 PV.

Effluent solutions from pore volume 1, 2, 3, 4, 5, 10, 20, 30, and 60 were analyzed from each replicated column to obtain data on pH, Al, Fe, Si, TOC, molar absorptivity, and fluorescence excitation-emission, using the methods described above. UV-Vis and fluorescence spectroscopy were determined on eluted solutions after a 3 fold dilution was obtained in order to minimize the inner filter effect (Hudson et al., 2007; Baker et al., 2008).

3 RESULTS

3.1 DOM sorption during reactive transport through pristine media (Phase 1)

During Phase 1, equivalent grassland DOM solutions were infiltrated into replicated columns of (i) Qtz, (ii) Al-Qtz, and (iii) Fe-Qtz, enabling an evaluation of the effects of mineral surface chemistry on DOM sorption/fractionation. Effluent pore volumes were analyzed for pH, DOC, UV-Vis absorption, and fluorescence emission. Treatment effects on reactive transport of DOM are apparent from the data comparing effluent solution pH, DOC, molar absorptivity and humification index (Figure 1) to values of the same for influent solution (blue 95% confidence bands in Figure 1). For the Qtz treatment, pH values were similar to influent solution, whereas for the Al-Qtz treatment, pH values of the first PVs were lower than influent, a maximum pH was reached at 10 PV, and then a subsequent decrease was observed with increasing solution flux through during the remainder of phase 1. In comparison to the Qtz treatment, Al and

Fe oxide surface coatings significantly diminished effluent solution concentrations of DOC for the initial 30 PV of Phase 1. Integrating the mass loss of DOC during the first 30 PV and normalizing that to the total mass of mineral media present in the columns gives sorbed concentrations of organic C at 30 PV of 244 ± 3 and 190 ± 13 mg kg^{-1} for Al-Qtz and Fe-Qtz, respectively. Importantly, net dissolution of the Al and Fe (oxy)hydroxide coatings was apparently minimal over the course of the experiment (both Phase 1 and Phase 2), as effluent solution concentrations of Al, Fe and Si were not elevated significantly above the influent concentrations (Figure E2, electronic annex). Total Si, Al and Fe concentrations in influent G-DOM were 7.72, 1.98, and 0.80 mg L^{-1} respectively, whereas for F-DOM, corresponding concentrations were 8.4, 1.9, and 0.84 mg L^{-1} . Concentrations of Al and Fe in effluent solutions remained roughly equivalent to influent concentrations throughout the course of the experiment, whereas sorptive release of Si was observed in the Qtz case, and its sorptive retention was observed in the Al-Qtz and Fe-Qtz cases.

Molar absorptivity (ϵ) values (Figure 1C) are UV absorbances at 280 nm normalized to the molar DOC concentrations and cuvette path length for influent (blue band) and effluent (data points) solutions. Molar absorptivity has been shown to correlate linearly with DOM aromaticity as measured by ^{13}C nuclear magnetic resonance spectroscopy (Chin et al., 1994) and hence here reflects the fractionation of aromatic DOM moieties relative to bulk constituents upon transport through the pristine mineral assemblages. Molar absorptivity values for the Qtz treatment were comparable to the influent value, indicating little fractionation, whereas ϵ values were diminished

significantly during the first 30 PV for the Al-Qtz and Fe-Qtz treatments, indicating preferential sorption of aromatic constituents. The ϵ values during phase 1 exhibited the following trend: Al-Qtz \leq Fe-Qtz \ll Qtz.

Humification index (HIX) values for effluent solutions from the Qtz treatment were (after 1 PV) similar to that of the influent solution (G-DOM HIX = 17.6, Figure 1D). For both Al-Qtz and Fe-Qtz treatments, HIX values were significantly reduced during the first 30 PV of phase 1. For these treatments, HIX values increased over time, eventually reaching values similar to influent solution. The lowest HIX values for Al-Qtz and Fe-Qtz treatments for early pore volumes were 1.04 and 2.13, respectively – similar to values reported by Kalbitz et al. (2003) that exhibit high biodegradation rates; therefore, indicative of significant “recalcitrant” DOM fractionation at pristine (oxy)hydroxide surfaces.

Chen et al. (2003) separated synchronous excitation-emission matrices (EEMs, i.e., the excitation-emission fluorescence “surface” as depicted e.g., in Figure 2 for grassland and forest DOM sources) into operational regions that have been adopted to quantify DOM molecular variation in the present study. The EEM was divided into five operational regions: I (aromatic protein I), II (aromatic protein II), III (fulvic acid-like), IV (soluble microbial by-product-like), and V (humic acid-like). The EEMs for unreacted grassland and mixed conifer DOM solutions, prior to column application, are shown in Figure 2. The EEM spectrum for grassland DOM solution shows two principal peaks (Ex: 210nm - Em: 450nm and Ex: 260nm - Em: 460nm) in regions III and V, respectively (Figure 2A).

To probe the EEM spectral “fingerprint” of DOM that was preferentially retarded during transport as sorbate organic matter (i.e., G-SOM) in each treatment, EEM spectra of effluent solution samples collected as a function of PV were subtracted from the unreacted G-DOM EEM (Fig. 2) to provide spectroscopic data on fluorophores removed from (and added to) solution. In this case, higher intensities (dark colors) are indicative of G-SOM fluorescent constituents (preferentially adsorbed and hence resulting in net loss of fluorescence in effluent relative to influent solution) (Fig. 3). In contrast, light colors (pale beige and white) are indicative of DOM desorbed or mobilized from the organo-mineral interface (i.e., net accumulation of fluorescence in effluent relative to influent solution) (Fig. 3). For Qtz, all EEM difference spectra showed little or no fluorescence emission in the fulvic and humic acid-like regions, indicating little or no adsorption to the quartz surface of compounds fluorescent in these regions. For both Al-Qtz and Fe-Qtz, PV 1-5 and 10 showed evidence of high depletions of fluorescence emission in regions III and V, suggesting preferential adsorption of fulvic and humic acid-like materials onto the Al or Fe oxide-coated quartz sand surfaces. By PV 20, the difference between influent and effluent EEMs was still present for these two treatments, but significantly diminished. Importantly, by 60 PV, desorption is observed, consistent with the DOC results showing effluent solutions exceeding influent concentrations (Fig. 1B). This result indicates that with progressive occupation of reactive interfacial sites, remobilization of kinetically-labile G-SOM occurs, particularly in region V of the EEM (Fig. 3 F and D), resulting in effluent concentrations in excess of influent (Fig. 1B). This is an interesting result, because region V [“humic acid-like” according to (Chen et al.,

2003)] is also the region of the EEM exhibiting the greatest preferential adsorption for early reaction times in the (oxy)hydroxide systems (Fig. 3 D and G).

3.2 DOM exchange during reactive transport through OM-mineral media (Phase 2)

At initiation of Phase 2, as a result of the earlier infusion of G-DOM, the Al-Qtz and Fe-Qtz columns contained 244 ± 3 and 190 ± 13 mg kg⁻¹ (C basis) of G-SOM (calculated at 30 PV assuming pseudo-steady state conditions). Columns were reinstalled at the pump and infused with F-DOM solution from the mixed conifer forest floor extractions. Relative to input F-DOM solution (shown in blue confidence bands), all treatments exhibited slightly lower than initial effluent pH values during the 1-2 pore volumes, but rapidly converged to within 0.2 pH units of influent values thereafter (Fig. 4A). In stark contrast to Phase 1, all Phase 2 treatments released DOC at concentrations in excess of influent concentrations throughout nearly all of the experiment (Fig. 4B). Values of DOC concentration were particularly elevated during the first 5 PVs and PV 20, indicating significant mobilization of G-SOM from the organo-mineral interface (Fig. 4B). An inverse relation was observed between pH and DOC concentration, even in the case of PV 20, which shows a pulsed DOC release (Fig. 4 A and B). It is noteworthy that this inverse correlation between pH and DOC mobilization is opposite of that observed in batch experiments comprising specimen (oxy)hydroxides and DOM, wherein surface protonation and increased positive surface charge (which favors increased DOM adsorption) increases with decreasing pH, resulting in increased surface retention of DOM (e.g., Gu et al., 1994; Gu et al., 1995; Meier et al., 1999; Chorover and Amistadi, 2001).

In contrast to Phase 1, molar absorptivity (ϵ) values of Phase 2 effluent DOM solutions were close (within 13%) of those of influent concentrations throughout all of the reaction, despite some clear and consistent trends in the data (Fig. 4C). However, it is important to note that the ϵ value for unreacted F-DOM ($478 \text{ L mol}^{-1} \text{ cm}^{-1}$) was much lower than that for G-DOM ($710 \text{ L mol}^{-1} \text{ cm}^{-1}$) consistent with G-DOM being more aromatic (Sanderman et al., 2008). Both Al-Qtz and Fe-Qtz treatments show lower than influent ϵ values for the first few pore volumes followed by an approach to near-influent values, consistent with mobilization of DOC being dominated by low aromaticity compounds. Conversely, early pore volumes from the Qtz system show the initial release of the high ϵ DOM followed by a progressive decrease toward influent ϵ values, i.e., an initial trend with PV that is opposite of the (oxy)hydroxide-coated surfaces. Furthermore, the pulsed DOC release at *ca.* PV 20 that occurs in all columns (Fig. 4B) was evidently comprised of relatively low molar absorptivity (ϵ) DOM in all cases (Fig. 4C). In addition to having a lower ϵ value than influent G-DOM, the influent F-DOM solution also had a lower HIX value (8.5 relative to 17.6 for G-DOM). Hence, effluent solutions showed consistently high HIX values relative to influent F-DOM during the entire experiment (Fig. 4D) consistent with displacement of higher HIX G-SOM that was preferentially removed from solution during Phase 1 (Fig. 1D).

All treatments showed that the large net G-SOM release occurring throughout the duration of the Phase 2 was the result of preferential release of fluorophores associated with regions V and III of the EEMs (Fig. 5), i.e., preferential desorption of G-SOM constituents characterized by humic acid-like and fulvic acid-like fluorescence,

respectively (Chen et al., 2003). According to the differential EEMs (“fingerprint”), which in this case are the *net effect* of release of desorbed G-SOM (and hence negative values depicted in the Fig. 5 EEMs) and uptake to the interface of F-DOM (which should diminish the magnitude of negative values resulting from G-SOM release). The greatest mobilization of G-SOM compounds was observed during the first pore volume for all treatments.

4 DISCUSSION

The current study modeled experimentally the infiltration and breakthrough of an initial G-DOM solution - characterized by high HIX and ϵ values - into pristine porous mineral media (Phase 1) followed by drying and then re-infiltration of a second F-DOM solution characterized by lower HIX and ϵ values. This design, applied across three mineralogical treatments (Qtz, Al-Qtz, and Fe-Qtz) permitted the testing of hypotheses related to the impacts of (oxy)hydroxide coatings on retardation of DOM during reactive transport, the impacts of progressive SOM coating on such retardation effects, and the effects of sorbate-coated surfaces on subsequent DOM breakthrough patterns and competitive exchange reactions. The infusion of two distinct DOM sources separated in time by a drying event models the field scenario of two hydrologic events that introduce distinct DOM sources into the soil column (e.g., via vertical and horizontal flow paths in a heterogeneously vegetated hillslope). Specifically, we postulated that Al and Fe (oxy)hydroxide coatings would exert a strong impact on DOM fractionation patterns during reactive transport (Gu et al., 1995; Kaiser and Zech, 1998a; Korshin et al., 1997;

Chorover and Amistadi, 2001; Heckman et al., 2011). Further, we hypothesized that formation of sorbate OM (SOM) coated surfaces would dramatically alter such fractionation patterns in subsequent DOM infusion events that would be characterized by competitive DOM molecular exchange reactions, revealing a kinetically-labile pool of SOM, similar to that described by Kleber et al. (2007). The experimental data support both hypotheses.

4.1 Effects of (oxy)hydroxide coatings on DOM transport through quartz sand

Surficial (oxy)hydroxide coatings play a major role in regulating the sorption-desorption reactions of DOM, particularly in sandy soils and aquifer sediments that are dominated, on a mass basis, by otherwise relatively non-DOM-reactive silicate surfaces, such as depicted in the Qtz treatment of the current study. Prior work has shown that oxide coatings strongly alter reaction affinity and molecular mechanisms of sorption of both organic and inorganic solutes (e.g., Benjamin et al., 1996; McMeen and Benjamin, 1997; Korshin et al., 1997; Axe and Trivedi, 2002; Dong et al., 2002; Gupta et al., 2005; Joo et al., 2008; Bekaroglu et al., 2010). In the present study, Al and Fe (oxy)hydroxide coatings significantly retarded DOM transport. From the breakthrough curve data (Fig. 1B), we calculate DOC sorption of 244 ± 3 and 190 ± 13 mg kg⁻¹ on the Al-Qtz and Fe-Qtz media, respectively, at pseudo-steady state (30 PV) of Phase 1. The SSA normalized DOC sorption values for Al-Qtz and Fe-Qtz media are 0.19 ± 0.002 and 0.15 ± 0.01 mg C m⁻², respectively. Gu et al. (1994) reported natural organic matter (NOM) adsorption maxima of 0.18 mg C m⁻² for iron oxide (hematite, α -Fe₂O₃) at pH 6.5. Also, Joo et al. (2008) reported DOC sorption values around 0.1 mg C m⁻² for Fe and Al coated sands

with DOM equilibrium concentration of 30 mg C L^{-1} at pH 4. Our results indicate that DOM exhibited a slightly higher affinity for Al-Qtz than for Fe-Qtz treatments. Similarly, Banaitis et al. (2006) reported a higher affinity of DOM for gibbsite (average sorption of $1,900 \pm 0.47 \text{ mg C kg}^{-1}$) than for goethite (average sorption of $720 \pm 0.32 \text{ mg C kg}^{-1}$).

Surface conditioning by both (oxy)hydroxide and sorbent organic matter (SOM) coatings were shown in this study to play a major role in subsequent surface reactivity toward DOM and the nature of ensuing fractionation reactions. Specifically, we found that while aromatic and high HIX moieties (predominantly attributable to lignin phenols) are preferentially adsorbed to pristine (oxy)hydroxide coated surfaces (Phase 1), introduction of a F-DOM solution of much lower aromaticity and HIX can however promote desorption and mobilization of high-affinity adsorptive G-DOM species (Phase 2). These findings are in agreement with those of Kaiser and Zech (1998a), who examined the sorption of a forest floor DOM and its hydrophilic and hydrophobic fractions to a B_s horizon before and after modifying the surface with DOM and (oxy)hydroxide (amorphous $\text{Al}(\text{OH})_3$, ferrihydrite, and goethite) coatings. They found that additions of DOM reduced the sorption of freshly added DOM. Similarly, Weigand and Totsche (1998) also reported high DOM mobilization after the re-application of DOM solution, attributing the effect to blockage of reactive sorption sites. The blockage of reactive sorption sites in the (oxy)hydroxide coatings used in this study can be tested by comparing specific surface area (SSA) in the unreacted (pristine mineral) vs. reacted minerals (at the end of phase 2). Initially (prior initial irrigation with G-DOM), Al-Qtz and Fe-Qtz exhibited a SSA of 1.28 ± 0.01 and $1.31 \pm 0.01 \text{ m}^2 \text{ g}^{-1}$, respectively. At the end

of phase 2 (after irrigation with F-DOM), the SSA of Al-Qtz was $0.78 \pm 0.03 \text{ m}^2 \text{ g}^{-1}$ and Fe-Qtz was $1.04 \pm 0.07 \text{ m}^2 \text{ g}^{-1}$, indicating less availability of reactive sorption sites in both minerals. A steady release of hydrophilic DOC has been reported when subsoil horizons are irrigated with DOC solutions, suggesting sorptive competition between DOC fractions (Kaiser and Zech, 1998b), similar to what was observed in the present study.

Insights into the implications of the current work for DOM bioavailability are afforded by spectroscopy that shows the time-evolution of their DOM molecular properties and, by inference, their inherent bioavailability. Compounds with high ϵ , high humification index (HIX), high molar mass and, low carbohydrate content tend to exhibit lower bioavailability (Kalbitz et al., 2003; Hunt and Ohno, 2007). Hence, the fractionation patterns observed in Phase 1 of the current work (pristine mineral surfaces) favor the removal from solution of compounds of (accordingly) greater inherent recalcitrance (from a biodegradation kinetics standpoint), leaving the more biologically labile pool as mobile to potential receiving ground water or surface water environments. Indeed, since such sorption reactions likely reduce the accessibility of otherwise available substrate to microbial and enzymatic degradation (Mikutta et al., 2007; Mikutta et al., 2011), these partially humified lignin residues would be retained at mineral surfaces with potentially long turnover times and low bioaccessibility.

4.2 Fluorophore-specific retardation and re-mobilization

Despite the observation in Phase 1 of G-DOM fractionation that favored sorption of high HIX and high ϵ components (Figures 1C and 1D), we observed in Phase 2 significant displacement and remobilization of these same constituents from G-SOM

(Figures 4C and 4D). That is, during re-irrigation (Phase 2), early porewater effluents showed high DOC concentrations indicating not only low sorption of F-DOM onto the mineral surface, but also solution phase re-mobilization of G-SOM (sorbate). The mechanisms underlying G-SOM desorption likely include an as yet unresolved combination of molecular interactions that include (1) exchange of *kinetically-labile* G-SOM by influent F-DOM constituents at a finite set of sorption sites on the G-SOM conditioned surfaces; (2) cation exchange reactions in ligand-bridging sites within G-SOM aggregates that interrupt the supramolecular (Kleber et al., 2007) or hemi-micellar (Wershaw, 1993) structures of G-DOM adsorbate; (3) promotion of G-SOM desorption via aqueous phase complexation with F-DOM derived hydrophilic organic ligands and/or cations (Sutton and Sposito, 2005); and reaction limited kinetics of molecular displacement from micro- and nano-porous domains, particularly prevalent in the hydrous oxide coated surfaces (Chorover and Brusseau, 2007; Kaiser et al., 2007). All of these cases derive from aqueous (bio)geochemical perturbations in the solution phase that subsequently affect the solid-solution exchange of interfacial species.

To examine the classes of fluorophores undergoing preferential retention and exchange, fluorescence regional integration (FRI) was calculated for all treatments (Chen et al., 2003). This quantitative technique was developed to integrate the volume within selected regions beneath an EEM. The volume (Φ_i) beneath region “i” of the EEM is calculated as follows:

$$(\Phi_i) = \sum_{\text{ex}} \sum_{\text{em}} I(\lambda_{\text{ex}}\lambda_{\text{em}}) \Delta_{\text{ex}}\Delta_{\text{em}} \quad (2)$$

where Δ_{ex} and Δ_{em} are the excitation and emission wavelength intervals (both 5 nm), respectively, and $I(\lambda_{\text{ex}}\lambda_{\text{em}})$ is the fluorescence intensity at each excitation-emission wavelength pair. The volume (Φ_1) beneath each region “i” was normalized to the volume of the same region in the unreacted DOM EEM spectrum (Φ_0). Values similar to unity indicate that fluorescence intensity of the effluent solution is similar to that of influent, implying no preferential adsorption of compounds fluorescing in that region at the mineral surface. Values < 1 indicate preferential adsorption and values > 1 indicate preferential desorption/mobilization.

During Phase 1 (Fig. 6, left side), adsorption to the Qtz surface results in only modest fractionation with apparent preference for sorption of aromatic protein-like fluorophores (regions I and II, Fig. 6A). Conversely, significant separation of fluorophore classes is observed for both the Al-Qtz and Fe-Qtz cases (Fig. 6 B and C). For the Al-Qtz treatment, FRI ratios indicate that fulvic acid-like, soluble microbial by-product-like, and humic acid-like compounds were preferentially adsorbed to the pristine mineral surface, particularly during early pore volumes, with preferential adsorption following a trend of $V > IV > III > II > I$ (Fig. 6B). Similarly, during the early pore volumes of Fe-Qtz treatment in Phase 1, FRI ratios suggested that compounds in regions II, III, IV, and V were preferentially adsorbed onto the Fe-hydroxide-coated quartz sand surface. The adsorption trend was as follows: $V > IV \geq III > II > I$ (Fig. 6C). The strong correlation between HIX and ϵ parameters in both sorbate (high values) and effluent (low values) is apparent from the left side of Figure 7 (Phase 1).

During Phase 2, FRI ratios were consistently close to or higher than unity (Fig. 6, right side). For those constituents exhibiting the greatest preferential adsorption in Phase 1 (regions III-V), the first pore volume exhibited the highest FRI ratios, particularly in systems comprising (oxy)hydroxide coatings. In these treatments, region V exhibited the highest ratios, indicating desorption and mobilization of humic acid-like compounds from the organo-mineral interface. The remobilization of high HIX and high ϵ G-SOM constituents is apparently the result of a continuous displacement and mixing of influent and sorbate OM constituents that produce a much narrower range of HIX and ϵ values over the course of Phase 2 (Fig. 7, right side) relative to Phase 1.

5 CONCLUSION

Flow-through column experiments were conducted to investigate the role of surficial (oxy)hydroxide coatings in DOM fractionation and stabilization during reactive transport. The experiments reveal that pristine Al and Fe (oxy)hydroxide coatings on quartz surfaces preferentially sequester aromatic and “humified” constituents into sorbate form, thereby significantly retarding the transport and, presumably, the bioavailability of these partially degraded lignin phenols. Meanwhile, less aromatic and “humified” constituents are transported with little retardation. However, progressive conditioning of the (oxy)hydroxide surfaces with sorbate organic matter results in distinctly different transport and retardation behavior in subsequent DOM infiltration events. Specifically, infusion of fresh DOM into SOM-(oxy)hydroxide-coated quartz sand results in displacement of the high affinity (aromatic and humified) sorbate forms, indicating that

SOM constituents occur in kinetically-labile and exchangeable forms that can be re-mobilized by perturbation of pore water chemistry.

Acknowledgements

This work was supported by National Science Foundation grants EAR-0724958 and DEB-0543130.

References

- Axe L. and Trivedi P. 2002. Intraparticle surface diffusion of metal contaminants and their attenuation in microporous amorphous Al, Fe, and Mn oxides. *J. Colloid Interface Sci.* 247:259-265.
- Baker A., Tipping E., Thacker S.A. and Gondar D. 2008. Relating dissolved organic matter fluorescence and functional properties. *Chemosphere* 73:1765-1772.
- Banaitis M.R., Waldrip-Dail H., Diehl M.S., Holmes B.C., Hunt J.F., Lynch R.P. and Ohno T. 2006. Investigating sorption-driven dissolved organic matter fractionation by multidimensional fluorescence spectroscopy and PARAFAC. *J. Colloid Interface Sci.* 304:271-276.
- Bekaroglu S.S.K., Yigit N.O., Karanfil T. and Kitis M. 2010. The adsorptive removal of disinfection by-product precursors in a high-SUVA water using iron oxide-coated pumice and volcanic slag particles. *J. Hazard. Mater.* 183:389-394.
- Benjamin M., Sletten R., Bailey R. and Bennett T. 1996. Sorption and filtration of metals using iron-oxide-coated sand. *Water Res.* 30:2609-2620.
- Bolster C., Mills A., Hornberger G. and Herman J. 2001. Effect of surface coatings, grain size, and ionic strength on the maximum attainable coverage of bacteria on sand surfaces. *J. Contam. Hydrol.* 50:287-305.
- Chen W., Westerhoff P., Leenheer J.A. and Booksh K. 2003. Fluorescence excitation - emission matrix regional integration to quantify spectra for dissolved organic matter. *Environ. Sci. Technol.* 37:5701-5710.

- Chi F.H. and Amy G.L. 2004. Kinetic study on the sorption of dissolved natural organic matter onto different aquifer materials: the effects of hydrophobicity and functional groups. *J. Colloid Interface Sci.* 274:380-391.
- Chin Y., Aiken G. and Oloughlin E. 1994. Molecular-weight, polydispersity, and spectroscopic properties of aquatic humic substances. *Environ. Sci. Technol.* 28:1853-1858.
- Chorover J. and Amistadi M.K. 2001. Reaction of forest floor organic matter at goethite, birnessite and smectite surfaces. *Geochim. Cosmochim. Acta* 65:95-109.
- Chorover, J. and M. L. Brusseau. 2008. Kinetics of sorption-desorption, Book chapter, pp. 109-149 in "Kinetics of Water-Rock Interaction" (S. L. Brantley, J. D. Kubicki and A. F. White, eds.), Springer, NY.
- Coston J., Fuller C. and Dacis J. 1995. Pb^{2+} and Zn^{2+} adsorption by a natural aluminum-bearing and iron-bearing surface coating on an aquifer sand. *Geochim. Cosmochim. Acta* 59:3535-3547.
- Dong H., Onstott T., Ko C., Hollingsworth A., Brown D. and Mailloux B. 2002. Theoretical prediction of collision efficiency between adhesion-deficient bacteria and sediment grain surface. *Colloid Surf. B-Biointerfaces* 24:229-245.
- Eusterhues K., Rumpel C. and Kogel-Knabner I. 2005. Organo-mineral associations in sandy acid forest soils: Importance of specific surface area, iron oxides and micropores. *Eur. J. Soil Sci.* 56:753-763.
- Eusterhues K., Rumpel C., Kleber M. and Kogel-Knabner I. 2003. Stabilisation of soil organic matter by interactions with minerals as revealed by mineral dissolution and oxidative degradation. *Org. Geochem.* 34:1591-1600.
- Goh K. 2004. Carbon sequestration and stabilization in soils: implications for soil productivity and climate change. *Soil Sci. Plant Nutr.* 50:467-476.
- Gu B., Schmitt J., Chen Z., Liang L. and McCarthy J. 1995. Adsorption and desorption of different organic-matter fractions on iron-oxide. *Geochim. Cosmochim. Acta* 59:219-229.
- Gu B., Schmitt J., Chen Z., Liang L. and McCarthy J. 1994. Adsorption and desorption of natural organic-matter on iron-oxide - mechanisms and models. *Environ. Sci. Technol.* 28:38-46.
- Guo M.X. and Chorover J. 2006. Leachate migration from spent mushroom substrate through intact and repacked subsurface soil columns. *Waste Manage.* 26:133-140.

- Guo M.X. and Chorover J. 2003. Transport and fractionation of dissolved organic matter in soil columns. *Soil Sci.* 168:108-118.
- Gupta V., Saini V. and Jain N. 2005. Adsorption of As(III) from aqueous solutions by iron oxide-coated sand. *J. Colloid Interface Sci.* 288:55-60.
- Harpold, A.A., Brooks P.D., Perdrial J., McIntosh J., Meixner T., Lohse K.A., Zapata-Rios X., Vazquez-Ortega A., and Chorover J. (In press) Quantifying variation in solute sources and nutrient cycling in montane headwater catchments. *Water Resources Research*.
- Heckman K., Vazquez-Ortega A., Gao X., Chorover J. and Rasmussen C. 2011. Changes in water extractable organic matter during incubation of forest floor material in the presence of quartz, goethite and gibbsite surfaces. *Geochim. Cosmochim. Acta* 75:4295-4309.
- Hernandez-Ruiz S., Abrell L., Wickramasekara S., Chefetz B. and Chorover J. 2012. Quantifying PPCP interaction with dissolved organic matter in aqueous solution: Combined use of fluorescence quenching and tandem mass spectrometry. *Water Res.* 46:943-954.
- Hudson N., Baker A. and Reynolds D. 2007. Fluorescence analysis of dissolved organic matter in natural, waste and polluted waters - A review. *River Res. Appl.* 23:631-649.
- Hunt J.F. and Ohno T. 2007. Characterization of fresh and decomposed dissolved organic matter using excitation-emission matrix fluorescence spectroscopy and multiway analysis. *J. Agric. Food Chem.* 55:2121-2128.
- Hunt J.F., Ohno T., He Z., Honeycutt C.W. and Dail D.B. 2007. Influence of decomposition on chemical properties of plant- and manure-derived dissolved organic matter and sorption to goethite. *J. Environ. Qual.* 36:135-143.
- Joo J.C., Shackelford C.D. and Reardon K.F. 2008. Association of humic acid with metal (hydr)oxide-coated sands at solid-water interfaces. *J. Colloid Interface Sci.* 317:424-433.
- Kaiser K. and Guggenberger G. 2000. The role of DOM sorption to mineral surfaces in the preservation of organic matter in soils. *Org. Geochem.* 31:711-725.
- Kaiser K. and Zech W. 1998a. Soil dissolved organic matter sorption as influenced by organic and sesquioxide coatings and sorbed sulfate. *Soil Sci. Soc. Am. J.* 62:129-136.

- Kaiser K. and Zech W. 1998b. Rates of dissolved organic matter release and sorption in forest soils. *Soil Sci.* 163:714-725.
- Kaiser K., Mikutta R. and Guggenberger G. 2007. Increased stability of organic matter sorbed to ferrihydrite and goethite on aging. *Soil Sci. Soc. Am. J.* 71:711-719.
- Kaiser K., Guggenberger G., Haumaier L. and Zech W. 1997. Dissolved organic matter sorption on subsoils and minerals studied by C-13-NMR and DRIFT spectroscopy. *Eur. J. Soil Sci.* 48:301-310.
- Kalbitz K., Schmerwitz J., Schwesig D. and Matzner E. 2003. Biodegradation of soil-derived dissolved organic matter as related to its properties. *Geoderma* 113:273-291.
- Kleber M., Sollins P. and Sutton R. 2007. A conceptual model of organo-mineral interactions in soils: Self-assembly of organic molecular fragments into zonal structures on mineral surfaces. *Biogeochemistry* 85:9-24.
- Korshin G., Benjamin M. and Sletten R. 1997. Adsorption of natural organic matter (NOM) on iron oxide: Effects on NOM composition and formation of organo-halide compounds during chlorination. *Water Res.* 31:1643-1650.
- Lam B. and Simpson A.J. 2008. Direct H-1 NMR spectroscopy of dissolved organic matter in natural waters. *Analyst* 133:263-269.
- Lattao C., Birdwell J., Wang J.J. and Cook R.L. 2008. Studying organic matter molecular assemblage within a whole organic soil by nuclear magnetic resonance. *J. Environ. Qual.* 37:1501-1509.
- McMeen C. and Benjamin M. 1997. NOM removal by slow sand filtration through iron oxide-coated olivine. *J. Am. Water Work Assoc.* 89:57-71.
- Meier M., Namjesnik-Dejanovic K., Maurice P., Chin Y. and Aiken G. 1999. Fractionation of aquatic natural organic matter upon sorption to goethite and kaolinite. *Chem. Geol.* 157:275-284.
- Mikutta R., Zang U., Chorover J., Haumaier L. and Kalbitz K. 2011. Stabilization of extracellular polymeric substances (*Bacillus subtilis*) by adsorption to and coprecipitation with Al forms. *Geochim. Cosmochim. Acta* 75:3135-3154.
- Mikutta R., Mikutta C., Kalbitz K., Scheel T., Kaiser K. and Jahn R. 2007. Biodegradation of forest floor organic matter bound to minerals via different binding mechanisms. *Geochim. Cosmochim. Acta* 71:2569-2590.

- Namjesnik-Dejanovic K., Maurice P., Aiken G., Cabaniss S., Chin Y. and Pullin M. 2000. Adsorption and fractionation of a muck fulvic acid on kaolinite and goethite at pH 3.7, 6, and 8. *Soil Sci.* 165:545-559.
- Ohno T., Chorover J., Omoike A. and Hunt J. 2007. Molecular weight and humification index as predictors of adsorption for plant- and manure-derived dissolved organic matter to goethite. *Eur. J. Soil Sci.* 58:125-132.
- Ohno T., Amirbahman A. and Bro R. 2008. Parallel factor analysis of excitation-emission matrix fluorescence spectra of water soluble soil organic matter as basis for the determination of conditional metal binding parameters. *Environ. Sci. Technol.* 42:186-192.
- Park S. and Kim S. 2010. Influence of (bi)carbonate on bacterial interaction with quartz and metal oxide-coated surfaces. *Colloids and Surfaces B-Biointerfaces* 76:57-62.
- Perdrial J., McIntosh J., Harpold A., Brooks P., Zapata-Rios X., Ray J., Troch P., Chorover J. (In review) Impact of winter climate change on stream water carbon characteristics in forested headwater streams.
- Sanderman J., Baldock J.A. and Amundson R. 2008. Dissolved organic carbon chemistry and dynamics in contrasting forest and grassland soils. *Biogeochemistry* 89:181-198.
- Scheel T., Dorfler C. and Kalbitz K. 2007. Precipitation of dissolved organic matter by aluminum stabilizes carbon in acidic forest soils. *Soil Sci. Soc. Am. J.* 71:64-74.
- Simpson A.J., Simpson M.J. and Soong R. 2012. Nuclear magnetic resonance spectroscopy and its key role in environmental research. *Environ. Sci. Technol.* 46:11488-11496.
- Six J., Conant R., Paul E. and Paustian K. 2002. Stabilization mechanisms of soil organic matter: Implications for C-saturation of soils. *Plant Soil* 241:155-176.
- Sutton R. and Sposito G. 2005. Molecular structure in soil humic substances: the new view. *Environ. Sci. Technol.* 39:9009-9015.
- Vázquez-Ortega A., Perdrial J.N., Harpold A., Zapata-Rios X., Amistadi M.K., Rasmussen C., McIntosh J., Schaap M., Chorover J. In prep. Rare earth elements as reactive tracers of biogeochemical weathering in forested rhyolitic terrain.
- von Luetzow M., Koegel-Knabner I., Ekschmitt K., Matzner E., Guggenberger G., Marschner B. and Flessa H. 2006. Stabilization of organic matter in temperate soils: mechanisms and their relevance under different soil conditions - a review. *Eur. J. Soil Sci.* 57:426-445.

- von Lutzow M., Kogel-Knabner I., Ludwig B., Matzner E., Flessa H., Ekschmitt K., Guggenberger G., Marschner B. and Kalbitz K. 2008. Stabilization mechanisms of organic matter in four temperate soils: development and application of a conceptual model. *J. Plant Nutr. Soil Sci. -Z. Pflanzenernahr. Bodenkd.* 171:111-124.
- Weigand H. and Totsche K.U. 1998. Flow and reactivity effects on dissolved organic matter transport in soil columns. *Soil Sci. Soc. Am. J.* 62:1268-1274.
- Wershaw R. 1993. Model for humus in soils and sediments. *Environ. Sci. Technol.* 27:814-816.
- Zhou Q., Maurice P. and Cabaniss S. 2001. Size fractionation upon adsorption of fulvic acid on goethite: equilibrium and kinetic studies. *Geochim. Cosmochim. Acta* 65:803-812.
- Zsolnay A., Baigar E., Jimenez M., Steinweg B. and Saccomandi F. 1999. Differentiating with fluorescence spectroscopy the sources of dissolved organic matter in soils subjected to drying. *Chemosphere* 38:45-50.

LIST OF TABLES:

Table 1 Chemical properties for the unreacted grassland DOM (G-DOM) and forest DOM (F-DOM) obtained from O horizons collected for the Zero Order Basin (ZOB). The chemical parameters were determined after dilution prior to use in the reactive transport.

Table 2 Specific surface area (SSA) for the unreacted oxides and adsorbed DOC on Al-Qtz and Fe-Qtz oxides after reactive transport. Adsorbed DOC is reported in mass (mg C kg^{-1}) and surface area (mg C m^{-2}) basis.

LIST OF FIGURES:

Figure 1 pH, DOC, molar absorptivity, and humification values for all treatments during the initial irrigation of fresh mineral media with Grassland DOM (Phase 1). Solid blue bands represent 95% confidence band for pH, DOC, molar absorptivity, or HIX values of the influent solution. Shaded blue bar represents the y-error (standard deviation) of the influent solution values.

Figure 2 EEM spectra for unreacted G-DOM (A) and F-DOM (B) solutions.

Figure 3 EEM spectral “fingerprint” of grassland sorbate organic matter (G-SOM) (obtained by subtracting effluent solution from influent G-DOM solution EEM) for the Qtz, Al-Qtz, and Fe-Qtz treatments during the initial irrigation of fresh mineral media with grassland DOM (Phase 1). Each spectrum corresponds to: (A) Qtz, PV 1, (B) Qtz, PV 20, (C) Qtz, PV 60, (D) Al-Qtz, PV 1, (E) Al-Qtz, PV20, (F) Al-Qtz, PV60, (G) Fe-Qtz, PV1, (H) Fe-Qtz, PV20, and (I) Fe-Qtz, PV 60. Positive values (dark colors) are indicative of G-SOM fluorescent constituents preferentially adsorbed and negative values (pale beige and white color) are indicative of DOM desorbed or mobilized from the organo-mineral interface.

Figure 4 pH, DOC, molar absorptivity, and humification values for all treatments during the re-irrigation of OM coated mineral surfaces with Mixed Conifer DOM (Phase 2). Solid blue line represents pH, DOC, molar absorptivity, or HIX values of the influent solution. Shaded blue bar represents the y-error (standard deviation) of the influent solution values.

Figure 5 EEM spectral “fingerprint” of G-SOM released from Qtz, Al-Qtz, and Fe-Qtz treatments during the re-irrigation of mineral-G-SOM surfaces with F-DOM solution (Phase 2). Each spectrum corresponds to: (A) Qtz, PV 1, (B) Qtz, PV 20, (C) Qtz, PV 60, (D) Al-Qtz, PV 1, (E) Al-Qtz, PV20, (F) Al-Qtz, PV60, (G) Fe-Qtz, PV1, (H) Fe-Qtz, PV20, and (I) Fe-Qtz, PV 60. Positive values (dark colors) are indicative of fluorescent constituents preferentially adsorbed and negative values (pale beige and white color) are indicative of DOM desorbed or mobilized from the organo-mineral interface.

Figure 6 Fluorescence regional integration of effluent DOM during (left column) G-DOM transport through porous media comprising initially pristine mineral surfaces and (right column) F-DOM solution influent to G-SOM coated porous media surfaces: (A, D) Qtz, (B, E) Al-Qtz, and (C, F) Fe-Qtz.

Figure 7 Scatterplots of humification index from fluorescence excitation-emission spectroscopy (HIX) versus molar absorptivity from UV 280 nm absorbance for Phase 1 (left) and Phase 2 (right) of the reactive transport experiments. Note the strong positive correlation between the two variables in Phase 1, during reaction of G-DOM with

initially pristine mineral surfaces. In contrast during Phase 2, the range in values of both variables with much narrower and no significant correlation is observed.

Table 1 Chemical properties for the unreacted grassland DOM (G-DOM) and forest DOM (F-DOM) obtained from O horizons collected for the Zero Order Basin (ZOB). The chemical parameters were determined after dilution prior to use in the reactive transport.

Parameters	G-DOM	F-DOM
TOC (mg L ⁻¹)	40.8±1.2	43.2±0.2
pH	7.95±0.05	8.00±0.03
ε ₂₈₀	710±10	478±4
HIX	17.8	8.4
Si (mg L ⁻¹)	7.72	8.37
Al (mg L ⁻¹)	1.98	1.91
Fe (mg L ⁻¹)	0.80	0.84

Table 2 Specific surface area (SSA) for the unreacted oxides and adsorbed DOC on Al-Qtz and Fe-Qtz oxides after reactive transport. Adsorbed DOC is reported in mass (mg C kg⁻¹) and surface area (mg C m⁻²) basis.

	Unreacted SSA ^a	Reacted SSA ^b	Adsorbed DOC ^c	Adsorbed DOC ^d
Mineral	m ² g ⁻¹	m ² g ⁻¹	mg C kg ⁻¹	mg C m ⁻²
Al-Qtz	1.28±0.01	0.78±0.03	244±3	0.19±0.002
Fe-Qtz	1.31±0.01	1.04±0.07	190±13	0.15±0.01

^a Pristine Al and Fe (oxy)hydroxide surfaces

^b End of phase 2.

^c per kilogram of coated sand

^d per specific surface area of coated sand

FIGURES

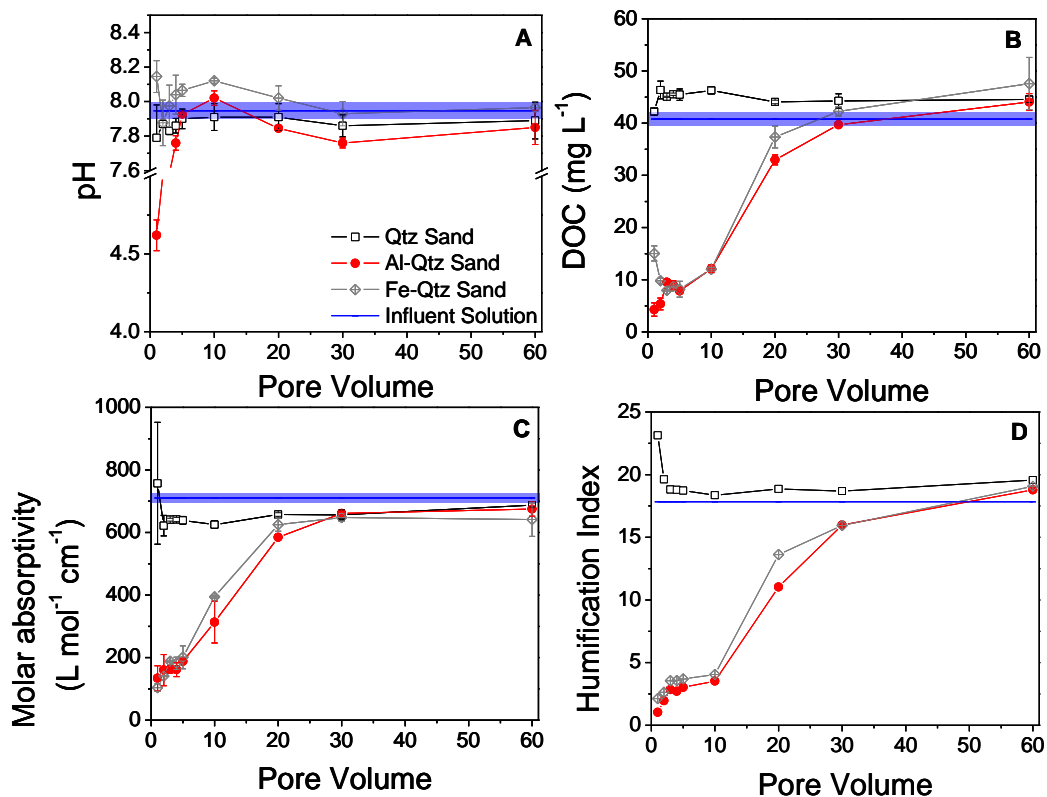


Figure 1 pH, DOC, molar absorptivity, and humification values for all treatments during the initial irrigation of fresh mineral media with Grassland DOM (Phase 1). Solid blue bands represent 95% confidence band for pH, DOC, molar absorptivity, or HIX values of the influent solution. Shaded blue bar represents the y-error (standard deviation) of the influent solution values.

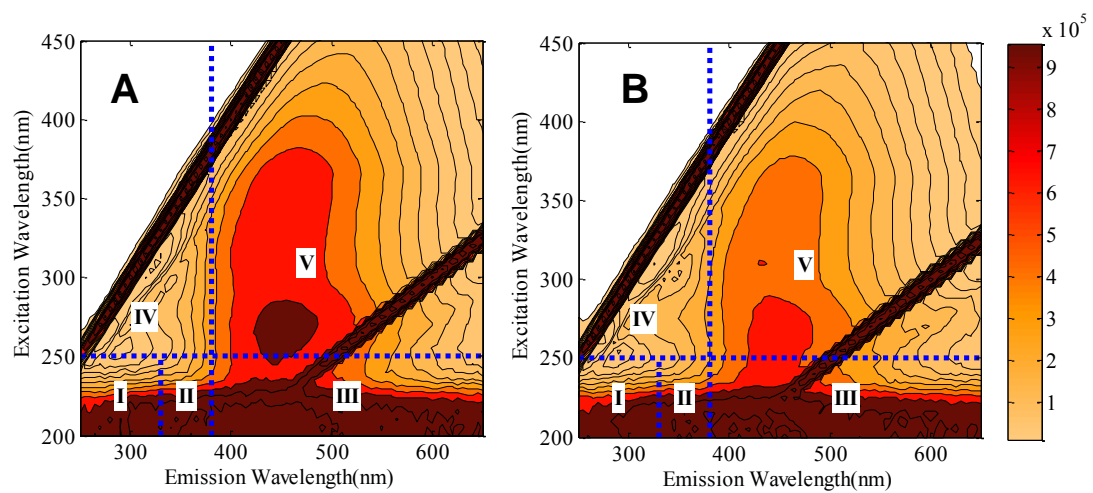


Figure 2 EEM spectra for unreacted G-DOM (A) and F-DOM (B) solutions.

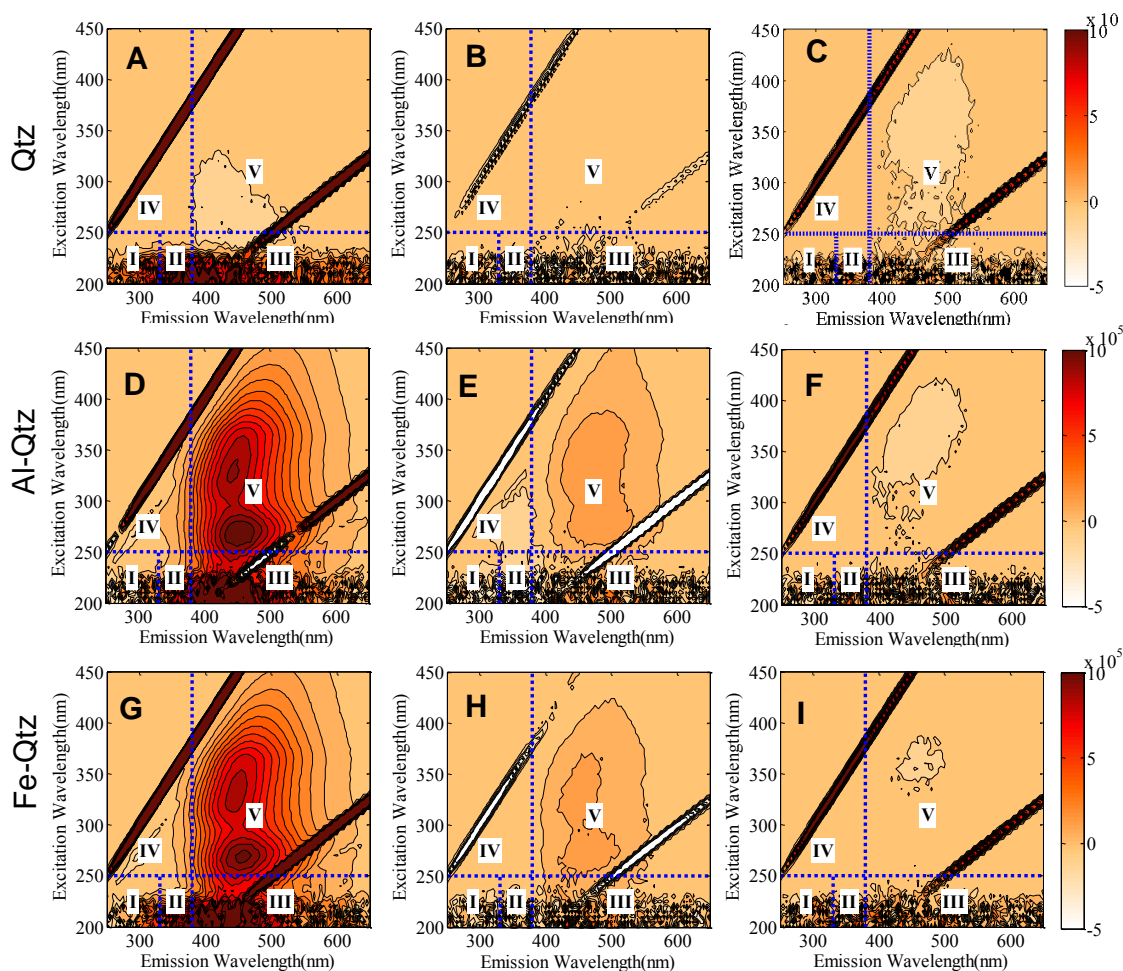


Figure 3 EEM spectral “fingerprint” of grassland sorbate organic matter (G-SOM) (obtained by subtracting effluent solution from influent G-DOM solution EEM) for the Qtz, Al-Qtz, and Fe-Qtz treatments during the initial irrigation of fresh mineral media with grassland DOM (Phase 1). Each spectrum corresponds to: (A) Qtz, PV 1, (B) Qtz, PV 20, (C) Qtz, PV 60, (D) Al-Qtz, PV 1, (E) Al-Qtz, PV20, (F) Al-Qtz, PV60, (G) Fe-Qtz, PV1, (H) Fe-Qtz, PV20, and (I) Fe-Qtz, PV 60. Positive values (dark colors) are indicative of G-SOM fluorescent constituents preferentially adsorbed and negative values (pale beige and white color) are indicative of DOM desorbed or mobilized from the organo-mineral interface.

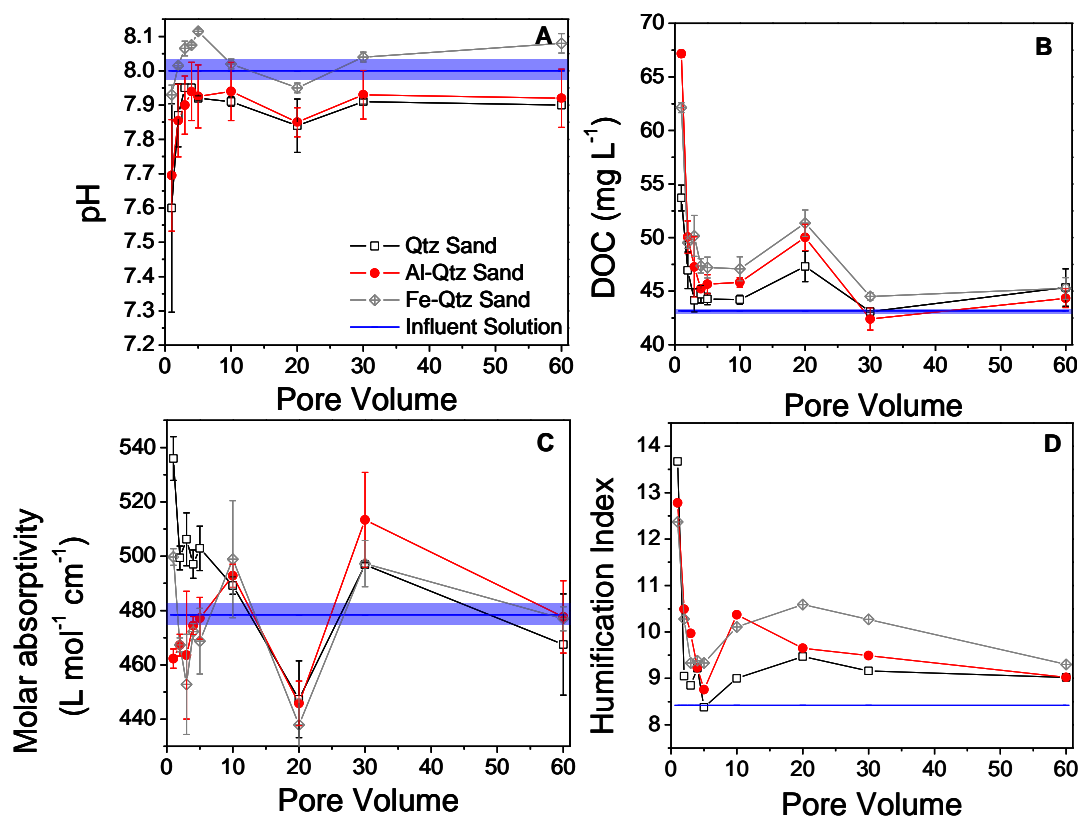


Figure 4 pH, DOC, molar absorptivity, and humification values for all treatments during the re-irrigation of OM coated mineral surfaces with Mixed Conifer DOM (Phase 2). Solid blue line represents pH, DOC, molar absorptivity, or HIX values of the influent solution. Shaded blue bar represents the y-error (standard deviation) of the influent solution values.

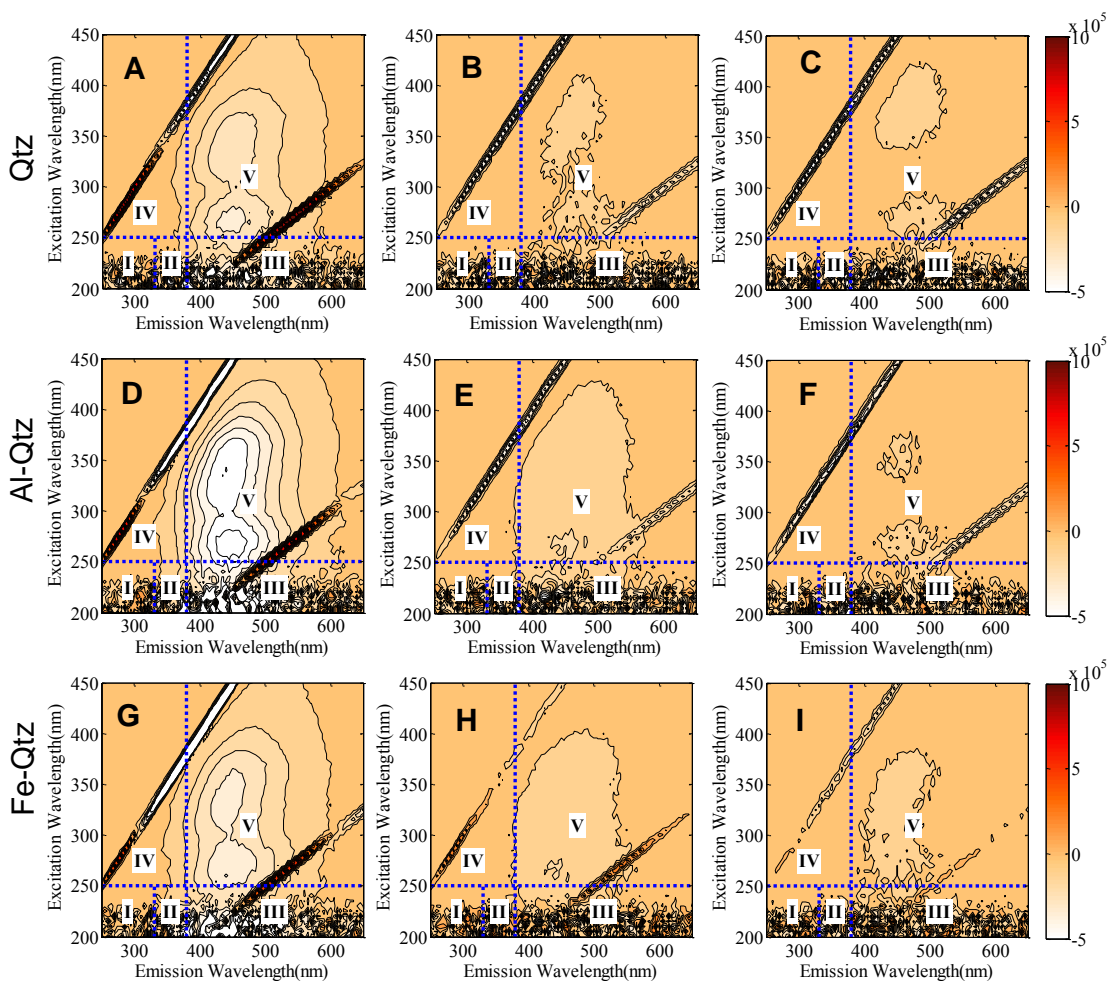


Figure 5 EEM spectral “fingerprint” of G-SOM released from Qtz, Al-Qtz, and Fe-Qtz treatments during the re-irrigation of mineral-G-SOM surfaces with F-DOM solution (Phase 2). Each spectrum corresponds to: (A) Qtz, PV 1, (B) Qtz, PV 20, (C) Qtz, PV 60, (D) Al-Qtz, PV 1, (E) Al-Qtz, PV20, (F) Al-Qtz, PV60, (G) Fe-Qtz, PV1, (H) Fe-Qtz, PV20, and (I) Fe-Qtz, PV 60. Positive values (dark colors) are indicative of fluorescent constituents preferentially adsorbed and negative values (pale beige and white color) are indicative of DOM desorbed or mobilized from the organo-mineral interface.

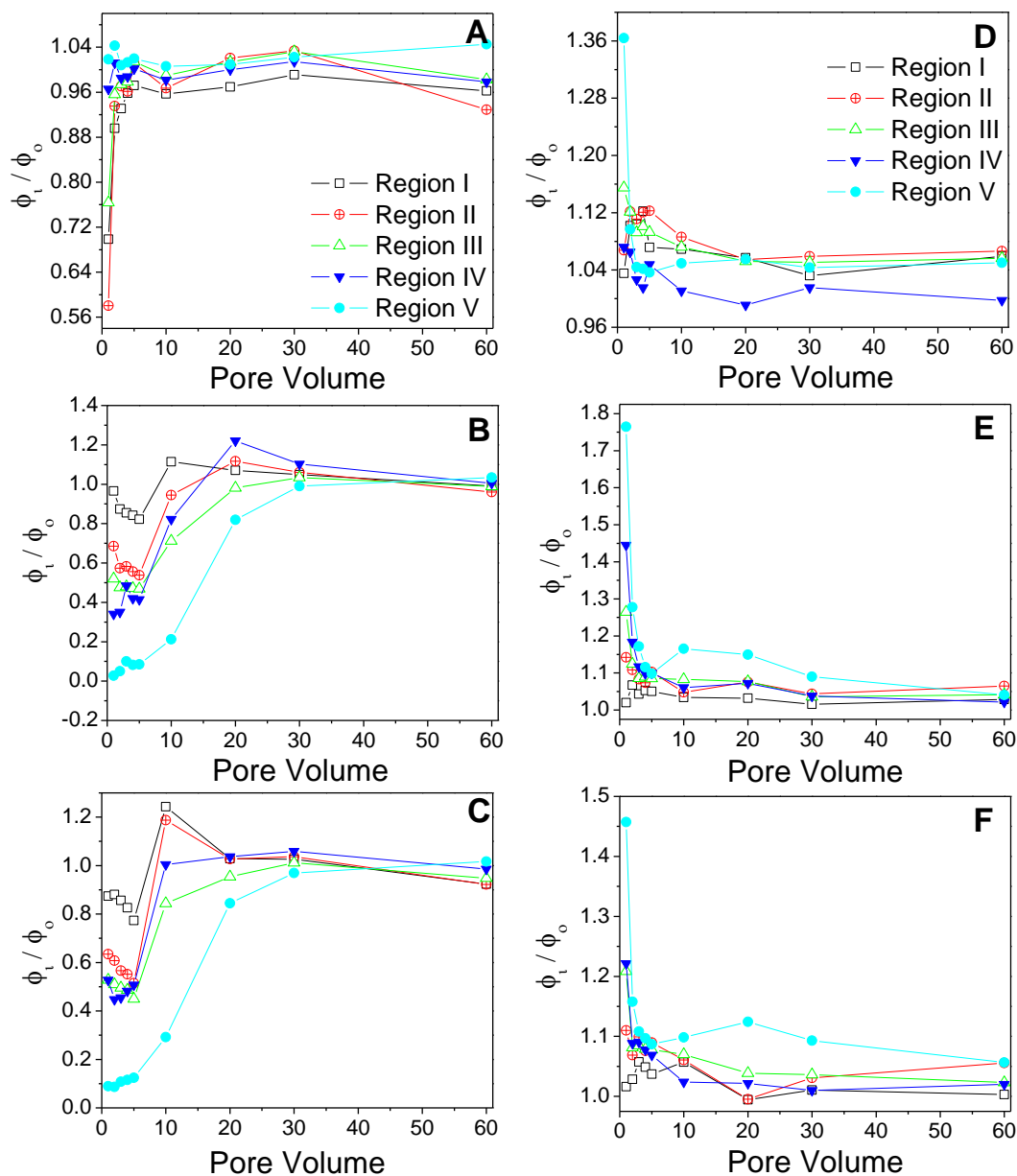


Figure 6 Fluorescence regional integration of effluent DOM during (left column) G-DOM transport through porous media comprising initially pristine mineral surfaces and (right column) F-DOM solution influent to G-SOM coated porous media surfaces: (A, D) Qtz, (B, E) Al-Qtz, and (C, F) Fe-Qtz.

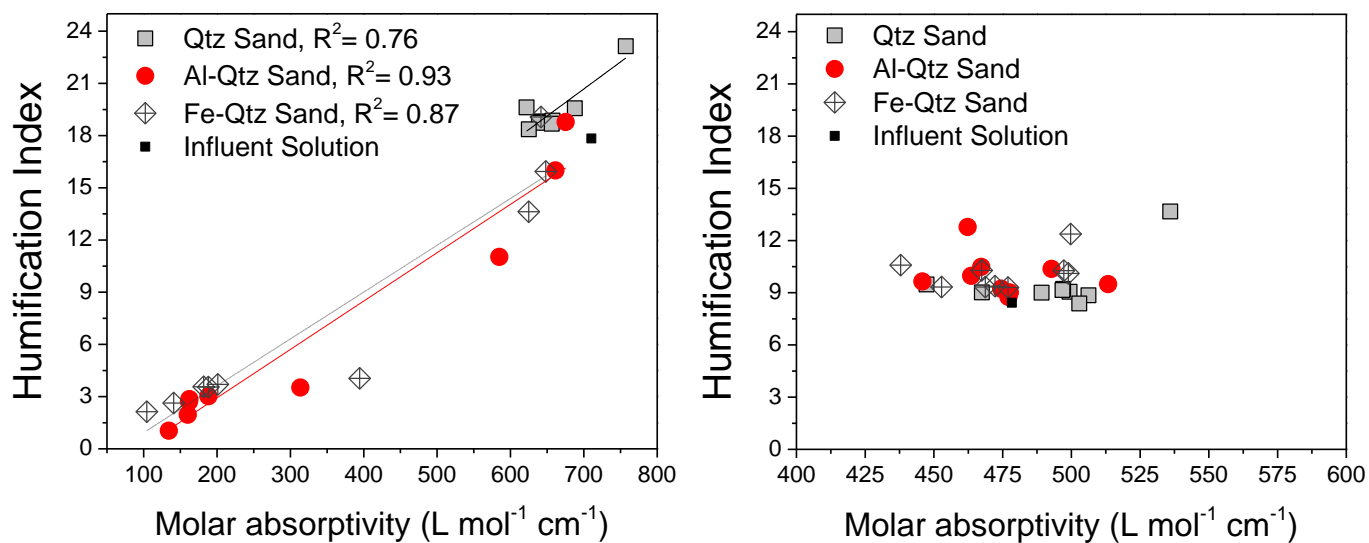


Figure 7 Scatterplots of humification index from fluorescence excitation-emission spectroscopy (HIX) versus molar absorptivity from UV 280 nm absorbance for Phase 1 (left) and Phase 2 (right) of the reactive transport experiments. Note the strong positive correlation between the two variables in Phase 1, during reaction of G-DOM with initially pristine mineral surfaces. In contrast during Phase 2, the range in values of both variables with much narrower and no significant correlation is observed.

APPENDIX B:

**RARE EARTH ELEMENTS AS REACTIVE TRACERS OF
BIOGEOCHEMICAL WEATHERING IN FORESTED RHYOLITIC TERRAIN**

Angélica Vázquez-Ortega^{a*}, Julia Perdrial^a, Adrian Harpold^{b1}, Xavier Zapata-Rios^b, Craig Rasmussen^a, Jennifer McIntosh^b, Marcel Schaap^a, Jon D. Pelletier^c, Mary Kay Amistadi^a,
Jon Chorover^a

^aDepartment of Soil, Water & Environmental Science, University of Arizona, 1177 East Fourth Street, Tucson, Arizona 85721-0038, USA

^bDepartment of Hydrology and Water Resources, University of Arizona, 1133 East James E. Rogers Way, Tucson, Arizona 85721-0011, USA

^cDepartment of Geosciences, University of Arizona, 1040 East Fourth Street, Tucson, Arizona 85721-0077, USA

¹Institute of Arctic and Alpine Research, University of Colorado, 1560 30th Street, Boulder, Colorado 80303-0450, USA

*Corresponding author: avazquez@email.arizona.edu; 520-626-8190

To be submitted to Geochimica et Cosmochimica Acta

ABSTRACT

Rare earth elements (REE) were evaluated as potential tracers of biogeochemical weathering at pedon, hillslope, and catchment scales in the Valles Caldera National Preserve (NM). We investigated time series of REE patterns in precipitation, soil pore water, ground water, and stream water, and related these data to REE composition of soil, rock and atmospheric dust. REE signatures in stream waters were dynamic, reflecting processes that occur along hydrologic flowpaths during transport to the stream, including organic complexation, primary and secondary mineral weathering, water/soil/bedrock interaction, and atmospheric deposition. Initial snowmelt reflected a stream water signature similar to that of soil solution, consistent with shallow subsurface flow. REE patterns consistent with deep groundwater contributions increased during the recession of the snowmelt hydrograph. The REE and dissolved organic carbon concentrations (DOC) in stream waters were strongly correlated during snowmelt, consistent with REE complexation and mobilization in association with organic ligands during the period of shallow subsurface flow. Most annual (bio)chemical denudation of REE occurred during the snowmelt-derived DOC pulse. Dust deposition, preferential dissolution of plagioclases, and hydrothermal alteration of parent materials (which induce a positive Eu-anomaly in the altered rock) likely contribute to positive Eu-anomalies observed in the soil matrix, soil solutions, and stream waters. In the zero order basin (ZOB) soils, cerium is preferentially accumulated in bottom horizons with respect to lanthanum and praseodymium. The Ce enrichment in bottom horizons can be attributed to Ce adsorption and co-precipitation by Fe- and Mn-oxides minerals. Negative Nd-anomalies in stream

waters are consistent with deep groundwater flow being the dominant contributor to hydrologic response in this system.

1 INTRODUCTION

Prior studies have shown the potential for lanthanide series elements (i.e., “rare earth elements” or REE) to serve as reactive tracers of surficial weathering processes (e.g., Leybourne and Johannesson, 2008; Shiller, 2010). The unique chemical properties of trivalent Lewis acid REE include a systematic increase in ionic potential (valence normalized to ionic radius) with increasing atomic number (Z). Systematic variation in metal-ligand chemical reactivity makes the REE useful for studying biological impacts on weathering in the critical zone (NRC, 2001) because of the documented variation in their tendency to form stable complexes with organic (carboxyl- and phenolic-OH) and inorganic (e.g., hydroxylated surfaces of Fe, Mn and Al oxide) ligands (Davranche et al., 2005; Pourret et al., 2007a; Pourret et al., 2007b; Pourret and Martinez, 2009; Davranche et al., 2004). Hence their mobilization from a weathering soil profile and into stream drainage waters (i.e., chemical denudation) is a strong function of localized incongruent weathering reactions and organic carbon flux (Dupre et al., 1999; Gruau et al., 2004; Pourret et al., 2010).

Since aqueous geochemical signatures of stream waters include dynamic mixing of waters deriving from distinct catchment locations (Nakajima and Terakado, 2003; Bailey et al., 2004; Voegelin et al., 2012), including biological “hot-spots” in the landscape (Harpold et al., WRR, in revision; McClain et al., 2003), occurrences of REE-enriched discharges, and their specific REE patterns may help to constraint the timing and spatial distribution of weathering in upland soils and to help resolve the temporal dynamics of catchment bio-weathering in particular (Dupre et al., 1999; Pourret et al., 2007a; Pourret

et al., 2007b; Pourret et al., 2010). To the extent that different critical zone water sources can be shown to produce distinct REE signatures and also dynamic changes therein over hydrologic events, we postulated that they may also be useful to resolving upgradient biological weathering processes in natural catchments.

REE are geochemical trace elements of atomic number 57 to 71, including La to Lu. The REEs occur principally as trivalent cations with ionic radii approximately twice that of Al^{3+} and Fe^{3+} , and with variation in geochemical properties across the series being attributed to trends in atomic mass, ionic radius, and potential variation in oxidation state (Laveuf and Cornu, 2009). REE fractionation patterns, when normalized to known standards, can provide insight into governing aqueous geochemical processes (Elderfield et al., 1990; Sholkovitz, 1992; Johannesson et al., 1997; Johannesson et al., 2004; Bau and Koschinsky, 2009; Steinmann and Stille, 2006; Stille et al., 2006; Steinmann and Stille, 2008; Stille et al., 2009; Davranche et al., 2011).

Geochemical weathering of primary minerals, such as Zr- and Ti-bearing phases (heavy minerals), phosphates, silicates and carbonates affect REE content in soil solutions and stream waters (Laveuf and Cornu, 2009; Aubert et al., 2001). Variation in chemical denudation of REE is tied to trends in their relative solubility and mobility; differential fractionation occurs upon release from primary minerals due to differences in reactivity toward aqueous complexation, adsorption and mineral precipitation reactions (Sonke and Salters, 2006; Laveuf and Cornu, 2009; Goyne et al., 2010). For example, dissolved organic matter (DOM) has been shown to be preferentially enriched in heavy (high Z) REEs (HREE: Dy to Lu) because these metals have smaller ionic radius (i.e., the

lanthanide contraction effect) (Sonke and Salters, 2006) favoring the formation of more stable complexes with acidic organic functional groups. Conversely, Davranche et al. (2011) reported middle (M)REE downward concavity patterns in soil solutions during wetland soil reduction, attributing to soil organic matter a tendency to concentrate MREE. REE form aqueous complexes with carboxylated organic ligands, such as acetate, citrate, malonate, oxalate, and succinate (Byrne and Li, 1995), and this complexation influences non-stoichiometric dissolution of primary minerals (Goynes et al., 2010) and the effective solubility and transport of REE in natural waters (Xiong, 2011). Pourret et al. (2007b) applied the Humic Ion Binding Model VI to experimental data and concluded that REE predominantly occur as organic complexes in DOM-containing aqueous solutions at circumneutral pH. Reference humic (HA) and fulvic (FA) acids have been shown to form complexes with REE (Sonke and Salters, 2006; Pourret et al., 2007b; Yamamoto et al., 2010), and several studies have suggested that carboxylic functional groups are the principal binding sites (Pourret et al., 2007b; Yamamoto et al., 2010); although phenolic moieties also play an important role (Pourret and Martinez, 2009).

Because of their cationic charge, REEs are subject to adsorption to the surfaces of secondary minerals (Bau, 1999; Bau and Koschinsky, 2009), and they can be scavenged by Fe and Al-(oxy)hydroxides via coprecipitation (Bau, 1999) and further released to pore waters during dissolution, either via reductive or non-reductive mechanisms (Pokrovsky and Schott, 2002; Davranche et al., 2011). Ohta and Kawabe (2001), using extended X-ray absorption fine structure (EXAFS) spectroscopy, reported that adsorbed

La, Pr, Nd, and Sm form inner-sphere complexes at the α -FeOOH_(s) surface. High specific surface area colloidal particles, when mobilized e.g., via pH or redox mechanisms, are known to facilitate REE transport (Viers et al., 1997; Braun et al., 1998; Thompson et al., 2006). Yttrium is also included in this study as in prior geochemical studies of the REE (e.g., Bau et al., 1999; Thompson et al., in press), because it has a charge and radius intermediate between Dy and Ho, but an electron structure and Misono softness that make it a harder Lewis acid. Hence, use of the full suite of rare earth elements and yttrium (REY) enables measurement of Y/Ho fractionation during incongruent geochemical weathering, which is particularly useful in bio-active soil environments. For example, Bau (1999) observed that Ho (relative to Y) fractionated preferentially to into Fe(III) (oxy)hydroxides (goethite and ferrihydrite) during oxidative precipitation in supersaturated Fe(II) groundwater discharge. Bao and Kochinsky (2009) observed positive Ce anomalies in Fe oxides precipitated into marine ferromanganese crusts, suggesting that in the marine system, oxidative scavenging of Ce is not restricted to Mn(IV) oxides, but also includes Fe(III) oxides. Since Fe and Mn oxides are common solid-phase (and hence profile-retained) products of pedogenesis accumulating in oxic landscape positions but depleted in anoxic ones, residual soils should contain an REY signature that serves as a proxy for prevalent redox conditions occurring over the course of pedogenesis. Similarly, time series of effluent solutions should reveal time-dynamics of anoxia occurring in upgradient landscape positions. Bao and Kochinsky (2009) further observed a decoupling of La, Ce, Gd, Y and Lu (M-type lanthanide tetrad effect) from their respective neighbors in the REY series during partitioning among Fe oxides, Mn

oxides and seawater. Thompson et al. (in press) observed comparable decoupling during long-term soil formation from Hawaiian basalt and used the results to interpret results from short-term soil dissolution experiments intended to model field pore-water dynamics. Silicate clay minerals also facilitate the transport of REE in weathering profiles. A review by Laveuf and Cornu (2009) reported that adsorbed REE form outer-sphere complexes on the basal surfaces of silicate clay under acidic pH and low ionic strength conditions; however, under alkaline pH they can be adsorbed as inner-sphere complexes at the edges.

Redox conditions can influence REE fractionation and sorption/desorption processes in soils, as well as in marine environments (Elderfield, 1988; Moffett, 1994; Bau and Koschinsky, 2009; Davranche et al., 2011). Europium and cerium are both redox sensitive elements; Eu occurs in (III) or (II) valence state, whereas Ce occurs in (III) or (IV) valence state. Reduction of Eu requires strong reducing conditions rarely encountered in low pressure-temperature systems (Panahi et al., 2000; Laveuf and Cornu, 2009), and Eu(II) predominates in magmatic systems, where primary silicate minerals such as feldspars often show positive Eu-anomalies because of substitution into Ca^{2+} sites, where the trivalent REE are excluded (Aubert et al., 2001). The oxidation of Ce(III) to Ce(IV) occurs at Eh values around than 300 mV (De Carlo and Wen, 1998), which is commonly encountered in oxic surficial environments. The oxidation of Ce induces changes in ionic charge and radius that induce the decoupling of Ce(IV) from the rest of the lanthanide group (REE), thereby promoting its solid phase incorporation, generating positive Ce anomalies in soils (Feng, 2010; Laveuf et al., 2012). Under sub-

oxic conditions, microbially-catalyzed dissolution of Fe(III)- and Mn(IV)-oxides occurs in preference to that of cerianite ($\text{CeO}_{2(s)}$), enabling a positive Ce-anomaly to persist despite reductive dissolution and soil profile loss of Fe- and Mn-oxides (Laveuf and Cornu, 2009). The anomalous behavior of Ce in soil and aqueous solutions can be used to trace redox conditions in natural systems.

Since bedrock and regolith weathering processes influence REE release, fractionation, and transport, these processes should be reflected in pore solutions and surface waters deriving from hillslope and catchment discharges. Hence, the REE signature in stream waters is expected to reflect not only chemical composition of parent rock but also hydrologic flowpaths and transit times. The REE signature for near-surface runoff can be obtained from organic matter-rich horizons impacted by dust deposition and flowpaths that are typically characterized by short transit time (Tetzlaff et al., 2007; Sanderman et al., 2009; Boyer et al., 1996; Lambert et al., 2011). Shallow groundwater (or subsurface flow) typically acquires its signature from the mineral horizons and is characterized by intermediate transit time (Dunn et al., 2008). Contributions from deep groundwater, which acquires its chemical signature from long-term water-mineral interaction within the aquifers, are likely to influence stream waters during baseflow (Hill, 1990). In upland forested catchments, which are the focus of the current study, the geochemical signature of the stream waters during snowmelt events is hypothesized to come from three idealized sources: precipitation (snow), shallow groundwater (springs and soil water), and deep groundwater (Liu et al., 2008; Harpold et al., WRR paper in press).

The current work sought to assess whether REE trends in rock, water and soil could be applied to resolve aspects of biogeochemical weathering resulting from snowmelt events in seasonally-snow covered nested catchments located in the Jemez River Basin Critical Zone Observatory (JRB-CZO). Based on this prior work, the principal objectives of the present study were (i) to explore whether REY patterns of critical zone catchment sources are reflected in time dynamics of stream water REY efflux, including their changes with time and spatial scale and (ii) to reveal biogeochemical processes influencing catchment REY fractionation during snowmelt events. Most of the precipitation in catchments of the western US occurs during the winter season and, at higher elevations, primarily as snow. Based on multi-technique evidence from prior studies at the same site (Harpold et al., in press; Perdrial et al., in review; Zapata-Rios et al., in review), snowmelt is consistently measured as the dominant source of deep groundwater recharge, as is common in western montane regions (Bales et al., 2006). We have also found that it carries with it a large seasonal pulse of reduced organic carbon through soil profiles (Perdrial et al., 2012) and into surface waters (Harpold et al., in press; Perdrial et al., in review). We postulate here that pore and stream waters of the snowmelt period will reveal REY signatures of biological weathering in the upland source areas such as enrichment in the MREE and HREE fractions.

2 MATERIALS AND METHODS

2.1 Study Site

The field experimental design takes advantage of the nested catchment infrastructure of the Jemez River Basin Critical Zone Observatory (JRB-CZO) (Chorover et al., 2011), located in the Valles Caldera National Preserve, in northern New Mexico (Fig. 1). The JRB-CZO is instrumented to monitor CZ processes from pedon to catchment scales (Fig. 1, also see <http://criticalzone.org/jemez-catalina/>). Pedon sites within a zero order basin (ZOB) on convergent hillslope (Fig. 1A) were instrumented in mixed conifer forest on Redondo Dome (35°52'56"N, 106°32'8"W) within the larger La Jara catchment (LJC, Fig. 1B). The ZOB is south-oriented with dominant SW and SE facing slopes. Like most of the larger East Fork Jemez watershed (EFJW, Fig. 1C) the ZOB is underlain by Tewa Group rhyolitic volcanoclastic materials of Pleistocene age, which comprises a mixture of fine-grained porphyritic rhyodacite and zeolitized Bandelier Tuff (<http://geoinfo.nmt.edu/publications/maps/geologic/ofgm/>). Catchment properties for ZOB, LJC, and EFJW are summarized in Table 1.

Water years 2010 and 2011 were hydrologically distinct (Harpold et al., WRR paper in press; Zapata-Rios et al., in review). The total annual precipitation recorded at the Redondo meteorological station for the WYs 2010 and 2011 was 658 mm and 546 mm, respectively (Table 2). Annual hydrologic flux is dominated by snowmelt and the stream hydrographs show a peak in discharge during the spring snowmelt period (Xapata et al., manuscript in preparation). Maximum discharge values during the snowmelt period for LJC during the WYs 2010 and 2011 were 1.5 and 0.19 mm d⁻¹, respectively

(Table 1). Maximum discharge values for EFJW during the WYs 2010 and 2011 were 7.69 and 0.07 mm d⁻¹, respectively (Table 1). In addition, the snow season of WY 2010 was characterized by a deep, long-duration snow pack, whereas WY 2011 was characterized by an unusually light snowpack and frozen soils, resulting in less flushing of soil constituents to streams during snowmelt (Table 2) (Perdrial et al., paper in review).

2.2 Sample Collection

Samples of porphyritic rhyodacite and zeolitized Bandelier Tuff rocks were collected in summer 2010 around Redondo Dome in order to span the range of lithologic variation. Soil samples were obtained from six soil pedons (Fig. 1A) excavated in La Jara ZOB in September 2010. Soil samples were collected by genetic horizon, composited in the field, sealed in zip-lock bags, and stored at 4°C. Upon return to the lab, soil materials were air dried, sieved to recover the < 2 mm fraction, homogenized, and stored at room temperature.

Atmospheric dust material was collected using field-deployed traps. Traps were constructed from a circular cake pan (area of 450 cm²) filled with glass marbles and covered with wire mesh (Reheis et al., 1999). The wire mesh was secured with plastic zip-ties. The trap was situated on a metal fence post approximately 1.5 m above ground surface. Dust traps were installed in two locations within JRB-CZO to assess inputs at higher elevation (3242 m, N 35.88929' W 106.53234') and middle elevation (2825 m, N 35.88555' W 106.51190') locations within the EFJW watershed (Fig. 1C), for collection over the 7/26/11 to 10/15/11 period. Deionized water was used to rinse marbles and wire

mesh for quantitative transfer to 1000 mL bottles. Dust samples were centrifuged and air dried.

Passive capillary wick samplers (PCaps) (Holder et al., 1991; Biddle et al., 1995) were used to collect soil solutions as a function of depth in each pedon under a constant negative pressure head of ca. 30 cm (~2.9 kPa). The samplers consist of a fiberglass wick covered high density poly ethylene (HDPE) plate that is propped via turnbuckles into contact with the bottom of the soil horizon of interest. Liquid samples were guided through tubing into a collection vessel that can be evacuated from the surface. PCaps have been shown to not sorb, release or fractionate organic carbon and REY, and are thus suitable for the present study (Perdrial et al., 2012). PCap samples were filtered through 0.7 μm combusted glass fiber filters and stored in acid washed HDPE bottles. Total sample volume was recorded for flux calculations. Soil solutions included in this study were collected in situ during the WY of 2011.

Temperature and water stage were recorded every 30 min at the ZOB and LJC outlets (Fig. 1A-B) with an in-situ level troll 500 and at the EFJW with a Hobo U20 (Fig. 1C). Stage was converted to discharge using a standard equation for Parshall flumes. Only a few water stage measurements at the ZOB during the snowmelt period were recorded due to freezing conditions. In order to obtain discharge measurements from the ZOB a correlation between volumetric moisture content and discharge was developed and applied during the WY 2011.

Stream water grab samples were collected at flume locations in combusted (475°C, 4 h) 1000 mL amber glass bottles (for carbon analyses) and 250 mL acid washed HDPE

bottles (for metals analyses). Bottles were rinsed three times with stream water, filled to eliminate headspace and stored cool (4°C) until samples were processed in the lab. In this study, La Jara ZOB spring, East Fork La Jara spring and South La Jara spring are considered representatives for shallow groundwater (Fig. 1B). Stream waters from Redondo Meadow (near a spring outlet) were used as a proxy for deep groundwater due to its representation of the low chloride and high silica concentration that characterize stream baseflow most of the year (Harpold et al., in press). Shallow groundwater grab samples were collected following the same protocol as stream water samples. All shallow groundwater samples were collected in June 2011 and only one replicate was collected for each spring. Snow samples were collected using a 30 cm snow tube that collects samples integrated across the entire snowpack depth for shallow conditions or in incremental layers within deeper snowpack. Mean values (n=19) for snow grab samples are reported in this study and were collected during 2/13/11 to 3/28/11.

For dissolved organic carbon (DOC) analysis, sample splits were filtered through combusted Whatman 0.7 µm glass fiber filters within 48 h of sampling and filtrate was stored at 4°C in combusted 60 mL amber glass bottles. For REY analysis, sample splits from the HDPE bottles were filtered through 0.45 µm nylon membranes and stored in 30 mL acid washed HDPE bottles that were acidified with concentrated HNO₃.

2.3 Analytical Methods

2.3.1 *Solid Phase Characterization*

Unweathered sections in the porphyritic rhyodacite and zeolitized Bandelier Tuff rocks and soil samples were analyzed for mineralogical and elemental composition.

Mineral composition was determined by quantitative x-ray diffraction at the University of Arizona Center for Environmental Physics and Mineralogy (CEPM) on a PANalytical X'Pert PRO-MPD x-ray diffraction system (PANalytical, Almelo, AA, The Netherlands). Prior to mineralogical determination, organic matter was removed (Jackson, 2005). After measurement, diffractograms were imported into RockJock (Eberl, 2003) with an expanded reference mineral library analyzed at the CEPM for determination of quantitative mineral composition (Electronic Annex, Table E.1). Particle size composition for soil samples was using laser diffractometry (Beckman Coulter LS 13 320) following pretreatment to remove organic matter (Jackson, 2005) (Electronic Annex, Table E.2). Sand, silt and clay are reported as a percentage of the mineral fraction.

Elemental composition was determined by lithium metaborate/tetraborate fusion followed by inductively coupled plasma optical emission spectrometry (ICP-OES) and mass spectrometry (ICP-MS) analysis of total elemental concentrations (Activation Laboratories, Ancaster, Ontario). Dust samples were acid (HF-HCl-HNO₃) digested and elemental composition was then determined by ICP-MS (Perkin Elmer DRC II, Shelton, CT).

2.3.2 *Aqueous Phase Analyses*

DOC concentrations were determined using high temperature oxidation followed by infrared detection of CO₂ (Shimadzu TOC-VCSH, Columbia, MD). Rare earth elements and yttrium (REY) concentrations were determined by ICP-MS.

2.3.3 REY Normalization and Anomalies

To enable comparison across the full suite of aqueous and solid phase samples, REY concentration data for soil and water samples were normalized by a weighted average of CZO rhyolitic bedrock concentrations. Since both porphyritic rhyodacite and zeolitilized Bandelier Tuff contribute to the parent rock composition of the site, their fresh rock compositions were analyzed for REY concentrations, and the mean REY signatures for ZOB, LJC and EFJW bedrock were calculated from the mapped fractional coverage of the two bedrock types in each catchment (<http://geoinfo.nmt.edu/publications/maps/geologic/ofgm/>). In order to permit direct comparison of normalized REY data sets from various water and soil sources, a mean REY pattern was generated from a weighted average of porphyritic rhyodacite (0.44) and zeolitilized Bandelier Tuff (0.56) compositions, since that corresponds to the average bedrock composition. All subsequent soil and water REY data are normalized to this weighted rhyodacite-tuff average composition, as denoted by the subscript “RT”.

Presence or absence of europium, cerium, and neodymium anomalies (Eu/Eu^* , Ce/Ce^* and Nd/Nd^*) were calculated as:

$$\frac{Eu}{Eu^*} = \frac{Eu_{RT}}{(Sm_{RT})^{0.5} \times (Gd_{RT})^{0.5}} \quad \mathbf{Eq. 1}$$

$$\frac{Ce}{Ce^*} = \frac{Ce_{RT}}{(La_{RT})^{0.5} \times (Pr_{RT})^{0.5}} \quad \mathbf{Eq. 2}$$

$$\frac{Nd}{Nd^*} = \frac{Nd_{RT}}{(Pr_{RT})^{0.5} \times (Sm_{RT})^{0.5}} \quad \mathbf{Eq. 3}$$

where Eu_{RT} , Sm_{RT} , Gd_{RT} , Nd_{RT} and Pr_{RT} correspond to REE concentrations normalized by the rhyodacite-tuff weighted value. Anomaly values significantly greater than (less than) 1 represent positive (negative) anomalies with respect to rhyodacite-tuff weighted values.

2.3.4 Pedon Mass Balance Calculations

Mass fraction calculations for soils collected at the ZOB were calculated using the following equation:

$$\tau = \left(\left[\frac{C_{a,soil}}{C_{Ti,soil}} \div \frac{C_{a,parent\ material}}{C_{Ti,parent\ material}} \right] - 1 \right) \quad \mathbf{Eq. 4}$$

Ti was chosen as the immobile element. C_a corresponds to the REY concentration and C_{Ti} to titanium concentration. The weighted rhyodacite-tuff average composition for La Jara ZOB was used as parent material. Tau values higher than (lower than) 0 represent enrichment (depletion) with respect to the rhyodacite-tuff weighted values.

2.3.5 Volume Weighted Mean Concentrations

For soil solutions, volumes weighted mean (VWM) concentration values for REY were calculated from:

$$VWM_a = \frac{1}{V_T C_{RT}} \sum_i C_{a,i} V_i \quad [\text{mg kg}^{-1}] \quad \mathbf{Eq. 5}$$

where a corresponds to the REY of interest, $C_{a,i}$ to the concentration of REY for sampling date i , V_i is the mass of solution (kg) collected for sampling date i , V_T is the

total mass of solution collected over the snowmelt event, and C_{RT} is the rhyodacite-tuff weighted average for each REY. Discharge values were used for the calculation of VWM concentrations in stream waters.

2.3.6 *Geochemical Modeling*

Geochemical modeling was conducted to assess saturation indices (Ω) of CZ waters with respect to colloidal Fe and Al-(oxyhydr)oxides phases (MINTEQA2 for Windows, Version 1.50, Allison Geoscience Consultants, Inc.). MINTEQA2 specialized sub-model for calculations involving dissolved organic matter was included in the calculations. DOC concentration and DOM site density (2.4×10^{-6} mol of sites per mg DOC) were required input parameters (Susetyo et al., 1991). Saturation indices were employed to assess gibbsite and goethite precipitation or dissolution. The value of the saturation index (Ω) describes quantitatively the relative saturation of an aqueous solution with respect to equilibrium with a solid phase:

$$\Omega = IAP/K_{so} \quad \text{Eq. 6}$$

here IAP is the measured ion activity product corrected for aqueous phase speciation and K_{so} is the solubility product constant.

3 **RESULTS**

3.1 **Characterization of REY Sources**

JRB-CZO parent rock materials (porphyritic rhyodacite and zeolitilized Bandelier Tuff) show similar REY patterns (Fig. 2) when normalized to upper continental crust (UCC, Taylor and McLennan, 1981) values. REY_{UCC} values higher than 1 represent

enrichment and REY_{UCC} values lower than 1 represent depletion with respect to UCC values. Bandelier tuff exhibits (i) lower REY concentrations overall ($\sum REY_{UCC} = 15.89$), (ii) a larger negative Eu anomaly ($[Eu/Eu^*]_{UCC} = 0.17$) and (iii) smaller concentration increase across the HREE (from Er to Lu) relative to the rhyodacite (Fig. 2, Table 3). Dust samples are depleted in REY relative to bedrock and also UCC ($\sum REY_{UCC} = 8.05$), with slightly negative Eu ($[Eu/Eu^*]_{UCC} = 0.80$) and Nd ($[Nd/Nd^*]_{UCC} = 0.79$) anomalies (Fig. 2, Table 3). According to X-ray diffraction (XRD) analysis, the mineralogical composition of rhyodacite is albite ($NaAlSi_3O_8$), quartz (SiO_2), and sanidine ($((K,Na)(Si,Al)_4O_8)$) and for tuff is Ca-clinoptilolite ($CaAl_3(Al,Si)_2Si_{13}O_{36} \cdot 12H_2O$), sanidine, and cristobalite (polymorph of SiO_2) (Table E.1). The crystalline mineralogical composition of the ZOB soils includes dominantly quartz, orthoclase ($KAlSi_3O_8$), muscovite ($KAl_2(Si_3Al)O_{10}(OH)_2$), oligoclase ($((Ca,Na)(Al,Si)_4O_8)$), biotite ($(K(Mg,Fe)_3AlSi_3O_{10}(OH)_2$), Ca-clinoptilolite, and kaolinite ($Al_2Si_2O_5(OH)_4$).

For internal consistency of comparison, REY data sets discussed in the remainder of this paper were normalized by the rhyodacite-tuff average composition (i.e., “WA all” shown in Fig. 2). A description of the shallow groundwater REY patterns will follow. The REY_{RT} pattern for La Jara ZOB spring shows high relative HREE concentrations ($[HREE/LREE]_{RT} = 7.7$) (Fig. 3). The lowest REY_{RT} values ($\sum REY_{RT} = 4.53 \times 10^{-6}$) were observed in East Fork La Jara spring. South La Jara spring was characterized by a pronounced negative Nd-anomaly ($[Nd/Nd^*]_{RT} = 0.10$), a positive Eu-anomaly ($[Eu/Eu^*]_{RT} = 2.05$), and $[Y/Ho]_{RT}$ ratio of 0.79. Deep groundwater showed pronounced positive Eu-anomaly ($[Eu/Eu^*]_{RT}$ ranges from 1.07 to 6.80, average = 2.35, n = 9) and a

negative Nd-anomaly ($[Nd/Nd^*]_{RT}$ ranges from 0 to 1.0, average = 0.23, n = 9). In addition, the average Eu- and Nd-anomalies for snow are 2.98 and 0.40, respectively.

3.2 REY Signatures of Soil Solid Phase

Light (L), middle (M) and heavy (H) REE can separated, respectively into the groups LREE (La to Nd), MREE (Sm to Tb), and HREE (Dy to Lu). In general, mineral soil solids in the ZOB pedons (locations shown in Fig. 1A) are depleted in LREE and enriched in HREE relative to parent material (Fig. 4), exhibiting the depletion trend $LREE > MREE \geq HREE$, consistent with preferential removal of LREE during pedogenesis. Surficial organic (O) horizons generally show greater depletion of HREE relative to underlying mineral horizons, with pedon 3 being an exception. The REE depletion trends are coherent within a given pedon but vary by pedon and with landscape position. For example, pedon 1 situated on a planar hillslope shows decreased depletion with depth (approaching bedrock), whereas pedon 5 situated in the convergent hillslope shows the inverse trend. Pedons 1, 2, 3, and 6 exhibited significant ($p < 0.01$) positive correlations between tau values and mass fraction of soil clay ($< 2 \mu m$ sized particles), with R^2 values to 0.83, 0.83, 0.46, and 0.97. But this positive relation was not consistently observed; weaker and even negative correlations between these two parameters were measured for pedons 4 ($R^2 = 0.54$) and 5 ($R^2 = 0.60$).

All horizons exhibited pronounced positive Eu-anomalies ($[Eu/Eu^*]_{RT}$ values from 1.79 to 2.52, mean = 2.18, n = 30) (Fig. 5), indicating soil enrichment in Eu relative to the rhyodacite-tuff (RT) parent material signature. Dust was the single source showing a sufficiently large Eu anomaly to match that measured in the pedons ($[Eu/Eu^*]_{RT}$ from

1.48 to 1.77, average = 1.66, n = 3). Cerium accumulates in lower horizons in preference to La and Pr ($[Ce/Ce^*]_{RT}$ from 0.70 to 1.29, average = 1.08, n = 30) (Figure E.2, electronic annex).

3.3 REY Signatures of Soil Pore Waters

Soil pore waters in instrumented pedons reveal distinctive REY patterns including, prominently, a depth dependent Eu anomaly (Fig. 6). Overall, REY patterns for the six pedons showed that specific locations in the landscape exhibit relatively consistent REY patterns, within a dynamic range characterized by seasonal variation. For example, representative time-series and volume-weighted-mean (VWM) data are shown for pedons 1 (planar hillslope location) and 5 (convergent hillslope location) for WY 2011. Volume weighted mean values (Fig. 6, *bottom*) show that REY concentrations are higher in surficial pore waters of pedon 1, but at depth in pedon 5. A prior study showed that water and reduced carbon fluxes over the same period were higher in the surface (than at depth) for planar pedon 1, whereas the inverse was true for the convergent pedon 5 (Perdrial et al., 2012). This result is consistent with the depletion patterns for these two pedons (Fig. 4), which shows greater solid-phase depletion of REY at the surface for pedon 1, and at depth for pedon 5. Quite low values in general are found in the near surface of pedon 5, situated in a convergent position, with a very slight trend favoring the HREE (Fig. 6D).

In both pedons, soil solutions at depth have a pronounced negative Nd anomaly (50-60 cm, Fig. 7) during early periods of snowmelt. The anomaly is smaller for the surface horizons and diminishes (approaching $Nd/Nd^* \sim 1$) later in spring snowmelt even at depth. Soil solutions in the upper horizon of pedon 1 exhibited negative Ce-anomalies

during snow melt ($[Ce/Ce^*]_{RT}$ from 0.31 to 0.58, mean = 0.49, n = 6) (Fig. E.3), whereas Ce anomalies for soil solutions are diminished with depth (e.g., $[Ce/Ce^*]_{RT}$ from 0.43 to 1.09, mean = 0.98, n = 30 for 59 cm in pedon 1).

Soil solutions were preferentially enriched in smaller ionic radius (and hence higher ionic potential, IP) REY (i.e., HREE>MREE>LREE) - a trend that is especially evident for the surface horizons (Fig. 6). These data suggest preferential release of higher IP REY from the soil matrix.

Given the potential control over REE concentrations exerted by DOC (Sonke and Salters, 2006; Pourret et al., 2007b; Tang and Johannesson, 2003; Tang and Johannesson, 2010), we correlated the sum of REE (Σ REE) (yttrium was excluded) concentrations against DOC in collected soil solutions. In contrast to the case for surface waters (discussed below) correlations were relatively weak for pore waters, with comparable total REE concentrations existing across a relatively large range in soil solution DOC (Pedon 1, 3cm: $R^2= 0.23$, n=5; Pedon 1, 59cm: $R^2= 0.21$, n=6; Pedon 5, 5cm: $R^2= 0.09$, n=3) (data not shown). In both pedons, the upper horizons give the highest VWM DOC concentration values (Table 4), but unlike “planar” pedon 1, “convergent” pedon 5 showed higher carbon and water flux at depth (Perdrial et al., 2012; Vazquez-Ortega et al., in prep.).

(Oxyhydr)oxide nano-particles and colloids, common weathering products in pedogenic environments, have been shown to facilitate the transport of REE in soil and water systems (Guo et al., 2010; Sholkovitz, 1992). We observed positive correlations between Σ REE and aqueous Al and Fe, potentially signaling an oxy-hydroxide colloid

effect on REE mobilization in soil pore waters (Fig. 8). For example, soil solutions collected at 3cm and 59 cm in pedon 1 show a positive correlation between ΣREE and Al ($R^2 = 0.92$ and 0.94 for surface and subsurface, respectively, Fig. 8A), and between ΣREE and Fe ($R^2 = 0.93$ and 0.78 for surface and subsurface, respectively, Fig. 8B).

3.4 REY Signatures of Surface Waters

Surface waters draining basins of increasing scale – i.e., zero order basin (ZOB), La Jara Catchment (LJC) and East Fork of the Jemez Watershed (EFJW) – showed distinct REY signatures (Fig. 9). Solutions collected at the ZOB outlet (WY 2011) were remarkably consistent in REY pattern over time and enriched in HREE and MREE relative to LREE ($[\text{LREE}/\text{MREE}]_{\text{RT}}$ ranged from 0.34 to 0.43, mean = 0.38, $n = 9$; $[\text{LREE}/\text{HREE}]_{\text{RT}}$ ranged from 0.19 to 0.29, mean = 0.26, $n = 9$) (Fig. 9A). A pronounced positive Eu-anomaly ($[\text{Eu}/\text{Eu}^*]_{\text{RT}}$ from 1.61 to 1.68, mean = 1.64, $n = 9$) was consistently observed at the ZOB scale. Whereas deep soil solutions had shown a strong negative Nd anomaly (section 3.3); Nd anomalies were not as pronounced in surface waters (e.g., ZOB $[\text{Nd}/\text{Nd}^*]_{\text{RT}}$ ranges from 0.65 to 1.03, mean = 0.74, $n = 9$) (Fig. 9A and Fig. 10), and ZOB patterns were more similar to near surface than deep soil solutions. High REY concentrations were observed during the initial snowmelt period (after 3/25/11).

Positive Eu-anomalies were also observed for LJC ($[\text{Eu}/\text{Eu}^*]_{\text{RT}}$ ranges from 1.09 to 2.27, average = 1.66, $n = 9$) and EFJW ($[\text{Eu}/\text{Eu}^*]_{\text{RT}}$ ranges from 1.44 to 2.05, average = 1.71, $n = 9$) stream waters during WY 2011. On average, LJC and EFJW stream waters deviated from the ZOB by showing a more pronounced negative Nd-anomaly (LJC mean $[\text{Nd}/\text{Nd}^*]_{\text{RT}} = 0.24$, $n = 9$; EFJW mean $[\text{Nd}/\text{Nd}^*]_{\text{RT}} = 0.44$, $n = 9$) (Fig. 9B and C, Fig.

10), similar to the pattern observed for deeper soil solutions. It is noteworthy that no Nd anomaly was observed 4/12/11, during which was sampled the first large flush of water produced during the onset of snowmelt (Fig. 10A and 10B). During the wetter WY 2010, LJC and EFJW exhibited higher REY VWM values than in 2011 (Fig. 9E and F, no WY 2010 data available for ZOB). Likewise, the VWM DOC values for LJC and EFJW were 1.8 and 3.1 times higher in the wetter 2010 relative to drier 2011 as well (Table 4), as discussed in detail elsewhere (Harpold et al., in press; Perdrial et al., in review).

Dissolved organic carbon concentrations were positively correlated with discharge for all surface water scales, with much higher values being achieved during the wetter 2010, which greatly strengthened the correlation for that year (e.g., R^2 values for correlation of DOC and discharge for LJC during WYs 2010 and 2011 were 0.94 and 0.12, respectively, and 0.48 and 0.01, respectively, for EFJW). High \sum REE concentrations were also positively correlated with discharge in WY 2010 (LJC: $R^2 = 0.73$; EFJW: $R^2 = 0.43$) (Fig. 11B), following similar trends as DOC. Therefore, \sum REE concentration was positively correlated with DOC across all catchments and both WYs 2010 and 2011 (Fig. 11C). The \sum REE - DOC correlations were again stronger for the wetter WY 2010 (LJC: $R^2 = 0.88$; EFJW: $R^2 = 0.99$), which provided a significantly wider range in both REE and DOC concentration, extending them to higher values. The \sum REE - DOC correlation was measured at the ZOB scale only in 2011, and nonetheless gave an $R^2 = 0.95$. Positive correlates with \sum REE included also: Al (ZOB WY 2011, $R^2 = 0.23$; LJC WY 2010, $R^2 = 0.56$; EFJW WY 2010, $R^2 = 0.67$), Fe (ZOB WY 2011, $R^2 =$

0.56; LJC WY 2010, $R^2 = 0.49$; EFJW WY 2010, $R^2 = 0.96$), and P (ZOB WY 2011, $R^2 = 0.19$; LJC WY 2010, $R^2 = 0.90$, EFJW WY 2010, $R^2 = 0.83$).

4 DISCUSSION

4.1 Influences of Biogeochemical Weathering processes on REE across Scales

Biogeochemical processes implicated in REE transport and fate in soil and stream water include, 1) weathering of primary phosphate and silicate minerals, 2) complexation with DOM, 3) adsorption and co-precipitation with secondary minerals (silicate clays and Mn-, Al-, Fe-(oxy)hydroxides), and 4) colloidal transport (Sonke and Salters, 2006; Pourret et al., 2007b; Tang and Johannesson, 2003; Tang and Johannesson, 2010). Phosphate minerals such as apatite or monazite can partially control the REE budget in soils, soil solutions, and stream waters (Aubert et al., 2001; Stille et al., 2009; Tang and Johannesson, 2003); for instance, low molecular weight organic acids (LMWOA) such as citrate, oxalate, and phthalate have been reported to enhance phosphate mineral weathering (Goyné et al., 2010). Porphyritic rhyodacite (parent material in the study site) and local dust contain substantive total phosphorus (Table 3), primarily associated with trace phosphate minerals. Furthermore, phosphorus content in the soil matrix was positively correlated with MREE followed by HREE (data not shown), suggesting possible phosphate minerals enrichment in MREE. However, the potential contribution of organic P to this correlation cannot be ignored, because of prior studies that have shown MREE enrichment in soil organic matter (Tang and Johannesson, 2010). We also observed that total phosphorus in stream waters exhibits a positive correlation with

Σ REE, suggesting that phosphate mineral weathering exerts control over total REE system fluxes (Figure 8).

The least REE depleted soils (pedons 1, 2, 3, and 6) according to mass calculations were also those most enriched in clay content, suggesting that solid phase pedogenic products play an important role diminishing REE transport and fate (data not shown). Cation exchange capacity (CEC) of silicate clay minerals have previously been shown to be predictive of REE sorption (Coppin et al., 2002). Pedon 5 (convergent hillslope location) showed increasing depletion of REY with depth, apparently associated with the greater water and carbon throughflux at depth resulting from lateral flow for that location (Vazquez-Ortega et al., in prep.). In the convergent location, total soil REY exhibit a positive correlation ($R^2 = 0.25$) with soil organic matter content, indicating that REY retention mechanisms vary across the landscape.

Soil solutions and stream waters at the outlet of ZOB exhibited higher VWM REY and VWM DOC concentrations than stream waters draining the larger LJC and EFJW (WY 2011)(Fig. 6 and 9, Table 4). The high aqueous REY concentrations and mobilization at the pedon and ZOB scales can be attributed to adsorption and/or co-precipitation with Al, Fe-(oxy)hydroxide colloids, as well as to the formation of REE-DOM complexes. Despite the fact that soil solutions (pedon scale) contain large amounts of DOC (DOC concentration ranges from 15 to 60 mg L⁻¹) weak correlations were observed between DOC and Σ REE as compared to those observed between Σ REE and total Al and Fe (Fig. 8). Fe and Al-(oxy)hydroxides colloids are continuously formed in soil pores during incongruent weathering processes and to the extent that they serve as

mobile nano-particulate sorbents for REE, they can be important transport vectors affecting catchment geochemical denudation using standard (e.g., 0.45 μm filtration) methods. Since nano-particulate forms of REE would be included in the “dissolved” pool as measured following filtration, we conducted geochemical modeling (MINTEQA2) to assess whether the analyzed solutions were indeed supersaturated with respect to Al and Fe-(oxy)hydroxides. Saturation index calculations were conducted following aqueous phase speciation that included the effects of complexation with DOM. This modeling exercise indicated that soil solutions were indeed supersaturated and the formation of micro-colloidal Al and Fe constituents was predicted thermodynamically (Electronic Annex, Table E.3). Such materials are likely very important to the development of depletion profiles in pedogenic environments, e.g., fine clays (<200 nm) enriched in Fe-(oxy)hydroxides, kaolinite, and gibbsite were the primary mobile colloids in reconstructed pedons of two Ultisols (Kaplan et al., 1997).

At the ZOB scale (WY 2011), a strong positive correlation between ΣREE and DOC was observed; REE mobilization appears to be primarily controlled by DOM complexation (Fig 11C), suggesting a strong role for biological mediation of REE chemical denudation. During the wetter WY 2010, DOC and ΣREE concentrations in stream waters at LJC and EFJW were positively correlated with discharge (Fig. 11A and B). In contrast, a poorer correlation was observed in drier WY 2011, suggesting that DOC and REE mobilization from catchment soils is strongly dependent on hydrologic fluxes (Fig 11A and B) that are, in turn a function of snowpack accumulation and snow water equivalent (Harpold et al., in press; Perdrial et al., in review). Likewise, ΣREE

concentrations in stream waters at LJC and EFJW (WY 2010) correlate strongly with DOC concentration (Fig 11C), suggesting that DOM complexation is one of the primary controls on REE mobilization from hillslope to catchment to watershed scale. Weaker correlations between DOC and $\sum\text{REE}$ during WY 2011 can be attributed to the low water flux in 2011 (Fig 11C), highlighting the fact that chemical denudation of organic-ligand-reactive metals occurs during pulsed episodes associated with snowmelt but with significant inter-annual variation depending on snowpack. Colloidal transport is also implicated in REE mobilization in LJC and EFJW (Fig. 12 and Table E.3). Sholkovitz (1992) conducted sequential filtrations on stream waters (pore sizes of 0.45, 0.2, and 0.025 μm) and concluded that a large portion of REE was in the colloidal load, indicating that colloids can control REE distribution in stream waters. Using cascade filtration, we have made similar observations during monsoon rainfall events in the Santa Catalina Mountains CZO (Pohlmann, MS thesis).

4.2 **Eu-anomaly: An Indicator of REE sources**

Among the patterns observed in the current study were pronounced positive Eu-anomalies in the soil matrix, soil solutions, and stream waters (Figures E.1, 6, and 9). Several processes can potentially contribute to the positive Eu-anomaly, including 1) dust deposition, 2) preferential weathering of plagioclase feldspars, and 3) alkaline hydrothermal alteration of the parent rocks.

Dust deposition inputs likely explain the Eu enrichment in bulk soils, soil solutions, and stream waters given that dust particles do not exhibit a pronounced negative Eu-anomaly when normalized to the parent rock (Fig. 2). In other words, dust is less

depleted in Eu when compare to the parent materials. Over long periods of time, Eu accumulation from dust deposition may induce the positive Eu-anomaly. Dust is primarily transported into the study site by winds that originate from the south (<http://www.wrcc.dri.edu/htmlfiles/westwinddir.html>), and the dominant dust sources are likely from the low-vegetation-cover geomorphic surfaces of the Rio Grande Valley and the playas of the Chihuahuan Desert. Several studies have reported that pore waters in upper soil horizons contain significant amounts of atmospheric derived REEs (Stille et al., 2009; Aubert et al., 2002).

Feldspar minerals tend to be enriched in Eu because, during primary mineral crystallization and growth from magma in the absence of molecular oxygen, Eu^{2+} substitutes into Ca^{2+} sites similar to Sr^{2+} (Aubert et al., 2001). Porphyritic rhyodacite (parent material in the study site) contains about 9% plagioclase (listed as oligoclase in Electronic Annex, Table E.1). When these rocks undergo surficial weathering in oxic environments, Eu^{2+} is released and readily oxidized (Panahi et al., 2000). Several studies (Ma et al., 2011; Brioschi et al., 2013) have reported positive Eu-anomalies in natural waters (pore and stream waters), and attributed this to preferential weathering of plagioclases. Ma et al. (2011) argues that the major element chemistry (bases on Na) in pore waters is consistent with preferential dissolution plagioclase in the regolith. No positive correlations in this study were found between oligoclase % and Eu-anomalies (or concentration, mg kg^{-1}) in the soil solid phase, suggesting that other processes are likely responsible for the large Eu enrichment in soils. An alternative hypothesis derives from Hopf (1993), who stated that REEs (with the unique exception of Eu) were depleted in

rhyodacite subjected to alkaline hydrothermal alteration, inducing a positive Eu-anomaly in the altered rock. Parent material alteration by hydrothermal activity, as evidenced by the prevalence of zeolite in the tuff matrix, may therefore contribute to the positive Eu-anomaly since hydrothermal activity has been reported in the study area (Goff and Gardner, 1988; Chipera, et al, 2008). Most likely, the positive Eu anomalies in our soils are a direct result of both dust deposition and hydrothermal alteration of parent materials.

4.3 Ce-anomaly: an indicator for redox conditions in the ZOB soils

Redox conditions can influence REE fractionation in soils, specifically the development of cerium (Ce) anomalies resulting from Ce(III) to Ce(IV) oxidation (Feng, 2010; Laveuf et al., 2012). The oxidation of Ce(III) to Ce(IV) occurs at Eh values near and above 300 mV (Ronov et al., 1967; Laveuf and Cornu, 2009). Tetravalent Ce is characterized by particularly low mobility due to strong interaction (via adsorption and/or coprecipitation) with Fe- and Mn-oxides (Laveuf et al, 2008). In addition, under favorable conditions (slightly acidic to neutral pH and sufficient aqueous Ce concentration), Ce(IV) can precipitate as cerianite (CeO₂) (Feng, 2010).

In our study site, soils exhibited a preferential accumulation of cerium in bottom horizons with respect to lanthanum and praseodymium (Fig. E.2, electronic annex). The Ce enrichment in lower horizons can be attributed to Ce retention at the surface of Fe-Mn-oxides via adsorption, coprecipitation, and/or intraparticle diffusion (Laveuf and Cornu, 2009). Several studies (Bau, 1999 and Bau and Koschinsky, 2009) have demonstrated that Ce(III) is oxidized by surface reaction and electron transfer to Fe(III)- and Mn(IV) centers of secondary (oxy)hydroxides. The oxidative scavenging of Ce by

these oxides has been described as consisting of a three-step process: (i) initial adsorption of trivalent REE (including Ce), (ii) incomplete oxidation of Ce(III) to Ce(IV), and (iii) preferential desorption of Ce(III) due to weaker interactions with the mineral surfaces (Bau et al., 1999; Bau and Kochinsky, 2009). De Carlo and Wen (1998) demonstrated (first proposed by Goldberg et al., 1963) that Ce is exclusively decoupled from trivalent REE under abiotic oxidation by Mn-oxides.

Soil solutions in the upper horizon of pedon 1 (planar hillslope location) exhibited negative Ce-anomalies during snowmelt WY 2011 (Fig. E.3, electronic annex). On the other hand, soil solutions at the bottom horizon of pedon 1 exhibited no anomalous Ce behavior during the beginning of the snowmelt, but towards the end of the snowmelt negative Ce-anomalies were observed, reaching values similar to those in the upper horizon. The negative Ce-anomalies in soil solutions in the upper horizon can be used as indicators of oxic conditions during the entire snowmelt event as Ce(IV) is retained at the surface of Fe- and Mn-oxides or precipitated as cerianite (and hence removed from soil solution) (Bau, 1999; Bau and Koschinsky, 2009; Feng, 2010). The evolving change in Ce anomaly at depth in pedon 1 is consistent with a progressive change in redox conditions from reducing to oxidizing conditions over the course of snowmelt. This likely results from a seasonal fluctuation of the near-surface groundwater table during snowmelt event, which imposes a potentially steep redox gradient. Soils with low water content remain oxic favoring Ce(IV) uptake to the solid phase leading to negative Ce-anomalies in the soil solution. High soil water content for prolonged periods likely induces reducing conditions favoring the reduction of Ce(IV) to Ce(III) releasing Ce to

soil solutions, and leading in some cases to positive Ce anomalies. Pedochemical processes controlling Ce behavior is the subject of ongoing work (Vazquez-Ortega et al., in prep.).

4.4 **Nd-anomaly: an indicator for hydrologic flowpaths**

Neodymium concentrations in the soils and parent materials of the study site did not exhibit strong anomalous behavior (Figure 2 and Electronic Annex, Fig. E.1), indicating that Nd is exhibiting small if any preferential immobilization during weathering processes. On the other hand, pronounced negative Nd-anomalies were observed in the fluids deriving from subsoils during early spring snowmelt (Fig. 7) as well as in deep and shallow groundwater sources (Figure 3).

At the beginning of snowmelt subsoils (e.g., deepest horizons in pedons 1 and 5) exhibited negative Nd-anomalies (Fig. 7). The Nd/Nd* values increased from 0.01 (beginning of snowmelt) to 1.05 (towards the end of snowmelt) reaching values similar to those in the soil matrix (no anomalous behavior). Low Nd concentrations in soil solutions in subsoils of the pedons can be attributed to preferential adsorption (adsorb onto the surface of silicate clay and/or oxy-hydroxide minerals) or to influent groundwater contributions, since shallow and deep ground waters exhibited pronounced negative Nd-anomalies. Several studies have reported that montmorillonite, kaolinite, and smectite exhibit high sorptive Nd affinity (Symeopoulos et al., 1996; Coppin et al., 2002). Sorption processes involved in Nd uptake by silicate clays are ion exchange, adsorption, and surface precipitation of Nd hydrolysis products (Symeopoulos et al., 1996).

Stream waters in the study site (ZOB, LJC, EFJW) during the snowmelt period obtain their chemical signature from precipitation (snow), shallow groundwater (springs and soil water), and deep groundwater (Redondo Meadow) (Harpold et al., WRR paper in press). Negative Nd-anomalies were observed in the surface waters of the ZOB (average $[\text{Nd}/\text{Nd}^*]_{\text{RT}} = 0.74$), LJC (average $[\text{Nd}/\text{Nd}^*]_{\text{RT}} = 0.24$), and EFJW (average $[\text{Nd}/\text{Nd}^*]_{\text{RT}} = 0.44$) (Fig. 10, section 3.4). Based on Nd-anomaly similarities, stream waters apparently acquire the negative Nd-anomaly when shallow (South La Jara spring, average $[\text{Nd}/\text{Nd}^*]_{\text{RT}} = 0.10$) and deep groundwaters (Redondo Meadow, average $[\text{Nd}/\text{Nd}^*]_{\text{RT}} = 0.23$) contribute to stream flow. Stream waters at the ZOB have contributions from near-surface runoff since the anomaly value is closer to 1 (more similar to the values observed in the soil solutions of the upper horizon in pedon 1). These patterns in Nd-anomaly in stream waters indicate that subsurface flow is a dominant hydrologic source to catchment and watershed scale discharges, consistent with other studies using unreactive tracers (Liu et al., 2008; Harpold et al., WRR paper in press).

5 SUMMARY AND CONCLUSIONS

REE were employed as reactive tracers to study weathering processes during snowmelt events at pedon (1-6), hillslope (ZOB), catchment (LJC) and watershed (EFJW) scales located within the Valles Caldera National Preserve, Jemez River Basin Critical Zone Observatory (JRB-CZO). Weighted rhyodacite-tuff normalized REE distribution patterns reveal positive Eu-anomalies in the soil matrix, soil solutions, and stream waters that can be attributed to 1) dust deposition and 2) preferential retention of

Eu in hydrothermally altered tuff. Cerium anomalies reflected spatially and temporally variable redox status, dominantly associated with seasons. Negative Ce-anomalies in soil solution can be used as a proxy for oxic conditions because of co-precipitation of Ce(IV) with Fe and Mn oxides. The precise fate of Ce in the ZOB soils is the subject of a companion study (Vazquez-Ortega et al., in prep.). Conversely, the lack of anomalous behavior ($[Ce/Ce^*]_{RT} \approx 1$) can be used as a proxy for anoxic conditions in which solid phase Ce(IV) is reduced to (or maintained in the form of) the more mobile Ce(III).

Negative Nd-anomalies in subsoils and also in stream waters suggests that subsoil lateral flows may be important flowpaths contributing to deep subsurface flows and stream water discharges. Pronounced negative Nd-anomalies observed in soil water samples in subsurface horizons and at the outlet of ZOB, LJC, and EFJW are potentially attributable to adsorption by silicate clay and/or oxy-hydroxide minerals at depth, but further investigation is underway to confirm or refute this hypothesis (Vazquez et al., in prep.). Similar negative Nd-anomalies were observed in Redondo Meadow (deep groundwater) and South La Jara spring (shallow groundwater) waters.

Since REE mobility can be affected by the same processes that influence trace metals (Cu, Cr, Co, Ni, Pb, U, Th) mobility in solution (Grybos et al., 2007); REE are postulated to be a very useful tool that allow us to learn more about the biogeochemical weathering processes occurring in natural systems that affect trace metal sorption/desorption and transport. In this study site, for instance, REE fractionation patterns in stream waters exhibited an increase from La to Lu (a.k.a. the lanthanide contraction), indicating the prevalence formation of organo-REE complexes (Tang and

Johannesson, 2010). Also, a strong positive correlation between DOC and Σ REE was observed in stream waters, suggesting a strong role for biological mediation of REE chemical denudation. This study also highlights the role of Fe and Al-(oxy)hydroxides colloids as mobile nano-particulate sorbents for REE (possibly other trace metals). Finally, the use of Ce-anomalies proved to be useful in describing redox fluctuations during the snowmelt period.

Acknowledgements

The Jemez-Santa Catalina Critical Zone Observatory is supported by the National Science Foundation, Grant # EAR-0724958 and EAR/IF-0929850. Thanks to Scott Compton, Caitlin Orem, Mercer Meding, and Courtney Porter for assistance with sampling and analysis. Thanks to Matej Durcik for help with GIS.

References

- Aubert D., Stille P. and Probst A. (2001) REE fractionation during granite weathering and removal by waters and suspended loads: Sr and Nd isotopic evidence. *Geochim. Cosmochim. Acta* **65**, 387-406.
- Aubert D., Stille P., Probst A., Gauthier-Lafaye F., Pourcelot L. and Del Nero M. (2002) Characterization and migration of atmospheric REE in soils and surface waters. *Geochim. Cosmochim. Acta* **66**, 3339-3350.
- Bailey S., Mayer B. and Mitchell M. (2004) Evidence for influence of mineral weathering on stream water sulphate in Vermont and New Hampshire (USA). *Hydrol. Process.* **18**, 1639-1653.
- Bales R. C., Molotch N. P., Painter T. H., Dettinger M. D., Rice R. and Dozier J. (2006) Mountain hydrology of the western United States. *Water Resour. Res.* **42**, W08432.

- Bau M. (1999) Scavenging of dissolved yttrium and rare earths by precipitating iron oxyhydroxide: experimental evidence for Ce oxidation, Y-Ho fractionation, and lanthanide tetrad effect. *Geochim. Cosmochim. Acta* **63**, 67-77.
- Bau M. and Koschinsky A. (2009) Oxidative scavenging of cerium on hydrous Fe oxide: evidence from the distribution of rare earth elements and yttrium between Fe oxides and Mn oxides in hydrogenetic ferromanganese crusts. *Geochem. J.* **43**, 37-47.
- Biddle D. L., Chittleborough D. J. and Fitzpatrick R. W. (1995) Field monitoring of solute and colloid mobility in a gneissic sub-catchment, South Australia. *Appl. Clay Sci.* **9**, 433-442.
- Boyer E., Hornberger G., Bencala K. and McKnight D. (1996) Overview of a simple model describing variation of dissolved organic carbon in an upland catchment. *Ecol. Model.* **86**, 183-188.
- Braun J. J., Viers J., Dupre B., Polve M., Ndam J. and Muller J. P. (1998) Solid/liquid REE fractionation in the lateritic system of Goyoum, east Cameroon: the implication for the present dynamics of the soil covers of the humid tropical regions. *Geochim. Cosmochim. Acta* **62**, 273-299.
- Brindley G.W. (1980) Chapter 7: Quantitative X-ray mineral analysis of clays, in: Brindley G.W., Brown G. (Eds.), *Crystal structures of clay minerals and their x-ray identification*. Mineralogical Society, London, 411-438
- Brioschi L., Steinmann M., Lucot E., Pierret M. C., Stille P., Prunier J. and Badot P. M. (2013) Transfer of rare earth elements (REE) from natural soil to plant systems: implications for the environmental availability of anthropogenic REE. *Plant Soil* **366**, 143-163.
- Byerne R. and Li B. (1995) Comparative complexation behavior of the rare-earths. *Geochim. Cosmochim. Acta* **59**, 4575-4589.
- Chipera S. J., Goff F., Goff C. J. and Fittipaldo M. (2008) Zeolitization of intracaldera sediments and rhyolitic rocks in the 1.25 Ma lake of Valles caldera, New Mexico, USA. *J. Volcanol. Geotherm. Res.* **178**, 317-330.
- Chorover J., Troch P. A., Rasmussen C., Brooks P. D., Pelletier J. D., Breshars D. D., Huxman T. E., Kurc S. A., Lohse K. A., McIntosh J. C., Meixner T., Schaap M. G., Litvak M. E., Perdrial J., Harpold A. and Durcik M. (2011) How water, carbon, and energy drive critical zone evolution: the Jemez-Santa Catalina Critical Zone Observatory. *Vadose Zone J.* **10**, 884-899.

- Coppin F., Berger G., Bauer A., Castet S. and Loubet M. (2002) Sorption of lanthanides on smectite and kaolinite. *Chem. Geol.* **182**, 57-68.
- Davranche M., Pourret O., Gruau G. and Dia A. (2004) Impact of humate complexation on the adsorption of REE onto Fe oxyhydroxide. *J. Colloid Interface Sci.* **277**, 271-279.
- Davranche M., Pourret O., Gruau G., Dia A. and Le Coz-Bouhnik M. (2005) Adsorption of REE(III)-humate complexes onto MnO₂: experimental evidence for cerium anomaly and lanthanide tetrad effect suppression. *Geochim. Cosmochim. Acta* **69**, 4825-4835.
- Davranche M., Grybos M., Gruau G., Pedrot M., Dia A. and Marsac R. (2011) Rare earth element patterns: a tool for identifying trace metal sources during wetland soil reduction. *Chem. Geol.* **284**, 127-137.
- De Carlo E., and Wen X. (1998) The influence of redox reactions on the uptake of dissolved Ce by suspended Fe and Mn oxide particles. *Aquatic Geochemistry* **3**, 357-389.
- Dunn S. M., Bacon J. R., Soulsby C., Tetzlaff D., Stutter M. I., Waldron S. and Malcolm I. A. (2008) Interpretation of homogeneity in delta(18)O signatures of stream water in a nested sub-catchment system in north-east Scotland. *Hydrol. Process.* **22**, 4767-4782.
- Dupre B., Gaillardet J., Rousseau D. and Allegre C. (1996) Major and trace elements of river-borne material: The Congo Basin. *Geochim. Cosmochim. Acta* **60**, 1301-1321.
- Dupre B., Viers J., Dandurand J., Polve M., Benezeth P., Vervier P. and Braun J. (1999) Major and trace elements associated with colloids in organic-rich river waters: ultrafiltration of natural and spiked solutions. *Chem. Geol.* **160**, 63-80.
- Eberl D.D. (2003) User's guide to a program for determining quantitative mineralogy from powder X-ray diffractions data. U.S. Geological Survey Open File Report 03-78.
- Elderfield H. (1988) The oceanic chemistry of the rare-earth elements. *Philos. Trans. R. Soc. A-Math. Phys. Eng. Sci.* **325**, 105-126.
- Elderfield H., Upstillgoddard R. and Sholkovitz E. (1990) The rare-earth elements in rivers, estuaries, and coastal seas and their significance to the composition of ocean waters. *Geochim. Cosmochim. Acta* **54**, 971-991.

- Feng J. (2010) Behaviour of rare earth elements and yttrium in ferromanganese concretions, gibbsite spots, and the surrounding terra rossa over dolomite during chemical weathering. *Chem. Geol.* **271**, 112-132.
- Gaillardet J., Dupre B. and Allegre C. (1999) Geochemistry of large river suspended sediments: Silicate weathering or recycling tracer? *Geochim. Cosmochim. Acta* **63**, 4037-4051.
- Goff F. and Gardner J. (1988) Valles Caldera region, New-Mexico, and the emerging continental scientific drilling program. *Journal of Geophysical Research-Solid Earth and Planets* **93**, 5997-5999.
- Goldberg E., Smith R., Koide M. and SCHMITT R. (1963) Rare-earth distributions in marine environment. *Journal of Geophysical Research* **68**, 4209-4217.
- Goyne K. W., Brantley S. L. and Chorover J. (2010) Rare earth element release from phosphate minerals in the presence of organic acids. *Chem. Geol.* **278**, 1-14.
- Gruau G., Dia A., Olivie-Lauqueta G., Davranche M. and Pinay G. (2004) Controls on the distribution of rare earth elements in shallow groundwaters. *Water Res.* **38**, 3576-3586.
- Guo H., Zhang B., Wang G. and Shen Z. (2010) Geochemical controls on arsenic and rare earth elements approximately along a groundwater flow path in the shallow aquifer of the Hetao Basin, Inner Mongolia. *Chem. Geol.* **270**, 117-125.
- Grybos M., Davranche M., Gruau G., Petitjean P. (2007) Is trace metal release in wetland soils controlled by organic matter mobility or Fe-oxyhydroxides reduction? *Journal of Colloid and Interface Science* **314**, 490-501.
- Harpold, A.A., Brooks P.D., Perdrial J., McIntosh J., Meixner T., Lohse K.A., Zapata-Rios X., Vazquez-Ortega A., and Chorover J. (In press) Quantifying variation in solute sources and nutrient cycling in montane headwater catchments. *Water Resources Research*
- Hill A. (1990) Ground-water flow paths in relation to nitrogen chemistry in the near-stream zone. *Hydrobiologia* **206**, 39-52.
- Holder M., Brown K., Thomas J., Zabcik D. and Murray H. (1991) Capillary-wick unsaturated zone soil pore water sampler. *Soil Sci. Soc. Am. J.* **55**, 1195-1202.
- Hopf S. (1993) Behavior of rare-earth elements in geothermal systems of New-Zealand. *J. Geochem. Explor.* **47**, 333-357.

- Jackson M.L. (2005) Soil chemical analysis: advanced course, 2nd Edition. Parallel Press, Madison, WI.
- Johnson C.E., Litaor M.I., Billet M.F., and Bricker O.P. (1994). Biogeochemistry of small catchments: a tool for environmental research. John Wiley & Sons Ltd. 323-341.
- Johannesson K., Stetzenbach K. and Hodge V. (1997) Rare earth elements as geochemical tracers of regional groundwater mixing. *Geochim. Cosmochim. Acta* **61**, 3605-3618.
- Johannesson K., Tang J., Daniels J., Bounds W. and Burdige D. (2004) Rare earth element concentrations and speciation in organic-rich blackwaters of the Great Dismal Swamp, Virginia, USA. *Chem. Geol.* **209**, 271-294.
- Kaplan D., Bertsch P. and Adriano D. (1997) Mineralogical and physicochemical differences between mobile and nonmobile colloidal phases in reconstructed pedons. *Soil Sci. Soc. Am. J.* **61**, 641-649.
- Klug H.P., and Alexander L.E. (1974) X-Ray Diffraction procedures for polycrystalline and amorphous materials, John Wiley & Sons, New York.
- Langmuir, D. (1997), Aqueous Environmental Geochemistry, New Jersey: Prentice-Hall, Inc.
- Lambert T., Pierson-Wickmann A., Gruau G., Thibault J. and Jaffrezic A. (2011) Carbon isotopes as tracers of dissolved organic carbon sources and water pathways in headwater catchments. *J. Hydrol.* **402**, 228-238.
- Laveuf C. and Cornu S. (2009) A review on the potentiality of rare earth elements to trace pedogenetic processes. *Geoderma* **154**, 1-12.
- Laveuf C., Cornu S. and Juillot F. (2008) Rare earth elements as tracers of pedogenetic processes. *C. R. Geosci.* **340**, 523-532.
- Laveuf C., Cornu S., Guilherme L. R. G., Guerin A. and Juillot F. (2012) The impact of redox conditions on the rare earth element signature of redoximorphic features in a soil sequence developed from limestone. *Geoderma* **170**, 25-38.
- Ledin A., Karlsson S., Duker A. and Allard B. (1994) The adsorption of europium to colloidal iron oxyhydroxides and quartz - the impact of pH and an aquatic fulvic-acid. *Radiochim. Acta* **66-7**, 213-220.

- Liu F., Parmenter R., Brooks P. D., Conklin M. H., Bales R. C. (2008) Seasonal and interannual variation of streamflow pathways and biogeochemical implications in semi-arid, forested catchments in Valles Caldera, New Mexico. *Ecohydrology* **1**, 239-52.
- Leybourne M. I. and Johannesson K. H. (2008) Rare earth elements (REE) and yttrium in stream waters, stream sediments, and Fe-Mn oxyhydroxides: fractionation, speciation, and controls over REE plus Y patterns in the surface environment RID B-2541-2009. *Geochim. Cosmochim. Acta* **72**, 5962-5983.
- Ma L., Jin L. and Brantley S. L. (2011) How mineralogy and slope aspect affect REE release and fractionation during shale weathering in the Susquehanna/Shale Hills Critical Zone Observatory. *Chem. Geol.* **290**, 31-49.
- McClain M., Boyer E., Dent C., Gergel S., Grimm N., Groffman P., Hart S., Harvey J., Johnston C., Mayorga E., McDowell W. and Pinay G. (2003) Biogeochemical hot spots and hot moments at the interface of terrestrial and aquatic ecosystems. *Ecosystems* **6**, 301-312.
- Meixner T. and Fenn M. (2004) Biogeochemical budgets in a mediterranean catchment with high rates of atmospheric N deposition - importance of scale and temporal asynchrony. *Biogeochemistry* **70**, 331-356.
- Moffett J. (1994) A radiotracer study of cerium and manganese uptake onto suspended particles in Chesapeake Bay. *Geochim. Cosmochim. Acta* **58**, 695-703.
- Nakajima T. and Terakado Y. (2003) Rare earth elements in stream waters from the Rokko granite area, Japan: effect of weathering degree of watershed rocks. *Geochem. J.* **37**, 181-198.
- NRC (2001) Basic research opportunities in earth sciences. National Academies Press. Washington, DC, National Research Council.
- Ohta A. and Kawabe I. (2001) REE(III) adsorption onto Mn dioxide (δ -MnO₂) and Fe oxyhydroxide: Ce(III) oxidation by δ -MnO₂. *Geochim. Cosmochim. Acta* **65**, 695-703.
- Panahi A., Young G. and Rainbird R. (2000) Behavior of major and trace elements (including REE) during Paleoproterozoic pedogenesis and diagenetic alteration of an Archean granite near Ville Marie, Quebec, Canada. *Geochim. Cosmochim. Acta* **64**, 2199-2220.

- Perdrial J., McIntosh J., Harpold A., Brooks P., Zapata-Rios X., Ray J., Troch P., Chorover J. (submitted) Impact of winter climate change on stream water carbon characteristics in forested headwater streams .
- Perdrial J. N., Perdrial N., Harpold A., Gao X., Gabor R., LaSharr K. and Chorover J. (2012) Impacts of sampling dissolved organic matter with passive capillary wicks versus aqueous soil extraction. *Soil Sci. Soc. Am. J.* **76**, 2019-2030.
- Pokrovsky O. and Schott J. (2002) Iron colloids/organic matter associated transport of major and trace elements in small boreal rivers and their estuaries (NW Russia). *Chem. Geol.* **190**, 141-179.
- Pohlmann M. (Thesis) Comparative aqueous and colloid chemistry of CZO and LEO: distribution of weathering products into dissolved and nano-particulate pools.
- Pourret O., Davranche M., Gruau G. and Dia A. (2007a) Organic complexation of rare earth elements in natural waters: Evaluating model calculations from ultrafiltration data. *Geochim. Cosmochim. Acta* **71**, 2718-2735.
- Pourret O., Davranche M., Gruau G. and Dia A. (2007b) Rare earth elements complexation with humic acid. *Chem. Geol.* **243**, 128-141.
- Pourret O. and Martinez R. E. (2009) Modeling lanthanide series binding sites on humic acid. *J. Colloid Interface Sci.* **330**, 45-50.
- Pourret O., Gruau G., Dia A., Davranche M. and Molenat J. (2010) Colloidal control on the distribution of rare earth elements in shallow groundwaters. *Aquat. Geochem.* **16**, 31-59.
- Rasmussen C., Southard R. and Horwath W. (2005) Modeling energy inputs to predict pedogenic environments using regional environmental databases. *Soil Sci. Soc. Am. J.* **69**, 1266-1274.
- Rasmussen C. and Tabor N. J. (2007) Applying a quantitative pedogenic energy model across a range of environmental gradients. *Soil Sci. Soc. Am. J.* **71**, 1719-1729.
- Rasmussen C., Troch P. A., Chorover J., Brooks P., Pelletier J. and Huxman T. E. (2011) an open system framework for integrating critical zone structure and function. *Biogeochemistry* **102**, 15-29.
- Reheis M. C., Budahn J. R. and Lamothe P. J. (1999) Elemental analysis of modern dust in Southern Nevada and California, USGS OFR 99-53, <http://pubs.usgs.gov/of/1999/ofr-99-0531/>.

- Ronov A., Balashov Y. and Migdisov A. (1967) Geochemistry of rare earths in sedimentary cycle. *Geochemistry International Ussr* **4**, 1-10.
- Sanderman J., Lohse K. A., Baldock J. A. and Amundson R. (2009) Linking soils and streams: sources and chemistry of dissolved organic matter in a small coastal watershed. *Water Resour. Res.* **45**, W03418.
- Shiller A. M. (2010) Dissolved rare earth elements in a seasonally snow-covered, alpine/subalpine watershed, Loch Vale, Colorado. *Geochim. Cosmochim. Acta* **74**, 2040-2052.
- Sholkovitz E. (1992) Chemical evolution of rare-earth elements - fractionation between colloidal and solution phases of filtered river water. *Earth Planet. Sci. Lett.* **114**, 77-84.
- Steinmann M. and Stille P. (2008) Controls on transport and fractionation of the rare earth elements in stream water of a mixed basaltic-granitic catchment basin (Massif Central, France). *Chem. Geol.* **254**, 1-18.
- Steinmann M. and Stille P. (2006) Rare earth element transport and fractionation in small streams of a mixed basaltic-granitic catchment basin (Massif Central, France). *J. Geochem. Explor.* **88**, 336-340.
- Stille P., Pierret M. -, Steinmann M., Chabaux F., Boutin R., Aubert D., Pourcelot L. and Morvan G. (2009) Impact of atmospheric deposition, biogeochemical cycling and water-mineral interaction on REE fractionation in acidic surface soils and soil water (the Strengbach case). *Chem. Geol.* **264**, 173-186.
- Stille P., Steinmann M., Pierret M. -, Gauthier-Lafaye F., Chabaux F., Viville D., Pourcelot L., Matera V., Aouad G. and Aubert D. (2006) The impact of vegetation on REE fractionation in stream waters of a small forested catchment (the Strengbach case). *Geochim. Cosmochim. Acta* **70**, 3217-3230.
- Sonke J. and Salters V. (2006) Lanthanide-humic substances complexation. I. experimental evidence for a lanthanide contraction effect. *Geochim. Cosmochim. Acta* **70**, 1495-1506.
- Środoń J., Drits V.A., McCarty D.K., Hsieh J.C.C., and Eberl D.D. (2001) Quantitative X-ray diffraction analysis of clay-bearing rocks from random preparations. *Clays Clay Miner.* **49**, 514-528.
- Stille P., Pierret M., Steinmann M., Chabaux F., Boutin R., Aubert D., Pourcelot L. and Morvan G. (2009) Impact of atmospheric deposition, biogeochemical cycling and

- water-mineral interaction on REE fractionation in acidic surface soils and soil water (the Strengbach case). *Chem. Geol.* **264**, 173-186.
- Susetyo W., Carreira L., Azarraga L. and Grimm D. (1991) Fluorescence techniques for metal-humic interactions. *Fresenius J. Anal. Chem.* **339**, 624-635.
- Symeopoulos B., Soupioni M., Misaelides P., Godelitsas A. and Barbayiannis N. (1996) Neodymium sorption by clay minerals and zeoliferous rocks. *J. Radioanal. Nucl. Chem. -Lett.* **212**, 421-429.
- Tang J., and Johannesson K. H. (2010) Ligand extraction of rare earth elements from aquifer sediments: Implications for rare earth element complexation with organic matter in natural waters. *Geochim. Cosmochim. Acta* **74**, 6690; 6690-6705.
- Tang J, Johannesson K. (2003) Speciation of rare earth elements in natural terrestrial waters: Assessing the role of dissolved organic matter from the modeling approach. *Geochimica et Cosmochimica Acta* **67**: 2321-39.
- Taylor S. and McLennan S. (1981) The composition and evolution of the continental-crust - rare-earth element evidence from sedimentary-rocks. *Philos. Trans. R. Soc. Lond. Ser. A-Math. Phys. Eng. Sci.* **301**, 381-399.
- Tetzlaff D., Soulsby C., Waldron S., Malcolm I. A., Bacon P. J., Dunn S. M., Lilly A. and Youngson A. F. (2007) Conceptualization of runoff processes using a geographical information system and tracers in a nested mesoscale catchment. *Hydrol. Process.* **21**, 1289-1307.
- Thompson A., Chadwick O. A., Boman S. and Chorover J. (2006) Colloid mobilization during soil iron redox oscillations. *Environ. Sci. Technol.* **40**, 5743-5749.
- Thompson A., Amistadi M.K., Chadwick O.A., and Chorover J. (In Press) Fractionation of yttrium and holmium during basaltic soil weathering. *Geochim. Cosmochim. Acta*
- Vázquez-Ortega A., Perdrial J.N., Huckle D., Amistadi M.K., Rasmussen C., McIntosh J., Chorover, J. (In prep) Redistribution of rare earth elements and yttrium (REY) in topographically distinct, rhyolite-derived pedons. *Geoderma*.
- Viers J., Dupre B., Polve M., Schott J., Dandurand J. and Braun J. (1997) Chemical weathering in the drainage basin of a tropical watershed (Nsimi-Zoetele site, Cameroon): comparison between organic-poor and organic-rich waters. *Chem. Geol.* **140**, 181-206.
- Voegelin A. R., Naegler T. F., Pettke T., Neubert N., Steinmann M., Pourret O. and Villa I. M. (2012) The impact of igneous bedrock weathering on the Mo isotopic

- composition of stream waters: natural samples and laboratory experiments. *Geochim. Cosmochim. Acta* **86**, 150-165.
- Walker J., Hays P. and Kasting J. (1981) A negative feedback mechanism for the long-term stabilization of earths surface-temperature. *Journal of Geophysical Research-Oceans and Atmospheres* **86**, 9776-9782.
- White A. and Blum A. (1995) Effects of climate on chemical-weathering in watersheds. *Geochim. Cosmochim. Acta* **59**, 1729-1747.
- Xiong Y. (2011) Organic species of lanthanum in natural environments: implications to mobility of rare earth elements in low temperature environments. *Appl. Geochem.* **26**, 1130-1137.
- Yamamoto Y., Takahashi Y. and Shimizu H. (2010) Systematic change in relative stabilities of REE-humic complexes at various metal loading levels. *Geochem. J.* **44**, 39-63.
- Zapata-Rios X., Troch P. A., McIntosh J., Broxton P., Harpold A., Brooks P., and Litvak M. (In review) Hydrological response of semi-arid mountain catchments to changes in winter precipitation. *Hydrological Processes*

LIST OF TABLES:

Table 1 Physical properties for the three study catchments Zero Order Basin (ZOB), La Jara Catchment (LJC), and East Fork Jemez Watershed (EFJW). Canopy coverage % was calculated using canopy height > 2m.

Table 2 Hydrometeorological properties during the water years 2010 and 2011 in the study site. Hydrometeorological measurements are reported from the upper CZO eddy-flux tower and nearby COSMOS snow pillow.

Table 3 REY values for rhyodacite and Bandelier tuff rock materials, and dust normalized to UCC values.

Table 4 Volume weighted mean (VWM) dissolved organic carbon (DOC) concentrations. Soil solution data was obtained during WY 2011. Surface water data was obtained during WYs 2010 and 2011.

LIST OF FIGURES:

Figure 1 Overview of field site at the Valles Caldera National Preserve (VCNP) in New Mexico. Digital elevation models show scales of inquiry for REY measurements in the current study. (A) Instrumented pedons (numbered 1-6, installed September 2010) are distributed within the SE and SW facing slopes of the La Jara zero order basin (ZOB). (B) The ZOB is nested within the northern section of the larger La Jara catchment (LJC) (flumes for both ZOB and LJC are shown in blue). (C) LJC and ZOB are contained within the western portion (on flank of Redondo Mountain) of the East Fork Jemez watershed (EFJW). In addition, spring sampling and dust trap locations and Redondo Meadow flume are also shown.

Figure 2 REY patterns for parent materials and dust normalized to upper continental crust (UCC) values reported in Taylor and McLennan (1981). Weighted average values (WA) for bedrock in LJ ZOB, LJC, and EFJW (based on fractional area coverage by rhyodacite and tuff) are included for rhyodacite fractions in ZOB, LJC, and EFJW of 0.47, 0.19, and 0.66, respectively.

Figure 3 REY fractionation patterns for shallow and deep groundwater and snow normalized by WA all. All shallow groundwater samples were collected in June 2011 and only one replicate was collected for each spring. In this study, La Jara ZOB spring, East Fork La Jara spring and South La Jara spring are defined as shallow groundwater. Mean values (n=9) are reported for Redondo Meadow stream waters (proxy for deep groundwater) and were collected during 3/28/11 to 6/14/11. Mean values (n=19) for snow grab samples are reported and were collected during 2/13/11 to 3/28/11.

Figure 4 Mass fraction (Tau values) for REE fractions as a function of depth for all pedons excavated in La Jara ZOB. The immobile element is titanium. All values were normalized by WA LJ ZOB. Tau values higher than 0 represent enrichment and Tau values lower than 0 represent depletion with respect to the parent materials. In this study LREE (La to Nd), MREE (Sm to Tb), and HREE (Dy to Lu) represent light, middle, and heavy rare earth elements, respectively.

Figure 5 Eu anomalies for all pedons (all horizons) excavated in La Jara ZOB, tuff, RT LJ ZOB, rhyodacite, and dust are included above. Range values are reported for tuff (n=3), rhyodacite (n=3), and, dust (n=3). All values were normalized by WA LJ ZOB.

Figure 6 REY fractionation patterns for soil solutions in (A) Pedon 1 at 3cm, (B) Pedon 1 at 59cm, (C) volume weighted mean for Pedon 1, (D) Pedon 5 at 5cm, (E) Pedon 5 at 54cm, and (F) volume weighted mean for Pedon 5. REY were normalized by WA all values.

Figure 7 Nd-anomalies in soil solutions sampled by wick lysimeter at pedon 1 during snowmelt WY 2011. All values were normalized by WA all.

Figure 8 Comparison between (A) \sum REE and Al, (B) \sum REE and Fe, (C) \sum REE and P in soil solutions for Pedons 1 and 5 during the snowmelt event (WY 2011). Eu was excluded. REE are in mg L^{-1} and were not normalized.

Figure 9 REY fractionation patterns for stream waters at the outlet of (A) La Jara ZOB, (B) volume weighted mean for La Jara ZOB, (C) La Jara catchment, (D) volume weighted mean for La Jara catchment, (E) EFJ watershed, and (F) volume weighted mean for EFJ watershed. REY were normalized by WA all values.

Figure 10 Nd-anomalies in stream waters at the outlet of La Jara ZOB, La Jara Catchment, and East Fork Jemez Watershed during snowmelt WY 2011. All values were normalized by WA all.

Figure 11 Comparison between (A) discharge versus DOC, (B) discharge versus \sum REE, and (C) DOC versus \sum REE for surface waters at the outlet of La Jara ZOB, La Jara catchment, and EFJ watershed during the snowmelt period for WYs 2010 and 2011. The coefficient of determination (R^2) for the entire data set presented in part C is 0.94. REE are in mg L^{-1} and were not normalized.

Table 1 Physical properties for the three study catchments Zero Order Basin (ZOB), La Jara Catchment (LJC), and East Fork Jemez Watershed (EFJW). Canopy coverage % was calculated using canopy height > 2m.

Catchment	Area (km ²)	Parent material fractional contribution		Max Discharge (mm/d) ^a		Slope ^c (degrees)	Elevation ^c (meters)	Canopy Coverage (%)
		rhyodacite	Bandelier tuff	WY 2010	WY 2011			
ZOB	0.15	0.47	0.53	no data	17.52 ^b	9.0 (0.0 - 35.1)	3027 (2986 – 3099)	45.2
LJC	3.67	0.19	0.81	1.5	0.19	15.8 (0.0 - 54.6)	3099 (2702 - 3429)	53.1
EFJW	110.98	0.66	0.34	7.69	0.07	11.3 (0.0 – 88.1)	2758 (2582 - 3432)	36.4

^aMaximum discharge during the snowmelt period.

^bPredicted max discharge based on a correlation between water content (upper horizon, pedon 2) and discharge at the outlet of the ZOB.

^cAverage values are followed by range values in parenthesis.

Table 2 Hydrometeorological properties during the water years 2010 and 2011 in the study site. Hydrometeorological measurements are reported from the upper CZO eddy-flux tower and nearby COSMOS snow pillow.

Water Year	Precipitation (mm)	Depth of Max SWE^a (mm)	Ambient Temperature (°C)^b	Soil Temperature at 5cm (°C)^b
2010	658	302	-2.1 (-15.1 to 9.6)	0.38 (-1.77 to 6.29)
2011	546	48	-1.2 (-23.8 to 13.8)	-0.91 (-2.77 to 4.41)

^aSWE stands for snow water equivalent.

^bAverage values are followed by range values in parenthesis.

Table 3 REY values for rhyodacite and Bandelier tuff rock materials, and dust normalized to UCC values. The phosphorous values are reported in mg kg⁻¹.

	Rhyodacite^b	Tuff^b	Dust^b
Σ REY	23.32±1.05	15.89±0.23	8.05±1.55
LREE/MREE ^a	1.30±0.08	1.29±0.04	0.90±0.07
LREE/HREE ^a	0.92±0.09	0.75±0.01	0.90±0.09
MREE/HREE ^a	0.71±0.02	0.58±0.02	1.00±0.03
Eu/Eu*	0.55±0.21	0.17±0.01	0.80±0.08
Nd/Nd*	0.98±0.01	0.93±0.01	0.79±0.03
Ce/Ce*	0.84±0.10	0.96±0.02	0.89±0.01
Phosphorous	262±0	44±0	911±243

^a LREE, MREE, and HREE represent light, middle, and heavy rare earth elements, respectively. LREE = La to Nd, MREE = Sm to Tb, HREE = Dy to Lu (Y not included).

^b Average values followed by standard deviation, n=3.

Table 4 Volume weighted mean (VWM) dissolved organic carbon (DOC) concentrations. Soil solution data was obtained during WY 2011. Surface water data was obtained during WYs 2010 and 2011.

Site		DOC ^a (mg/L)	VWM for DOC (mg/L)
Pedon 1, Soil Solution	3cm	24.0 – 63.0	40.7
	59cm	15.7 – 30.2	17.6
Pedon 5, Soil Solution	5cm	23.1 – 35.9	26.5
	54cm	9.8 ^b	9.8
La Jara ZOB	WY 2011	5.1 – 12.1	10.0
La Jara Catchment	WY 2010	1.8 – 5.2	3.8
	WY 2011	1.7 – 2.8	2.1
EFJ Watershed	WY 2010	2.9 – 14.1	10.2
	WY 2011	1.3 – 6.8	3.2

^aRange for DOC concentrations in soil solutions and stream waters.

^bn=1, for pedon 5 at 54cm during the snowmelt event.

FIGURES

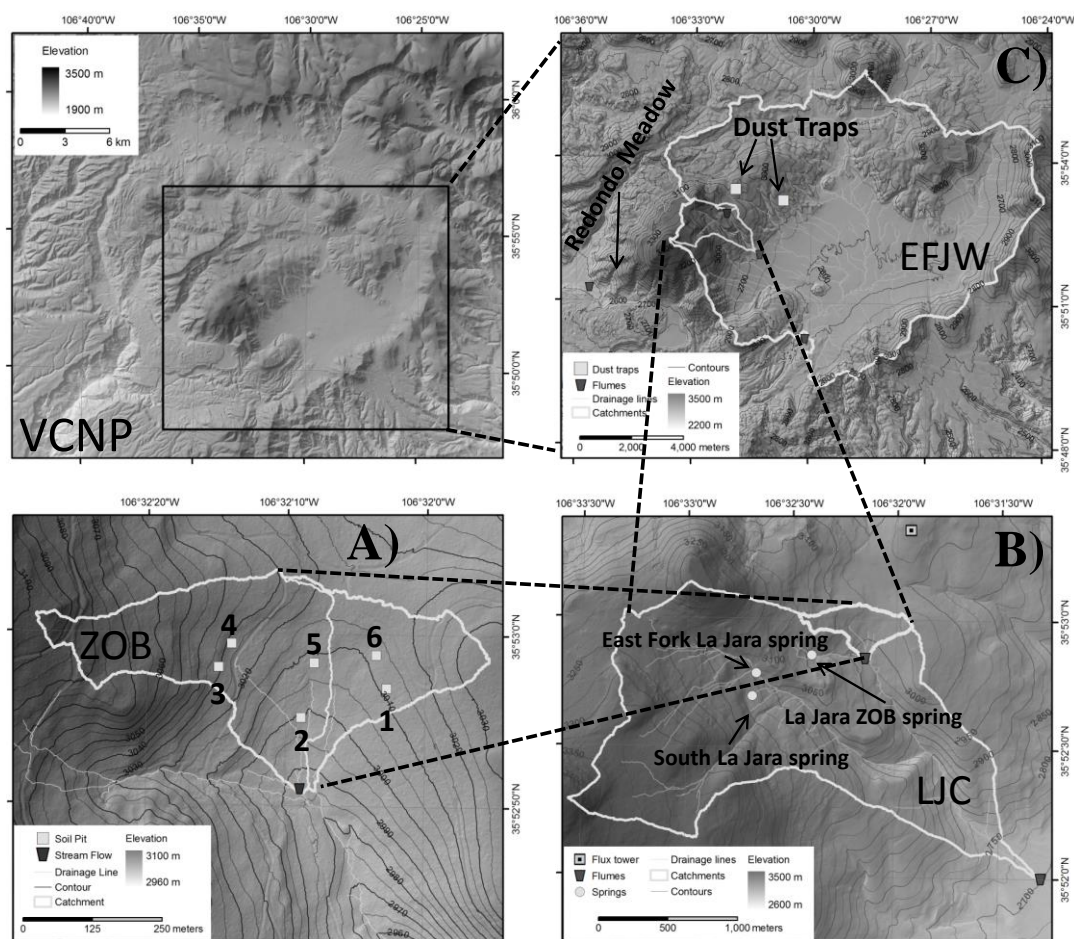


Figure 1 Overview of field site at the Valles Caldera National Preserve (VCNP) in New Mexico. Digital elevation models show scales of inquiry for REY measurements in the current study. (A) Instrumented pedons (numbered 1-6, installed September 2010) are distributed within the SE and SW facing slopes of the La Jara zero order basin (ZOB). (B) The ZOB is nested within the northern section of the larger La Jara catchment (LJC) (flumes for both ZOB and LJC are shown in blue). (C) LJC and ZOB are contained within the western portion (on flank of Redondo Mountain) of the East Fork Jemez watershed (EFJW). In addition, spring sampling and dust trap locations and Redondo Meadow flume are also shown.

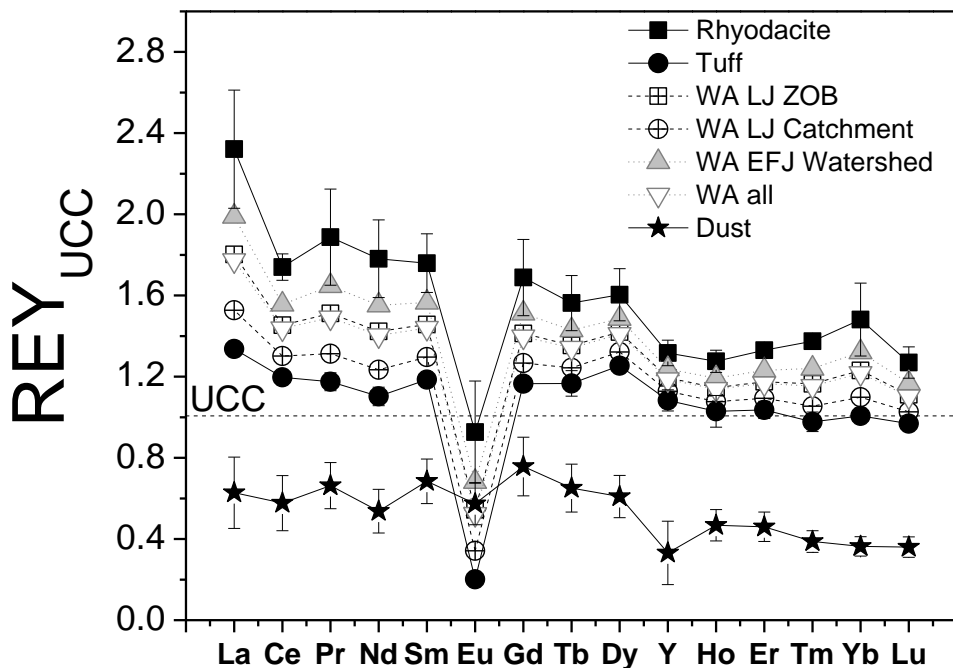


Figure 2 REY patterns for parent materials and dust normalized to upper continental crust (UCC) values reported in Taylor and McLennan (1981). Weighted average values (WA) for bedrock in LJ ZOB, LJC, and EFJW (based on fractional area coverage by rhyodacite and tuff) are included for rhyodacite fractions in ZOB, LJC, and EFJW of 0.47, 0.19, and 0.66, respectively.

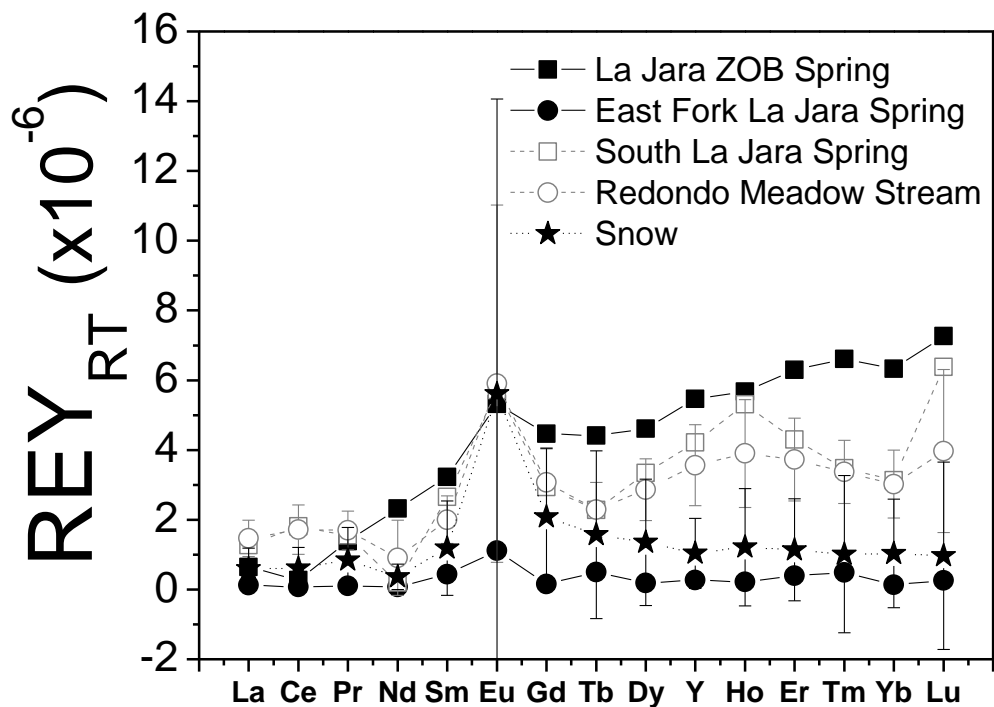


Figure 3 REY fractionation patterns for shallow and deep groundwater and snow normalized by WA all. All shallow groundwater samples were collected in June 2011 and only one replicate was collected for each spring. In this study, La Jara ZOB spring, East Fork La Jara spring and South La Jara spring are defined as shallow groundwater. Mean values (n=9) are reported for Redondo Meadow stream waters (proxy for deep groundwater) and were collected during 3/28/11 to 6/14/11. Mean values (n=19) for snow grab samples are reported and were collected during 2/13/11 to 3/28/11.

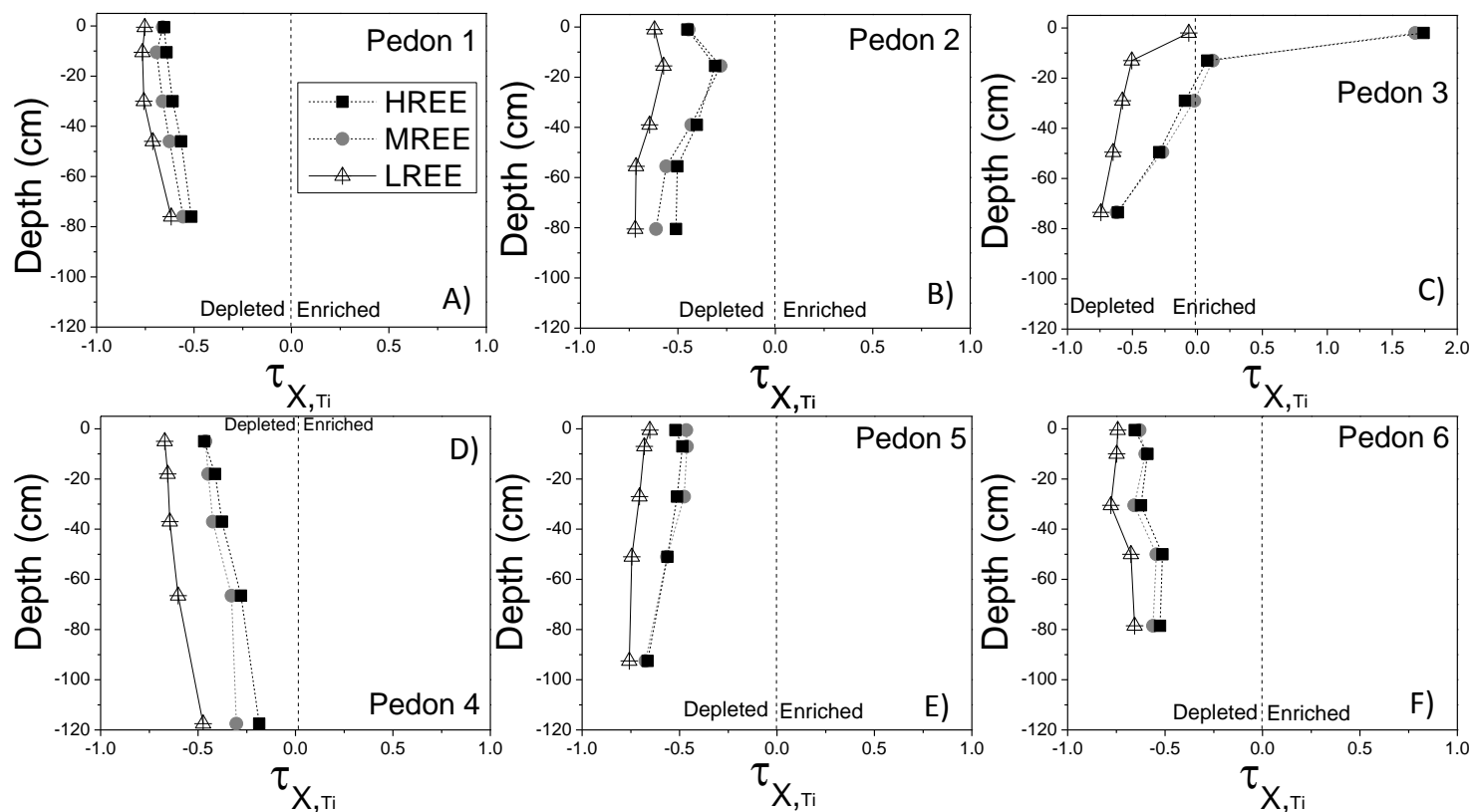


Figure 4 Mass fraction (Tau values) for REE fractions as a function of depth for all pedons excavated in La Jara ZOB. The immobile element is titanium. All values were normalized by WA LJ ZOB. Tau values higher than 0 represent enrichment and Tau values lower than 0 represent depletion with respect to the parent materials. In this study LREE (La to Nd), MREE (Sm to Tb), and HREE (Dy to Lu) represent light, middle, and heavy rare earth elements, respectively.

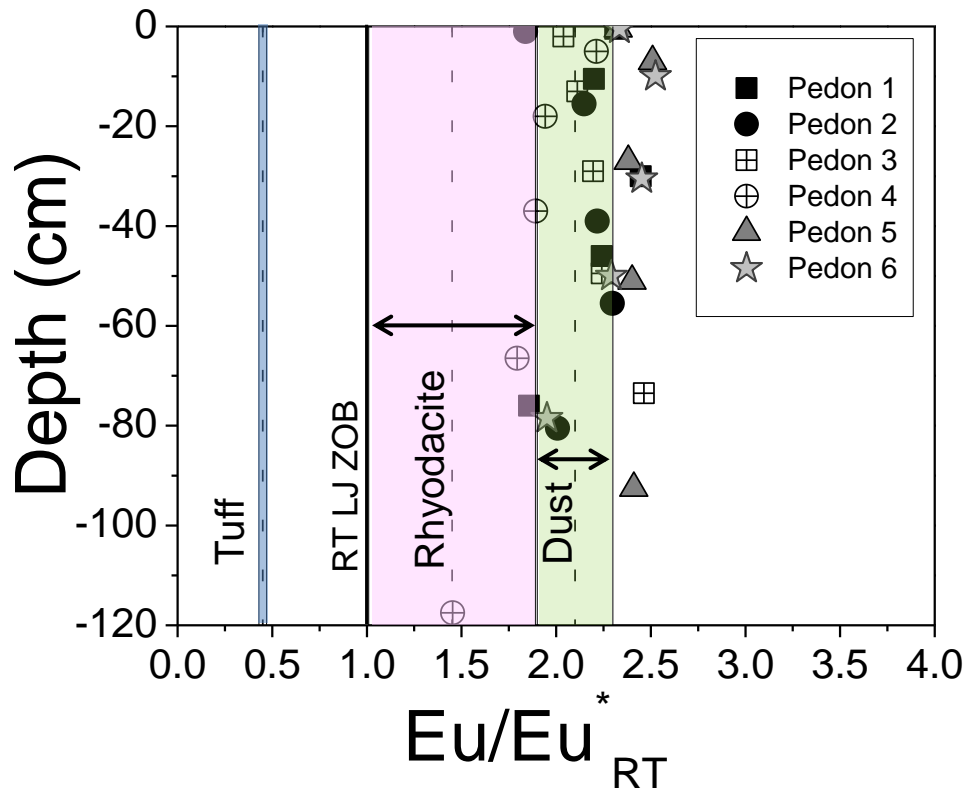


Figure 5 Eu anomalies for all pedons (all horizons) excavated in La Jara ZOB, tuff, RT LJ ZOB, rhyodacite, and dust are included above. Range values are reported for tuff (n=3), rhyodacite (n=3), and, dust (n=3). All values were normalized by WA LJ ZOB.

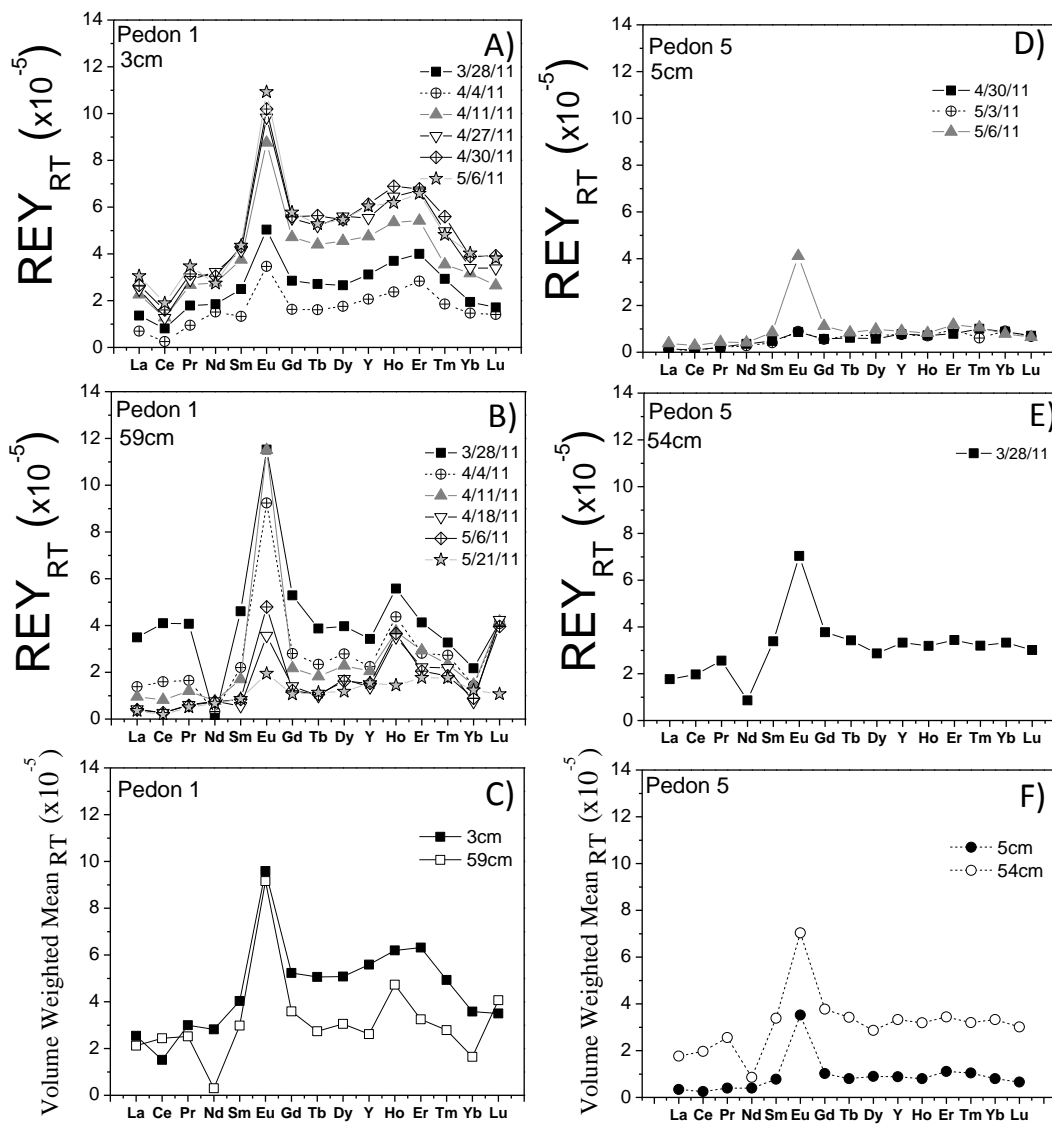


Figure 6 REY fractionation patterns for soil solutions in (A) Pedon 1 at 3cm, (B) Pedon 1 at 59cm, (C) volume weighted mean for Pedon 1, (D) Pedon 5 at 5cm, (E) Pedon 5 at 54cm, and (F) volume weighted mean for Pedon 5. REY were normalized by WA all values.

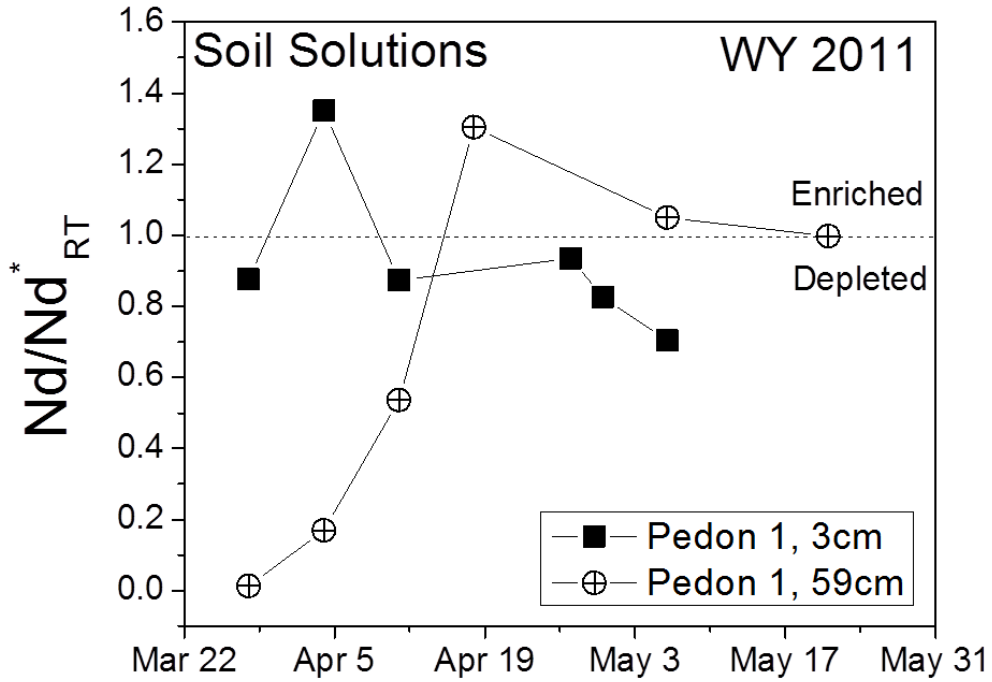


Figure 7 Nd-anomalies in soil solutions sampled by wick lysimeter at pedon 1 during snowmelt WY 2011. All values were normalized by WA all.

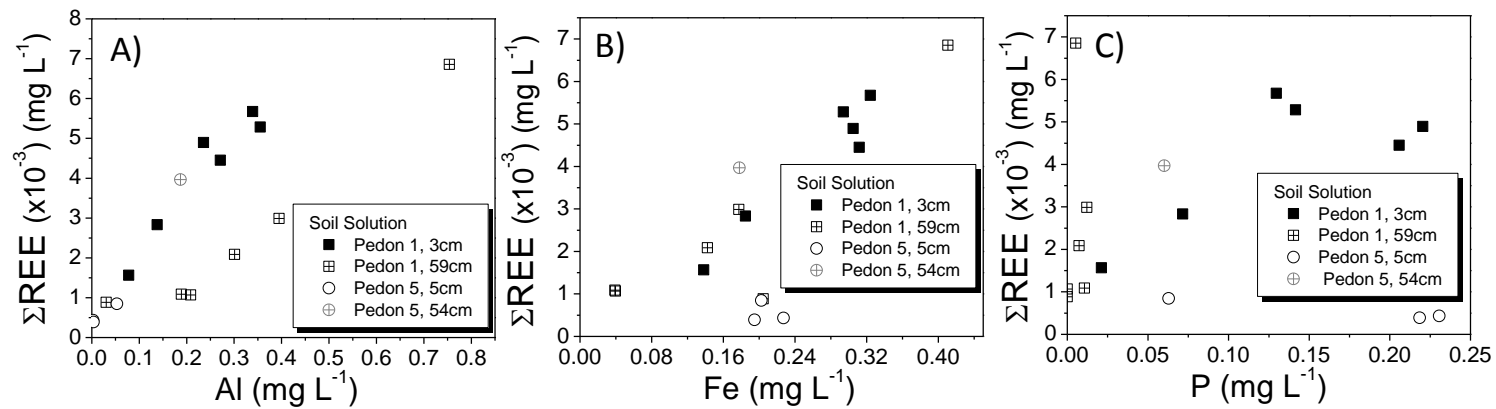


Figure 8 Comparison between (A) ΣREE and Al, (B) ΣREE and Fe, (C) ΣREE and P in soil solutions for Pedons 1 and 5 during the snowmelt event (WY 2011). Eu was excluded. REE are in mg L^{-1} and were not normalized.

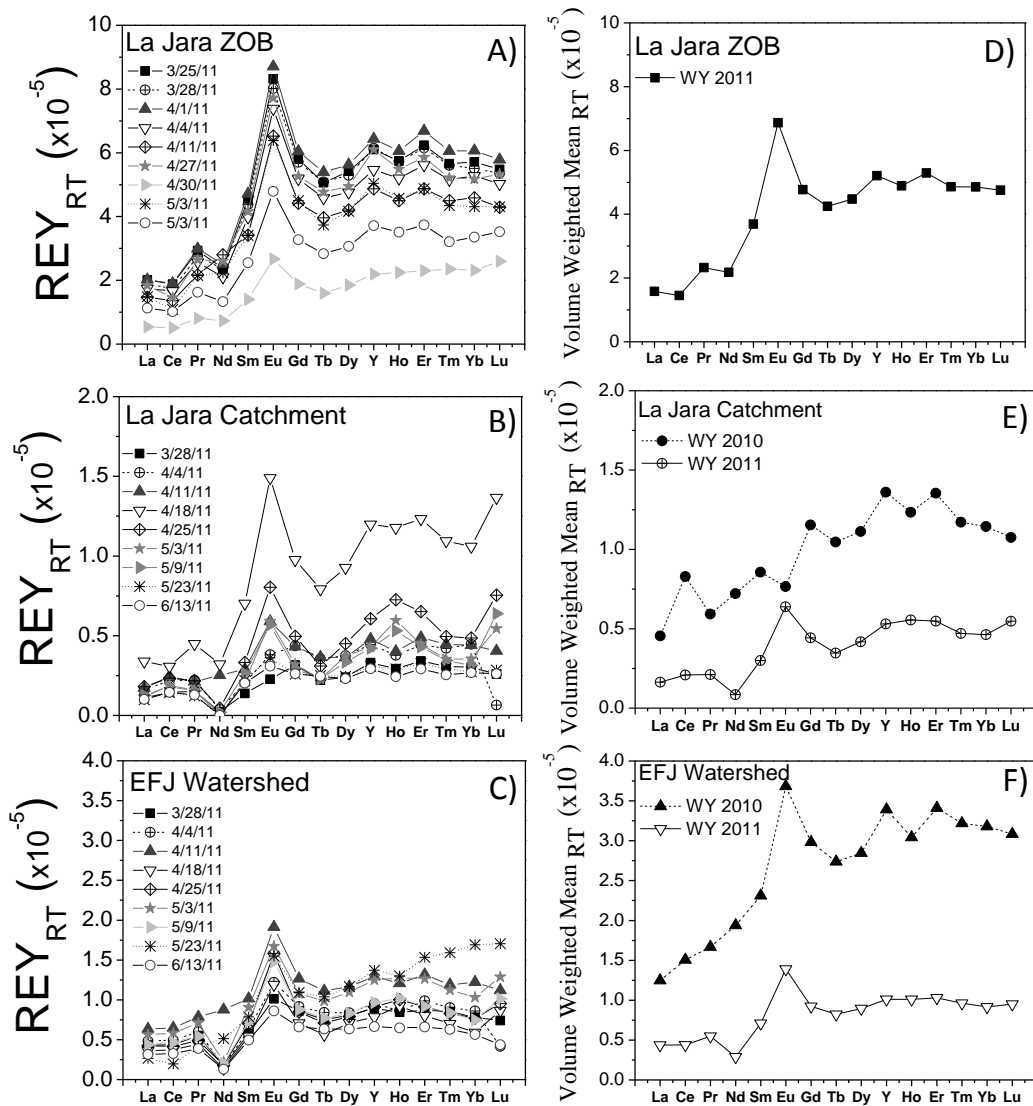


Figure 9 REY fractionation patterns for stream waters at the outlet of (A) La Jara ZOB, (B) volume weighted mean for La Jara ZOB, (C) La Jara catchment, (D) volume weighted mean for La Jara catchment, (E) EFJ watershed, and (F) volume weighted mean for EFJ watershed. REY were normalized by WA all values.

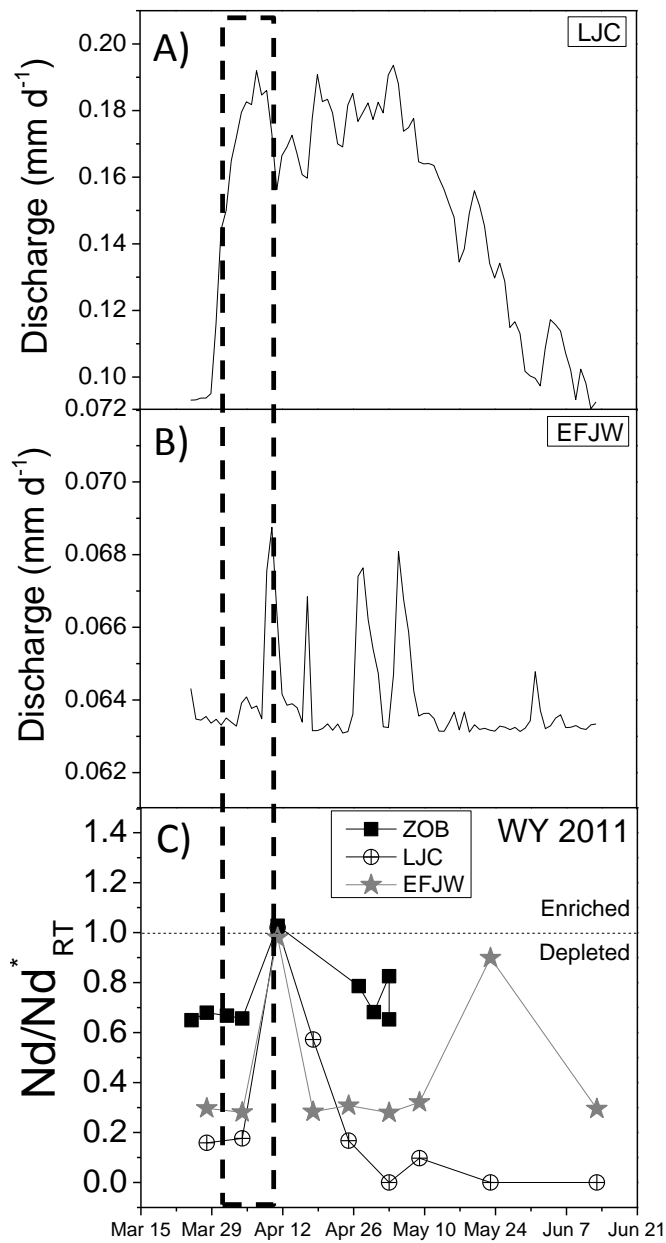


Figure 10 Nd-anomalies in stream waters at the outlet of La Jara ZOB, La Jara Catchment, and East Fork Jemez Watershed during snowmelt WY 2011. All values were normalized by WA all.

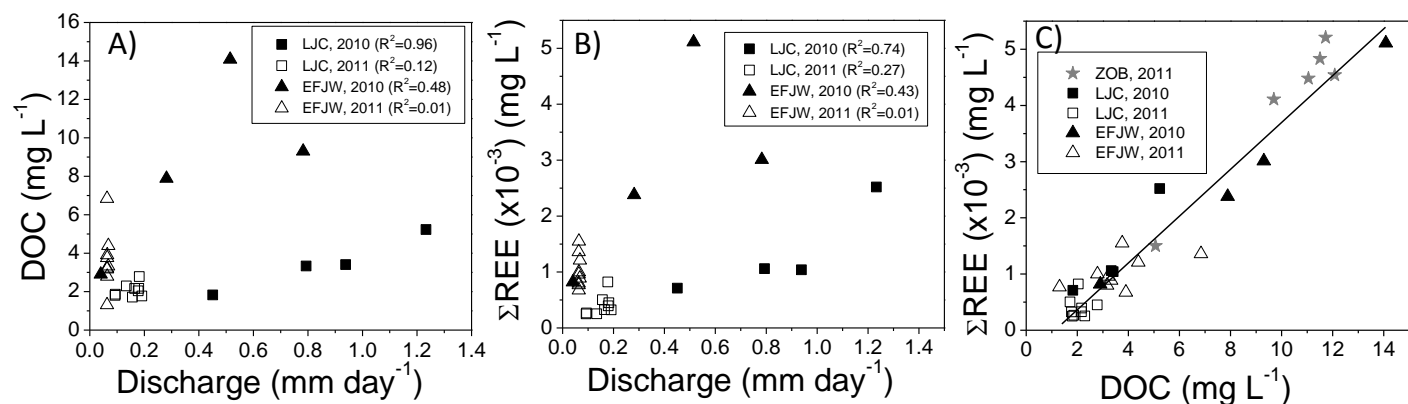


Figure 11 Comparison between (A) discharge versus DOC, (B) discharge versus Σ REE, and (C) DOC versus Σ REE for surface waters at the outlet of La Jara ZOB, La Jara catchment, and EFJ watershed during the snowmelt period for WYs 2010 and 2011. The coefficient of determination (R^2) for the entire data set presented in part C is 0.94. REE are in mg L^{-1} and were not normalized.

APPENDIX C:

**REDISTRIBUTION OF RARE EARTH ELEMENTS AND YTTRIUM (REY) IN
TOPOGRAPHICALLY DISTINCT, RHYOLITE-DERIVED PEDONS**

Angélica Vázquez-Ortega^{a*}, Julia Perdrial^a, David Huckle^b, Craig Rasmussen^a, Mary Kay Amistadi^a, Jennifer McIntosh^b, and Jon Chorover^a

^aDepartment of Soil, Water & Environmental Science, University of Arizona, 1177 East Fourth Street, Tucson, Arizona 85721-0038, USA

^bDepartment of Hydrology and Water Resources, University of Arizona, 1133 East James E. Rogers Way, Tucson, Arizona 85721-0011, USA

*Corresponding author: avazquez@email.arizona.edu

To be submitted to Geoderma

ABSTRACT

Prior studies indicate that patterns of lanthanide series or “rare earth element” and yttrium (REY) depletion or enrichment in soil weathering systems are sensitive to variation not only in lithology, but also in climatic and/or biological processes. For example, organic ligands vary in the stability of their complexes with different lanthanide series metals, which can result in solid-solution fractionation during primary mineral dissolution. Similarly, REY fractionation during precipitation of solution phase metals into solid phase weathering products – such as iron or manganese (oxy)hydroxides, layer silicate clays, or soil organic matter – can be non-stoichiometric, varying with sorbent affinity and aqueous (bio)geochemistry along fluid flow paths. We postulated that patterns of REY fractionation during pedogenic weathering will exhibit coherent trends as a function of depth in the soil profile, and also as influenced by topographic position of the pedon. In soil profiles derived from rhyolitic bedrock overlain by mixed conifer forest in the Jemez River Basin Critical Zone Observatory (JRB-CZO), we observed that REY depletion trends with depth correlate with topographically-induced variation in water and dissolved organic carbon fluxes that occur predominantly during winter snowmelt. To elucidate the secondary weathering products that sequester the fractionated REY in residual soils thus impacted, and to resolve the cause of previously observed depth-dependent trends in europium and cerium anomalies, we conducted sequential chemical extraction of the soils targeting exchangeable, organic, poorly-crystalline to well-crystalline reducible, and residual silicate pools, as a function of depth and location. Higher throughflux of water and carbon through subsurface horizons in the convergent

hillslope position (from lateral flow) resulted in much greater fractionation of REY into subsurface organo-metal colloid forms than occurred in a planar hillslope position, where vertical water and carbon flux was most prevalent. Preferential sequestration of Eu by Mn(IV)-oxides apparently explain patterns of enrichment of Eu in the soil matrix. Positive Ce-anomalies in the solid phase of the ZOB soils were highly correlated with Fe-(oxy)hydroxides as revealed by reductive dissolution of short range order (SRO) and long range order (SRO) Fe-oxides (e.g., ferrihydrite and goethite, respectively).

1 INTRODUCTION

The lanthanide series or “rare earth elements” – elements of atomic number (Z) 57 through 71 – have been used as reactive tracers to elucidate soil biogeochemical weathering processes such as mineral dissolution, argilluviation, redox processes, and biological cycling among others (Vazquez-Ortega et al., in review; Braun et al., 1990; Nezat et al., 2007; Laveuf et al., 2008; Laveuf and Cornu, 2009; Laveuf et al., 2012; Stille et al., 2006a; Stille et al., 2006b; Stille et al., 2009; Goyne et al., 2010; Ma et al., 2011). Dissolution of phosphate minerals such as apatite and monazite have been implicated in controlling REY concentrations in the soil profile (Aubert et al., 2001). By using the MREE-enrichment and the Eu-anomaly, argilluviation has been traced in soils in which the eluviated horizon will display enrichment in MREE and Eu (Cullers et al., 1975). Redox processes have been implicated with preferential immobilization of Ce during pedogenesis, in which Ce is mainly associated with Fe- and Mn-(oxy)hydroxides (Laveuf et al., 2012). Concentrations of REY in natural terrestrial waters, for example, have been shown to correlate strongly with dissolved organic carbon (DOC) concentration, suggesting biological mediation of REY chemical denudation (Johannesson et al., 2004; Tang and Johannesson, 2003). Stille et al. (2006) reported that plants in the Strengbach catchment (mainly beech trees) were preferentially uptaking LREE. Because yttrium (Y, atomic number 39) has a similar outer electron shell structure it is often included as a pseudo-lanthanide with an ionic radius nearly identical to that of holmium (Ho) and consequently similar chemical behavior (Bau et al., 1995; Bau, 1999; Thompson et al., in press).

In low temperature biogeochemical systems, the rare earth elements and yttrium (REY) occur principally as trivalent cations (with the exception of Eu and Ce that can occur as Eu^{2+} or Ce^{4+} depending on redox status) and variation in behavior across the series is therefore attributed to trends in atomic mass, ionic radius (i.e., lanthanide contraction effect), electron configuration, and variation in oxidation state (Bau et al., 1995; Bau, 1999; Ohta and Kawabe, 2001; Davranche et al., 2004; Pourret et al., 2007; Bau and Koschinsky, 2009; Davranche et al., 2011). Plots of REY concentrations across the lanthanide series are typically normalized to reference geological media in order to account for differences in natural abundance, thereby enabling assessment of their fractionation. References used in REY normalization include, but are not limited to, parent materials, soil horizons from the system under investigation or published values such as the upper continental crustal (UCC) mean or chondritic samples (Taylor and McLennan, 1981; Evensen et al., 1978; Anders and Grevesse, 1989). Normalized REY values less than (greater than) unity indicate depletion (enrichment) relative to the selected reference. Preferential enrichment or depletion of individual REY can be assessed by concentration ratios obtained relative to neighboring elements. The distinctive chemical properties that lead to series wide trends in incorporation into (or exclusion from) secondary minerals and/or complexes with natural organic matter make them appropriate for studies of biogeochemical weathering and subsequent solute denudation from the soil profile (Elderfield et al., 1990; Sholkovitz, 1992; Johannesson et al., 1997).

Chemical reactions with dissolved inorganic and organic ligands, solid phase organic matter, layer silicate clays, Fe, Mn, and Al (oxy)hydroxides, as well as variation in redox status have all been reported to influence REY fractionation, transport, and fate in soils (Cullers et al., 1975; Pourret et al., 2007; Laveuf et al., 2008; Laveuf and Cornu, 2009; Goyne et al., 2010; Laveuf et al., 2012). Soluble organic matter forms complexes with REY because of their polyvalent cationic charge (Byrne and Li, 1995; Goyne et al., 2010; Yamamoto et al., 2005). Complexes with natural organic ligands usually favor REE of intermediate (MREE, from Sm to Tb) and heavy (HREE, from Dy to Lu) mass that, because of their smaller ionic radii, tend to form more stable complexes with carboxyl and phenolic hydroxyl groups (Tang and Johannesson, 2010; Pourret et al., 2007; Pourret and Martinez, 2009).

Such effects can influence REY fate during incongruent dissolution reactions. For example, metal-ligand complex stability constants for REE with aliphatic carboxylates (e.g., oxalate) typically increase by over an order of magnitude from La (Z 57) to Lu (Z 71) (Schijf and Byrne, 2001), and these stability constants were shown to correlate with preferential dissolution of higher mass REE from specimen apatite in the presence versus absence of oxalate (Goyne et al., 2010). Complexation of free REE with dissolved fulvic acid in solution has been shown to favor middle rare earth element (MREE) enrichment (Pourret et al., 2007), and capillary electrophoresis studies of REE complexation with a range of humic substances showed REE-humic complex stability increasing by 2-3 orders of magnitude across the lanthanide series, consistent with the lanthanide contraction effect.

Differential reactivity of REY with complexing ligands likely also affects their partitioning into secondary solids where fractionation occurs during both adsorption (Ohta and Kawabe, 2001) and co-precipitation (Braun et al., 1993; Bau, 1999; Bau and Koschinsky, 2009). Iron and manganese oxides, in particular, scavenge REY through one or a combination of co-precipitation, adsorption (surface complex formation and/or ion exchange), and lattice diffusion (Bau, 1999; Ohta and Kawabe, 2001; Bau and Koschinsky, 2009; Davranche et al., 2011; De Carlo and Wen, 1998). Amorphous Fe- and Mn-oxides are postulated to be more enriched in REY than crystalline oxides because as the minerals undergo solid-state transformation and ripening, REY may be expelled from the increasingly constrained crystal structure. However, the degree to which that occurs, and the associated fractionation patterns remain poorly resolved. Fractionation upon secondary (and further) solid formation includes not only that associated with lanthanide contraction, but also radius-independent fractionation. For example, outer electron shell structure is thought to affect systematic variation in Y/Ho ratios that reflect exclusion of Y from co-precipitation in neo-formed Fe(III) oxyhydroxides (Bau, 1999; Bau and Koschinsky, 2009; Thompson et al., in press).

REY patterns affected by soil redox conditions include prominently the development of cerium (Ce) anomalies that can result from Ce(III) to Ce(IV) oxidation. Tetravalent Ce is characterized by particularly low mobility due to strong interaction (via adsorption and/or coprecipitation) with Fe- and Mn-oxides (Laveuf et al., 2008) and, under favorable conditions ($E_h > 300$ mV, slightly acidic to neutral pH, sufficient aqueous Ce concentration), Ce(IV) can precipitate as cerianite (CeO_2) (Feng, 2010).

Cerium oxidation can be coupled to several electron accepting processes - including Mn(IV) oxide (e.g., birnessite) reduction - thereby generating positive Ce anomalies in soils. Under sub-oxic conditions, microbially-catalyzed dissolution of Fe(III)- and Mn(IV)-oxides occurs in preference to that of cerianite, enabling a positive Ce-anomaly to persist despite reductive dissolution and soil profile loss of Fe- and Mn-oxides (Laveuf and Cornu, 2009). Prior studies have shown that amorphous or crystalline Fe-Mn-oxides, nodules, or concretions display a positive Ce-anomaly, highlighting the role of secondary redox active (oxy)hydroxides in Ce fate in soils (Laveuf and Cornu, 2009; Braun et al., 1990; Laveuf et al., 2012).

The REE are adsorbed to the surface of layer silicate clays and (oxy)hydroxides, and the transport of these colloids can result in mobilization of the REY within the soil profile (Coppin et al., 2002). Coppin et al. (2002) reported that at low ionic strength and pH (acidic conditions), REE are adsorbed as outer-sphere complexes onto the basal siloxane surface of smectites. Clay associated mobilization of REY impacts profile-scale patterns because specific silicate clay types can exhibit distinct REY enrichment or depletion; for instance, montmorillonite and kaolinite can exhibit a negative Eu-anomaly attributed to inheritance from source rocks or during diagenesis (Cullers et al., 1975).

The current study relates to our objective of investigating the partitioning of REY between mobile waters and residual weathered soil and rock across a range of sample types and spatial scales in forested terrain derived from rhyolitic bedrock the Jemez River Basin – Santa Catalina Mountains Critical Zone Observatory (JRB-SCM CZO). We seek to evaluate the extent to which lanthanide series mass fractionation can be used to

quantify the relative contributions of “biological weathering”, as reflected e.g., in organic ligand-promoted REY fractionation between mobile fluids and weathering residuum.

Our prior work (Vazquez-Ortega et al., in review) showed that total REY concentrations in catchment effluent (surface water) solutions – ranging from zero order basin (ZOB), to catchment (La Jara) and finally to watershed (East Fork Jemez River) scales – were strongly controlled by DOC concentration. The ZOB in our study site is characterized by the formation of an "intermittent" stream during snowmelt and monsoon periods. Furthermore, that work showed that pedons distributed in different landscape positions contributing to these biotically-driven catchment effluxes of REY exhibited: (1) distinct depth-dependent chemical depletion patterns; (2) pronounced positive Eu-anomalies; and (3) an increase in positive Ce-anomalies with depth (preferential accumulation of Ce in deeper horizons with respect to the parent materials). We hypothesized (i) that REY depletion patterns reflect pedon-specific patterns of water and reduced carbon flux at the pedon scale; (ii) that the positive Eu-anomalies observed in the soil matrix were attributed to the influence of dust deposition and preferential accumulation by secondary (oxy)hydroxide minerals; (iii) that Ce is preferentially accumulated in lower horizons by adsorption onto the surface of layer silicate clays and co-precipitation with Fe-Mn-oxide minerals; and (iv) depth dependent trends in Y/Ho ratio reflect differential incorporation of these elements in pedogenic Fe-(oxy)hydroxide precipitates; despite the fact that no systematic variations in Y/Ho ratios were observed in bulk soils. Therefore, the principal objective of the present study was to quantify mineral and organic phases controlling the retention of REY as a function of depth in pedons

located in distinct landscape positions. To accomplish this in the context of the incongruent weathering reactions of interest (as reviewed above), a sequential chemical extraction procedure was executed to quantify the mass fraction of REY incorporated into soils as adsorbed (and exchangeable) species, versus a variety of potential pedogenic sinks including Mn-oxides (e.g., birnessite), organo-metal colloids, short range order (SRO) Fe-oxides (e.g., ferrihydrite), long range order (LRO) Fe-oxides, (e.g., goethite), and residual silicate materials (Land et al., 1999; Laveuf et al., 2012).

2 MATERIALS AND METHODS

2.1 Study Site and Sample Collection

Soil samples for the present work were obtained from two distinct pedons (pedon 1: planar hillslope position and pedon 5: convergent hillslope position) excavated and instrumented in September 2010 in the Valles Caldera National Preserve, Jemez Spring, NM, within a 0.15 km² mixed conifer zero order basin (ZOB) of the larger La Jara catchment that is part of the East Fork Jemez River Watershed. The instrumented ZOB is the focus of inter-disciplinary surface earth process studies within the Jemez River Basin – Santa Catalina Mountains Critical Zone Observatory (JRB-SCM CZO). The ZOB is south-oriented with dominant SW and SE facing slopes separated by a convergent hollow that displays negligible surface flows outside of high discharge events and then only at the ZOB outlet (flume location). Soils are established on rhyolitic volcanoclastic parent materials of Pleistocene age. Bedrock comprises a mixture of fine-grained porphyritic rhyodacite and zeolitilized Bandelier Tuff

(<http://geoinfo.nmt.edu/publications/maps/geologic/ofgm/>). Outcrop samples of porphyritic rhyodacite and zeolitized Bandelier Tuff rocks (parent materials) were collected in summer 2010 around Redondo Dome in order to span the range of lithologic variation. Soil samples were collected by genetic horizon, sealed in zip-lock bags and stored at 4°C, until further analysis. Upon return to the lab, soil samples were air dried, sieved to recover the < 2 mm fraction, homogenized, and stored at room temperature prior to further chemical analysis.

The same pedons from which samples are derived were instrumented in September 2010 with a set of subsurface biogeochemistry instrumentation that included passive capillary soil solution (i.e., “PCap” or “wick”) samplers (Perdrial et al., 2012). Flux values for dissolved organic carbon (DOC) were determined by taking the product of water mass (kg) and DOC concentration (mg kg^{-1}) for each sampling date, summing these products across all sampling dates over the water year, and normalizing the result to the cross-sectional area of the wick sampler plate. The same was done to calculate total dissolved REY fluxes. Samples were filtered through combusted 0.7 μm glass fiber filters (GF/F, Whatman, Alameda Chemical & Scientific Inc., Oakland, CA) for DOC or through 0.45 μm nylon filters (Millipore, Thermo Fisher Scientific) for metals, into separate acid washed HDPE bottles and transported in cool conditions ($\sim 4^\circ\text{C}$) to the laboratory within a maximum of 2 d after sampling.

2.2 Solid Phase Characterization

Bulk soil samples (planar and convergent positions) and parent materials (porphyritic rhyodacite and zeolitized Bandelier Tuff) were analyzed for total elemental

composition by lithium metaborate/tetraborate fusion followed by inductively coupled plasma optical emission spectrometry (ICP-OES) and mass spectrometry (ICP-MS) analysis of total elemental concentrations (Activation Laboratories, Ancaster, Ontario). Total organic carbon in the bulk solid samples was determined by high temperature oxidation followed by infrared detection of CO₂ using a Shimadzu TOC-VCSH system equipped with a solid sample module SSM-5000A (Columbia, MD). Mineralogy and particle size composition for soils included in this study were described in Vazquez-Ortega et al., in review.

2.3 Sequential Chemical Extractions

Two soil profiles – planar and convergent hillslope positions- were selected for the detailed investigation described herein because of their distinctive REY chemical depletion trends (Figure 2, top). Genetic horizons from both of these pedons were subjected to a five-step sequential extraction (SE) scheme, summarized in Table 1 (adapted from Land et al., 1999 and Laveuf et al., 2012). Sequential extractions were performed in triplicate on 1.0 g samples of air dried soil (with mass measured to four decimal places). The SE scheme resulted in six chemically distinct REY fractions targeting those that are bound to the solid phase as species that are (Table 1): adsorbed (exchangeable) (Step 1), in reducible Mn-oxides (Step 2), in organo-metal complexes and dispersible colloids (Step 3), in reducible short range order (SRO) Fe-oxides (Step 4), in long range order (LRO) Fe-oxides (Step 5), and retained in the residual pool, mainly consisting of silicate minerals. Each extraction step was followed by a rinse with

ultrapure water for 30 min with a 1:20 solid to solution mass ratio at room temperature. Extractions and rinses were shaken at 100 rpm followed by centrifugation at 18,500 relative centrifugal force (RCF) for 30 min and finally filtered through a 0.2 μm cellulose acetate membrane. The rinses were combined into the supernatant solutions for each extraction, with the residual solids subjected to further extraction. Soil-free controls ('blanks') for the five steps were carried out in triplicate as well.

Dissolved organic carbon (DOC) concentrations in PCap water samples and associated with the organo-metal colloid (step 3) and SRO Fe-oxide (step 4) of the SE were determined by high temperature combustion followed by infrared detection of CO_2 (Shimadzu TOC-VCSH, Columbia, MD). Rare earth element and yttrium (REY) concentrations in soil water and extraction solutions were determined by ICP-MS (Perkin Elmer DRC II, Shelton, CT). The reported isotopes include: ^{56}Fe , ^{27}Al , ^{31}P , ^{89}Y , ^{139}La , ^{140}Ce , ^{141}Pr , ^{142}Nd , ^{147}Sm , ^{153}Eu , ^{157}Gd , ^{159}Tb , ^{164}Dy , ^{165}Ho , ^{166}Er , ^{169}Tm , ^{174}Yb , ^{175}Lu . Rhodium (Rh) was included as an internal standard for Fe, Al and P and Indium (In) was used for REY based on similarities in first ionization potential. Customized calibration standards were prepared for each sequential extraction step matching the matrix composition to that of the samples prepared for ICP-MS analysis.

2.4 Mass Balance and Fractionation Calculations

REY concentrations per unit mass of sample for each extraction ($\mu\text{g kg}^{-1}$) were normalized by the total corresponding elemental mass concentration for the genetic horizon for which the extraction was performed.

Non-dimensionalized europium and cerium anomalies (Eu/Eu^* and Ce/Ce^*) and Y/Ho ratios were calculated as (Braun et al., 1998):

$$\frac{Eu}{Eu^*} = \frac{Eu}{(Sm)^{0.5} \times (Gd)^{0.5}} \quad \mathbf{Eq. 1}$$

$$\frac{Ce}{Ce^*} = \frac{Ce}{(La)^{0.5} \times (Pr)^{0.5}} \quad \mathbf{Eq. 2}$$

where Eu, Sm, Gd, Ce, La and Pr correspond to REE concentrations (per unit mass of soil) in a given extract normalized by the total for a given genetic horizon. Eu/Eu^* and Ce/Ce^* values (in extracted fraction) higher than unity represent positive anomalies (enrichment) and values lower than unity represent negative anomalies (depletion) with respect to the genetic horizon.

Chemical enrichment or depletion relative to parent rock for bulk soils collected at the ZOB were determined using the following equation (Brantley et al., 2007):

$$\tau = \left(\left[\frac{C_{a,soil}}{C_{Ti,soil}} \div \frac{C_{a,parent\ material}}{C_{Ti,parent\ material}} \right] - 1 \right) \quad \mathbf{Eq. 3}$$

where Ti was chosen as the representative “immobile” element, C_a corresponds to the REY concentration in the bulk soil ($mg\ kg^{-1}$), and C_{Ti} corresponds to Ti concentration in the parent material ($mg\ kg^{-1}$). In order to permit direct comparison of the REY tau values for all hillslope positions, REY concentration data were normalized to a weighted average of ZOB bedrock concentrations. Since both porphyritic rhyodacite and zeolitilized Bandelier Tuff contribute to the parent rock composition of the site, their fresh rock compositions were analyzed for REY concentrations, and the mean REY signatures were calculated from the mapped fractional coverage of the two bedrock types in the ZOB (<http://geoinfo.nmt.edu/publications/maps/geologic/ofgm/>). The tau values

were generated from a weighted average based in the following abundances of porphyritic rhyodacite (0.44) and zeolitized Bandelier Tuff (0.56), since that corresponds to the average bedrock composition. Tau values higher than (less than) zero represent enrichment (depletion) relative to parent rock.

3 RESULTS

3.1 Water, DOC and REY through-flux in Planar and Convergent Pedon

Locations

The planar and convergent hillslope locations exhibit distinct patterns in water, DOC, and REY through-flux, as measured with passive capillary samplers (PCaps) installed at the time of soil sampling in September 2010 (Perdrial et al., 2012) and monitored for the water years 2011-2013. Higher carbon flux at depth in the convergent site is evident, and it attributes to this site the greater amount of accumulated solid phase OC at depth (Fig. 1 and 2).

3.2 REY Signatures of Landscape Location

The planar and convergent hillslope locations exhibit distinctly different depth-dependent chemical depletion (Eq. 3) trends in the solid phase for the light, medium and heavy rare earth elements (LREE, MREE and HREE), respectively (Fig. 2, *top*). For the planar site, depletion decreases with depth from the surface, whereas the inverse trend is observed for the convergent site. These divergent trends, which are qualitatively consistent with site-specific differences in the depth distribution of water, DOC and REY flux (Fig. 1) motivated the SE study.

The total mass of REY (Σ REY) depicted in the top of Figure 2 was differentially fractionated across operationally-defined metal pools as shown quantitatively for planar and convergent hillslope locations, respectively (Figure 2, *bottom*). In planar site, the largest REY fraction was associated with the residual (mainly silicate minerals) pool ranging from 0.77 to 0.80, depending on depth (Figure 2C). Among all non-silicate pools targeted in the sequential extraction, “organo-metal colloids” comprised the largest fraction of the O horizon, and then showed a decrease with depth (from 0.2 to 0.04). The second most abundant fraction was released during extraction targeting the SRO Fe-oxides, and this fraction showed an incremental increase with depth (from 0.05 to 0.1). A small “exchangeable” REY fraction increased with depth (from 0.007 to 0.03), whereas Mn-oxide associated REY were highest in the B1 horizon (0.05). A small (0.02 to 0.05) fraction was consistently released during extraction targeting LRO Fe-oxides.

In the convergent site, REY abundance in extracted fractions decreased in the order: residual (0.46 to 0.88), organo-metal colloids (0.03 to 0.3), SRO Fe-oxides (0.02 to 0.07), LRO oxides (0.01 to 0.07), exchangeable (0.01 to 0.05), and Mn-oxides (0.003 to 0.06). Organo-metal colloids comprised a much larger fraction of the total REY pool in the convergent (relative to planar) hillslope location. In contrast, the residual pool was smaller in the convergent site.

3.3 REY Signatures of Extractable Pools

To explore radius-dependent fractionation trends, REY patterns are plotted for all SE extraction steps in Figures 3-4 using the convention of Bau and co-workers, where Y is included to the left of Ho, consistent with its ionic radius. These plots (discussed in

order of SE step below) also reveal that coherent lanthanide contraction effects control the fractionation of REY among the operationally-defined pools for all soil samples.

3.3.1 *Exchangeable REY*

Step 1 targeted the REY cations adsorbed to negatively-charged soil particle surfaces that are exchangeable with Na^+ at pH 5.5. In both landscape positions, the exchanged REY showed an enrichment in MREE relative to HREE (hillslope: MREE/HREE ranging from 1.73 to 3.16; convergent: MREE/HREE ranging from 1.15 to 1.75) (Figures 3A and D). Pronounced positive Eu-anomalies were observed for this extraction in all horizons; planar site Eu/Eu^* values range from 1.2 to 6.0, convergent site Eu/Eu^* values range from 1.2 to 2.0 (Fig. 5A). In contrast, the exchangeable REY exhibited “negative” (i.e., downward) Ce-anomalies (Ce/Ce^*) ranging from 0.14 to 0.72 for the planar site and from 0.18 to 0.71 for the convergent site (Fig. 6A). No systematic variations in Y/Ho ratios were observed in the “exchangeable” REY fraction (Fig. 7A).

3.3.2 *Mn-oxide-bound REY*

In both soil profiles, the Mn-oxide extraction gave rise to pronounced positive Eu-anomalies (Eu/Eu^*) in almost all horizons: from 1.00 to 33.04 in the planar site and from 1.15 to 10.34 in the convergent site, with the larger value attributed to the O horizon in both locations (Fig. 5B). Aside from the surface (O) horizon in planar profile and the deepest subsurface (B3) horizon in convergent profile, which showed small and large positive Ce anomalies, respectively, the Mn oxide fraction exhibited a small negative Ce anomaly. The Mn-oxide fraction exhibited Y enrichment with coherent dependent decrease in Y/Ho ratios as a function of depth (Fig. 7B).

3.3.3 REY in organo-metal colloids

In the planar site surface (O and A horizon) soils, the Na-pyrophosphate dispersible organo-metal colloids showed MREE enrichments ranging from 1.23 to 1.48 (MREE/HREE) (Figure 3C). In contrast, deeper horizons exhibited a slight LREE enrichment (B2 horizon: LREE/HREE = 1.10 and B3 horizon: LREE/HREE = 1.45). Slightly negative Eu-anomalies were observed in organo-metal colloids of the lowest horizons (Eu/Eu^* ranges from 0.83 to 0.89) (Fig. 5C). The organo-metal colloid pool exhibited coherent dependent increase in Ce/Ce^* as a function of depth (Fig. 6C). In the convergent soils, all horizons showed a MREE enrichment with respect to the LREE fraction (LREE/MREE ranging from 0.62 to 0.76) (Fig. 4C), Eu concentrations did not exhibit anomalous behavior (Fig. 5C), and only the B3 horizon exhibited a pronounced Ce-anomaly ($[\text{Ce}/\text{Ce}^*] = 3.10$) (Fig. 6C). Middle horizons in both sites showed slightly depletion in Y (determined from Y/Ho ratios) (Fig. 7C). The dispersible organic carbon (OC) in the planar hillslope soils decreased as a function of depth, but in the convergent soils it remained relatively high and similar to the upper horizons (Figure 8A). In general, higher concentrations of pyrophosphate dispersible OC were observed in the convergent site relative to planar site.

3.3.4 SRO Fe-oxide-bound REY

The SRO Fe-oxides in both profiles were depleted in HREE (LREE/HREE ranges from 1.21 to 2.71) and, for the planar site, the depletion trends increase with depth (Figure 4 A and D), with the exception of B3 horizon (LREE/HREE = 0.62). For the planar site, positive Eu-anomalies were observed for SRO Fe-oxides in the O, A, and B3

horizons (Fig. 5D), whereas for the convergent site, Eu concentrations did not exhibit anomalous behavior (Fig. 5D). This extraction revealed an incremental increase in Ce/Ce^* as a function of depth for the planar site, whereas for the convergent site, only the B3 horizon exhibited a Ce-anomaly ($[Ce/Ce^*] = 1.81$) (Fig. 6D). The SRO Fe-oxides fraction exhibited Y depletion (exception of O horizon) with coherent dependent decrease in Y/Ho ratios as a function of depth (Fig. 7D). Lower OC concentrations were observed in the SRO Fe-oxide extraction as compared to the organo-metal colloid extraction (Figure 8B).

3.3.5 *LRO Fe-oxide-bound REY*

In the planar site, a small fraction of REY was associated with the LRO Fe-oxides (i.e., goethite) with the O horizon being most enriched (Figure 4E) and Eu/Eu^* ranged from 0.96 to 1.72, with the largest value associated with the B3 horizon (Fig. 5E). An incremental increase in Ce/Ce^* was observed as a function of depth in the LRO Fe-oxide phase (Fig. 6E), similar to the trend observed for SRO Fe-oxides. In contrast to the planar site, Ce/Ce^* values in the convergent soils decreased with depth (Fig. 6E). The LRO Fe-oxides fraction exhibited Y depletion with coherent dependent decrease in Y/Ho ratios as a function of depth (Fig. 7E).

3.3.6 *Residual REY signatures*

Residual (non-extracted) materials in both hillslope locations showed a concave upward pattern, although this was particularly evident for the convergent site signaling enrichment in HREE and depletion of MREE. For planar site, MREE/HREE ranges from 0.43 to 0.61, whereas for the convergent site it ranges from 0.30 to 0.63) (Figures 4C and

F). Residual materials were in both hillslope locations generally depleted in Eu (Figures 4C and F). Ce/Ce^* values of SE residual decreased with depth in both sites, with slightly negative and slightly positive anomalies in the planar and convergent hillslopes, respectively (Fig. 6F). No systematic variations in Y/Ho ratios were observed in the residual fraction (Fig. 7F).

4 DISCUSSION

4.1 Role of water and dissolved organic carbon flux on REY fraction

The influence of water and dissolved organic carbon flux on REY fractionation and transport in temperate soils located in a mixed conifer ZOB was evaluated using two distinct soil profiles, planar and convergent sites. Higher reduced organic carbon and water fluxes at depth in the convergent site were observed across all sampling dates over the water years 2011, 2012, and 2013, resulting in higher REY transport (determined from $\sum REY$ fluxes) relative to the planar site (Fig. 1). Soil profiles exhibited a distinct depth-dependent REY depletion patterns, attributing to the convergent site a higher degree of depletion with depth than in the planar site (Fig. 2). Water and DOC fluxes (WY 2011, 2012, and 2013) were correlated with $\sum REY$ in the solid matrix ($mg\ kg^{-1}$) (data not shown) for both sites, resulting in negative correlations which indicate that high water and DOC fluxes are inducing a REY depletion in the solid matrix. These results highlight the key role of organo ligand-promoted REY fractionation between mobile fluids and weathering residuum.

Among the non-silicate fractions, the organo-metal complexes and dispersible colloids (Step 3 in the SE) displayed a large mass fraction of REY associated with this operationally-defined pool. REY concentrations associated with the colloidal fraction in the convergent site remained relatively high and similar across the soil profile. A MREE downward concavity was evidenced in the REY fractionation patterns of the colloidal fraction, indicating the preferential MREE transfers from primary (silicates) to secondary (organic and Al-, Fe-(oxy)hydroxide colloids) phases.

Tang and Johannesson (2010) indicated that in the absence of organic ligands, a small amount of REE was extracted from aquifer sediments. In contrast, when dissolved organic matter extracting solutions were employed, a larger amount of REE was released from the system and a MREE downward concavity pattern was observed in the extracted solutions (in agreement with our observations). The $\sum\text{REE}/\text{DOC}$ molar ratios (REE loading effect) have been used to predict the apparent stability constants between REE and organic matter complexes (Tang and Johannesson 2010; Yamamoto et al., 2005; Sonke and Salters, 2006; Pourret et al., 2007; Yamamoto et al., 2010). The $\sum\text{REE}/\text{DOC}$ molar ratios in our extraction solutions (in specific, in organo-metal colloids) ranged from 9×10^{-5} to 6×10^{-4} for the planar site and from 2×10^{-4} to 3×10^{-4} for the convergent site. Our results are in agreement to those reported in Tang and Johannesson (2010). The authors concluded that the MREE downward concavity pattern was observed as a consequence of the apparent stability constants of REE and humic substance complexes.

4.2 Weathering controls on REY pattern formation

Biogeochemical processes affecting REY fractionation and mobilization include: 1) organo-metal complexes (dissolved organic matter or colloidal), 2) adsorption and co-precipitation by neo-precipitated Fe and Mn-(oxy)hydroxides, and 3) redox conditions among others (De Carlo and Wen, 1998; Bau, 1999; Ohta and Kawabe, 2001; Davranche et al., 2004; Johannesson et al., 2004; Steinmann and Stille, 2006; Steinmann and Stille, 2008; Bau and Koschinsky, 2009; Laveuf and Cornu, 2009; Davranche et al., 2011; Xiong, 2011).

4.2.1 Processes that favor Ce anomalies in soil profiles

It is known that redox conditions can influence Ce fractionation and sorption/desorption processes in soils (Braun et al., 1990; Davranche et al., 2011; Bau, 1999; Ohta and Kawabe, 2001; Bau and Koschinsky, 2009; Laveuf et al., 2012). The oxidation of Ce (III) induces changes in ionic charge and radius that induces the decoupling of Ce(IV) from the rest of the lanthanide group (REE), thereby promoting its solid phase incorporation, generating positive Ce anomalies in soils (Feng, 2010; Laveuf et al., 2012). Fe- and Mn-oxides have been reported to display positive Ce-anomalies (De Carlo and Wen, 1998; Braun et al., 1990; Ohta and Kawabe, 2001; Laveuf et al., 2008; Laveuf et al., 2012; Bau, 1999; Bau and Koschinsky, 2009).

In the planar site, a large mass fraction of Ce (obtained from SE) was associated with the SRO Fe-oxide pool in which Ce concentrations increased with depth (Fig E.1, electronic annex). In contrast, in the convergent site, Ce was mainly associated with the organo-metal colloid pool. Distribution coefficients (K_d) for Ce reported by Ohta and

Kawabe (2001) indicate that Mn-oxides have a higher affinity for Ce than for Fe-(oxy)hydroxides. Interestingly, Ce in our study has an apparently higher affinity for Fe-(oxy)hydroxides than for Mn-oxides . Also, pronounced positive Ce-anomalies (in the planar site) were revealed after the reductive dissolution of the SRO and LRO Fe-oxides in which the anomalies increased systematically with depth, suggesting preferential accumulation of Ce in these pools (Figures 6D and E). Mass balance values for Ce were more similar to Fe than to Mn, indicating probably higher association of Ce with Fe-oxides in the ZOB bulk soils (Figure 9). It is important to emphasize that Fe concentrations (reported in g kg⁻¹) in the bulk soil of the planar site were several orders of magnitude higher than Mn (Table 2). The higher abundance of Fe in the bulk soils can indicate a large prevalence of Fe-oxides over Mn-oxides, attributing to Fe-oxides higher reactivity (active sites readily available for Ce sequestration). Also, a small mass fraction of Mn was extracted during the reductive dissolution of the SRO and LRO Fe-oxide steps (steps 4 and 5), attributing primarily the Ce signature to the Fe-oxide pools (Table 3). Bau and Koschinsky (2009) observed positive Ce anomalies in Fe-oxides precipitated into marine ferromanganese crusts, suggesting that in the marine system, oxidative scavenging of Ce is not restricted to Mn(IV) oxides, but also includes Fe(III) oxides.

Vazquez-Ortega et al (paper in review) reported an incremental increase in positive Ce-anomalies as a function of depth in the solid phase of the ZOB soils (current study site). In addition, the study reported negative Ce-anomalies in soil solutions at the upper horizon of the planar site during the snowmelt of WY 2011. The negative anomalies indicated the prevalence of Ce⁺⁴ (oxic conditions) which exhibit high solid

phase retention; therefore, soil solutions were depleted in Ce (Feng, 2010). On the other hand, soil solutions at the bottom horizon ranged from no anomalous behavior to negative Ce-anomalies during the snowmelt period (WY 2011), indicating a progressive change in redox conditions from reducing to oxidizing conditions and further accumulation of Ce to the solid phase. In summary, the systematic increase of the positive Ce-anomalies in the bulk soil with depth (Vazquez-Ortega et al, in review) and their correlation with Ce-anomalies in the SRO (i.e., ferrihydrite) and LRO (i.e., goethite) Fe-oxide pools (SE in the planar site) with depth provided strong evidence on the role of Fe-oxides on Ce sequestration.

4.2.2 Processes that favor Eu anomalies in soil profiles

Reduction of Eu requires strong reducing conditions rarely encountered in low pressure-temperature systems (Panahi et al., 2000; Laveuf and Cornu, 2009), and Eu(II) predominates in magmatic systems, where primary silicate minerals such as feldspars often show positive Eu-anomalies because of substitution into Ca^{2+} sites, where the trivalent REE are excluded (Aubert et al., 2001). When these rocks undergo surficial weathering in oxic environments, Eu^{2+} is released and readily oxidized (Panahi et al., 2000). The fractionation, transport and fate of Eu in soils can be influenced by the biogeochemical processes involved during soil pedogenesis (e.g. incorporation onto silicate clay and Mn-oxide minerals and organic phases).

The current study revealed that among all the chemical extraction steps, the reductive dissolution of Mn-oxides (Step 2) exhibited the largest positive Eu-anomalies and the anomalies decreased systematically with depth in both soil profiles (Figure 5B),

indicating preferential sequestration of Eu by this pool with respect to Sm and Gd (neighbors in the periodic table). Manganese oxides have been reported to scavenge REY (Bau, 1999; Ohta and Kawabe, 2001; Bau and Koschinsky, 2009; Davranche et al., 2011; De Carlo and Wen, 1998). Mn-oxides are characterized by having negative structural and pH-dependence charge due to the presence of Mn(III), vacant sites and soil solution pH conditions; as a result, metal cations (including REY) are adsorbed to cancel the negative charge. At deeper horizons, Mn-oxides can be subjected to reducing conditions due to fluctuations in water table inducing the reductive dissolution of Mn-oxides; therefore, soluble Mn^{+2} along with associated Eu can be leached from the lower horizons, explaining the lower mass fraction of Eu associated with this pool with depth. It is likely that during the formation Mn(IV)-oxides, Eu was incorporated into the oxides contributing to pronounced positive Eu-anomalies in the soil matrix. In addition, among the non-silicate minerals, a large mass fraction of Eu was associated with the organo-metal colloid pool (to a larger extent in the convergent site), suggesting that this pool play an important role on Eu transport and fate as well (Fig E.1, electronic annex).

4.2.3 Processes that favor Y/Ho fractionation

The outer electron shell structure of Y^{3+} with empty $4f$ electron shell induces a low polarizability (less propensity of charge distribution) and tendency to form less covalent metal-ligand bonds with organic acids (Peppard et al., 1969; Byrne and Lee, 1993). The Misono softness parameter ' Y ' is employed to characterize the Lewis acid hardness of REY. Yttrium exhibits a Misono softness of 0.20 (lowest among all REY), leading to expect anomalous Y behavior. Systematic variation in Y/Ho ratios in soils that reflect

exclusion of Y from co-precipitation in neo-formed Fe(III) oxyhydroxides has been previously reported (Bau, 1999; Bau and Koschinsky, 2009; Thompson et al., in press).

The chemical extraction revealed that Fe-oxides (SRO and LRO) in the planar and convergent hillslope profiles were depleted in Y (exception of O horizon) with coherent dependent decrease in Y/Ho ratios as a function of depth. The anomalous Y/Ho ratios reflect differential incorporation of these elements in pedogenic Fe-(oxy)hydroxide precipitates. Contrary, Mn-oxides were enriched in Y with a larger enrichment in the upper horizons. Bau and Koschinsky (2009) reported Lu-normalized apparent mineral/seawater partition coefficients for Mn- and Fe-oxides ($K_D^{\text{REY-Oxide/REY-sw}}_{\text{Lu}}$) and concluded that Y was more depleted in the Fe-oxides than in the Mn-oxides. Furthermore, among the non-silicate minerals, a large mass fraction of Y and Ho was associated with the organo-metal colloid pool (to a larger extent in the convergent site), suggesting that this pool play an important role on Y and Ho transport and fate in the ZOB soils (Fig E.2, electronic annex).

5 SUMMARY AND CONCLUSIONS

This study seeks to evaluate the use of the lanthanide series (REE) and yttrium (“geochemical twin” of Ho) as reactive tracers of biogeochemical weathering processes on soil profiles with topographically-induced variation in water and dissolved organic carbon fluxes. For this purpose, REY fractionation patterns and mass fraction calculations were obtained from operationally defined chemical extractions in two distinct soil profiles (planar and convergent sites). The experiments were designed to

quantify mineral or organic phases controlling the retention of REY as a function of depth to further understand the REY fractionation between mobile fluids and weathering residuum in soil profiles.

In the convergent site, REY fractionation during pedogenic exhibited coherent depletion trends with depth. Opposite trends were observed in the planar site, attributing higher degree of depletion to the upper horizons. The REY fractionation patterns, in the planar site, developed after the reductive dissolution of Fe-oxides (SRO and LRO) revealed pronounced positive Ce-anomalies with systematically increase with depth, suggesting preferential accumulation of Ce in these pools. These results are consistent with a large mass fraction of Ce associated with the SRO Fe-oxides, providing strong evidence on the role of Fe-oxides on Ce sequestration.

Preferential sequestration of Eu by Mn(IV)-oxides apparently explain patterns of enrichment of Eu in the soil matrix. Also, a large mass fraction of Eu was associated with the organo-metal colloids, highlighting the key role of organo ligand-promoted REY fractionation. The systematic decrease in Y/Ho ratios in both sites for the Fe-oxide pools reflected differential incorporation of these elements in pedogenic Fe-(oxy)hydroxide precipitates.

Since REE mobility can be affected by the same processes that influence trace metals (Cu, Cr, Co, Ni, Pb, U, Th) mobility in solution (Grybos et al., 2007); REE have been postulated to be a very useful tool that allow us to learn more about biogeochemical weathering processes in natural systems. In this study site, for instance, a MREE downward concavity pattern was revealed in the organo-metal colloid pool, suggesting

the formation of stable REE and humic substance complexes. The organo-metal colloid pool strongly influenced trace metal mobilization in the convergent site which was characterized by high water and reduced OC fluxes at depth. This study also highlights the significant role of Mn and Fe -(oxy)hydroxides pools as sorbents for REE (possibly other trace metals).

Acknowledgements

The Jemez-Santa Catalina Critical Zone Observatory is supported by the National Science Foundation, Grant # EAR-0724958 and EAR/IF-0929850. Thanks to Mary Kay Amistadi, Juliana Gil, Mark Losleben, Scott Compton, Caitlin Orem, and Mercer Meding for assistance with sampling and analysis. Thanks to Matej Durcik for help with GIS.

References

- Aubert, D., Stille, P. and Probst, A., 2001. REE fractionation during granite weathering and removal by waters and suspended loads: Sr and Nd isotopic evidence. *Geochim. Cosmochim. Acta*, 65:387-406.
- Anders, E. and Grevesse, N., 1989. Abundances of the elements - meteoritic and solar. *Geochim. Cosmochim. Acta*, 53:197-214.
- Aubert, D., Stille, P. and Probst, A., 2001. REE fractionation during granite weathering and removal by waters and suspended loads: Sr and Nd isotopic evidence. *Geochim. Cosmochim. Acta*, 65:387-406.
- Bau, M., 1999. Scavenging of dissolved yttrium and rare earths by precipitating iron oxyhydroxide: experimental evidence for Ce oxidation, Y-Ho fractionation, and lanthanide tetrad effect. *Geochim. Cosmochim. Acta*, 63:67-77.
- Bau, M., Dulski, P. and Moller, P., 1995. Yttrium and holmium in south-pacific seawater - vertical-distribution and possible fractionation mechanisms. *Chem Erde-Geochem.*, 55:1-16.

- Bau, M. and Koschinsky, A., 2009. Oxidative scavenging of cerium on hydrous Fe oxide: evidence from the distribution of rare earth elements and yttrium between Fe oxides and Mn oxides in hydrogenetic ferromanganese crusts. *Geochem. J.*, 43:37-47.
- Brantley, S.L., Goldhaber, M.B. and Ragnarsdottir, K.V., 2007. Crossing disciplines and scales to understand the Critical Zone. *Elements*, 3:307-314.
- Braun, J.J., Viers, J., Dupre, B., Polve, M., Ndam, J. and Muller, J.P., 1998. Solid/liquid REE fractionation in the lateritic system of Goyoum, east Cameroon: the implication for the present dynamics of the soil covers of the humid tropical regions. *Geochim. Cosmochim. Acta*, 62:273-299.
- Braun, J., Pagel, M., Herbillon, A. and Rosin, C., 1993. Mobilization and redistribution of REEs and thorium in a syenitic lateritic profile - a mass-balance study. *Geochim. Cosmochim. Acta*, 57:4419-4434.
- Braun, J., Pagel, M., Muller, J., Bilong, P., Michard, A. and Guillet, B., 1990. Cerium anomalies in lateritic profiles. *Geochim. Cosmochim. Acta*, 54:781-795.
- Byrne, R. and Lee, J., 1993. Comparative yttrium and rare-earth element chemistries in seawater. *Mar. Chem.*, 44:121-130.
- Byrne, R. and Li, B., 1995. Comparative complexation behavior of the rare-earths. *Geochim. Cosmochim. Acta*, 59:4575-4589.
- Coppin, F., Berger, G., Bauer, A., Castet, S. and Loubet, M., 2002. Sorption of lanthanides on smectite and kaolinite. *Chem. Geol.*, 182:57-68.
- Cullers, R., Chaudhuri, S., Arnold, B., Lee, M. and Wolf, C., 1975. Rare-earth distributions in clay-minerals and in clay-sized fraction of Lower Permian Havensville and Eskridge shales of Kansas and Oklahoma. *Geochim. Cosmochim. Acta*, 39:1691-1703.
- Davranche, M., Pourret, O., Gruau, G. and Dia, A., 2004. Impact of humate complexation on the adsorption of REE onto Fe oxyhydroxide. *J. Colloid Interface Sci.*, 277:271-279.
- Davranche, M., Grybos, M., Gruau, G., Pedrot, M., Dia, A. and Marsac, R., 2011. Rare earth element patterns: a tool for identifying trace metal sources during wetland soil reduction. *Chem. Geol.*, 284:127-137.
- De Carlo E., and Wen X., 1998. The influence of redox reactions on the uptake of dissolved Ce by suspended Fe and Mn oxide particles. *Aquatic Geochemistry*, 3:357-389.

- Elderfield, H., Upstillgoddard, R. and Sholkovitz, E., 1990. The rare-earth elements in rivers, estuaries, and coastal seas and their significance to the composition of ocean waters. *Geochim. Cosmochim. Acta*, 54:971-991.
- Evensen, N., Hamilton, P. and Onions, R., 1978. Rare-earth abundances in chondritic meteorites. *Geochim. Cosmochim. Acta*, 42:1199-1212.
- Feng, J., 2010. Behaviour of rare earth elements and yttrium in ferromanganese concretions, gibbsite spots, and the surrounding terra rossa over dolomite during chemical weathering. *Chem. Geol.*, 271:112-132.
- Goyne, K.W., Brantley, S.L. and Chorover, J., 2010. Rare earth element release from phosphate minerals in the presence of organic acids. *Chem. Geol.*, 278:1-14.
- Grybos, M., Davranche, M., Gruau, G., Petitjean, P., 2007. Is trace metal release in wetland soils controlled by organic matter mobility or Fe-oxyhydroxides reduction? *Journal of Colloid and Interface Science.*, 314:490-501.
- Tang J. and Johannesson, K.H., 2010. Ligand extraction of rare earth elements from aquifer sediments: Implications for rare earth element complexation with organic matter in natural waters. *Geochim. Cosmochim. Acta*, 74:6690; 6690-6705/6705; 6705.
- Johannesson, K., Stetzenbach, K. and Hodge, V., 1997. Rare earth elements as geochemical tracers of regional groundwater mixing. *Geochim. Cosmochim. Acta*, 61:3605-3618.
- Johannesson, K., Tang, J., Daniels, J., Bounds, W. and Burdige, D., 2004. Rare earth element concentrations and speciation in organic-rich blackwaters of the Great Dismal Swamp, Virginia, USA. *Chem. Geol.*, 209:271-294.
- Land, M., Ohlander, B., Ingri, J. and Thunberg, J., 1999. Solid speciation and fractionation of rare earth elements in a spodosol profile from northern Sweden as revealed by sequential extraction. *Chem. Geol.*, 160:121-138.
- Laveuf, C. and Cornu, S., 2009. A review on the potentiality of rare earth elements to trace pedogenetic processes. *Geoderma*, 154:1-12.
- Laveuf, C., Cornu, S., Guilherme, L.R.G., Guerin, A. and Juillot, F., 2012. The impact of redox conditions on the rare earth element signature of redoximorphic features in a soil sequence developed from limestone. *Geoderma*, 170:25-38.
- Laveuf, C., Cornu, S. and Juillot, F., 2008. Rare earth elements as tracers of pedogenetic processes. *C. R. Geosci.*, 340:523-532.

Ma, L., Jin, L. and Brantley, S.L., 2011. How mineralogy and slope aspect affect REE release and fractionation during shale weathering in the Susquehanna/Shale Hills Critical Zone Observatory. *Chem. Geol.*, 290:31-49.

Nezat, C.A., Blum, J.D., Yanai, R.D. and Hamburg, S.P., 2007. A sequential extraction to determine the distribution of apatite in granitoid soil mineral pools with application to weathering at the Hubbard Brook Experimental Forest, NH, USA. *Appl. Geochem.*, 22:2406-2421.

Ohta, A. and Kawabe, I., 2001. REE(III) adsorption onto Mn dioxide (δ -MnO₂) and Fe oxyhydroxide: Ce(III) oxidation by δ -MnO₂. *Geochim. Cosmochim. Acta*, 65:695-703.

Panahi, A., Young, G. and Rainbird, R., 2000. Behavior of major and trace elements (including REE) during Paleoproterozoic pedogenesis and diagenetic alteration of an Archean granite near Ville Marie, Quebec, Canada. *Geochim. Cosmochim. Acta*, 64:2199-2220.

Peppard, D., Mason, G. and Lewey, S., 1969. A tetrad effect in liquid-liquid extraction ordering of lanthanides(3). *Journal of Inorganic & Nuclear Chemistry*, 31:2271-2272.

Perdrial, J.N., Perdrial, N., Harpold, A., Gao, X., Gabor, R., LaSharr, K. and Chorover, J., 2012. Impacts of sampling dissolved organic matter with passive capillary wicks versus aqueous soil extraction. *Soil Sci. Soc. Am. J.*, 76:2019-2030.

Pourret, O., Davranche, M., Gruau, G. and Dia, A., 2007. Rare earth elements complexation with humic acid. *Chem. Geol.*, 243:128-141.

Pourret, O. and Martinez, R.E., 2009. Modeling lanthanide series binding sites on humic acid. *J. Colloid Interface Sci.*, 330:45-50.

Schijf, J. and Byrne, R., 2001. Stability constants for mono- and dioxalato-complexes of Y and the REE, potentially important species in groundwaters and surface freshwaters. *Geochim. Cosmochim. Acta*, 65:1037-1046.

Sholkovitz, E., 1992. Chemical evolution of rare-earth elements - fractionation between colloidal and solution phases of filtered river water. *Earth Planet. Sci. Lett.*, 114:77-84.

Sonke, J. and Salters, V., 2006. Lanthanide-humic substances complexation. I. experimental evidence for a lanthanide contraction effect. *Geochim. Cosmochim. Acta*, 70:1495-1506.

Steinmann, M. and Stille, P., 2008. Controls on transport and fractionation of the rare earth elements in stream water of a mixed basaltic-granitic catchment basin (Massif Central, France). *Chem. Geol.*, 254:1-18.

Steinmann, M. and Stille, P., 2006. Rare earth element transport and fractionation in small streams of a mixed basaltic-granitic catchment basin (Massif Central, France). *J. Geochem. Explor.*, 88:336-340.

Stille, P., Pierret, M.-., Steinmann, M., Chabaux, F., Boutin, R., Aubert, D., Pourcelot, L. and Morvan, G., 2009. Impact of atmospheric deposition, biogeochemical cycling and water-mineral interaction on REE fractionation in acidic surface soils and soil water (the Strengbach case). *Chem. Geol.*, 264:173-186.

Stille, P., Steinmann, M., Pierret, M.-., Gauthier-Lafaye, F., Chabaux, F., Viville, D., Pourcelot, L., Matera, V., Aouad, G. and Aubert, D., 2006a. The impact of vegetation on REE fractionation in stream waters of a small forested catchment (the Strengbach case). *Geochim. Cosmochim. Acta*, 70:3217-3230.

Stille, P., Steinmann, M., Pierret, M., Gauthier-Lafaye, F., Aubert, D., Probst, A., Viville, D. and Chabaux, F., 2006b. The impact of vegetation on fractionation of rare earth elements (REE) during water-rock interaction. *J. Geochem. Explor.*, 88:341-344.

Tang, J. and Johannesson, K., 2003. Speciation of rare earth elements in natural terrestrial waters: Assessing the role of dissolved organic matter from the modeling approach. *Geochim. Cosmochim. Acta*, 67:2321-2339.

Taylor, S. and McLennan, S., 1981. The composition and evolution of the continental-crust - rare-earth element evidence from sedimentary-rocks. *Philos. Trans. R. Soc. Lond. Ser. A-Math. Phys. Eng. Sci.*, 301:381-399.

Thompson, A., Amistadi, M.K., Chadwick, O.A., and Chorover, J., In Press. Fractionation of yttrium and holmium during basaltic soil weathering. *Geochim. Cosmochim. Acta*

Vázquez-Ortega, A., Perdrial, J.N., Harpold, A., Zapata-Rios, X., Amistadi, M.K., Rasmussen, C., McIntosh, J., Schaap, M., Chorover, J., In review. Rare earth elements as reactive tracers of biogeochemical weathering in forested rhyolitic terrain. *Geochim. Cosmochim. Acta*.

Xiong, Y., 2011. Organic species of lanthanum in natural environments: implications to mobility of rare earth elements in low temperature environments. *Appl. Geochem.*, 26:1130-1137.

Yamamoto, Y., Takahashi, Y. and Shimizu, H., 2005. Systematics of stability constants of fulvate complexes with rare earth ions. *Chem. Lett.*, 34:880-881.

Yamamoto, Y., Takahashi, Y. and Shimizu, H., 2010. Systematic change in relative stabilities of REE-humic complexes at various metal loading levels. *Geochem. J.*, 44:39-63.

LIST OF TABLES:

Table 1 Sequential extraction scheme for soils at La Jara ZOB. Mass:volume ratio, shaking time, and extraction temperature are also included. Adapted from Laveuf et al. (2012) and Land et al. (1999).

Table 2 Organic carbon (OC), Mn, and Fe concentrations (reported in g kg^{-1}) in the bulk soil for the planar (pedon 1) and convergent (pedon 5) soils located in the ZOB.

Table 3 Extractable concentrations for P, Al, Mn, and Fe as a function of depth for the planar (Pedon 1) hillslope profile. Concentrations associated with the target phases are associated with the following chemical extractions: 1.0 M CH_3COONa (pH 5.5), 0.1M $\text{NH}_2\text{OH}\cdot\text{HCl}$ (pH 2), 0.1 M $\text{Na}_4\text{P}_2\text{O}_7$ (pH 10), 0.25 M $\text{NH}_2\text{OH}\cdot\text{HCl}$ (pH 1.5), and 1.0 M $\text{NH}_2\text{O HCl}$ (pH 1).

Table 4 Extractable concentrations for P, Al, Mn, and Fe as a function of depth for the convergent (Pedon 5) hillslope profile. Concentrations associated with the target phases are associated with the following chemical extractions: 1.0 M CH_3COONa (pH 5.5), 0.1M $\text{NH}_2\text{OH}\cdot\text{HCl}$ (pH 2), 0.1 M $\text{Na}_4\text{P}_2\text{O}_7$ (pH 10), 0.25 M $\text{NH}_2\text{OH}\cdot\text{HCl}$ (pH 1.5), and 1.0 M $\text{NH}_2\text{O HCl}$ (pH 1).

LIST OF FIGURES:

Figure 1 Water (*top*), dissolved organic carbon (*middle*), and Σ REY (*bottom*) fluxes through depth increments of the planar hillslope profile (*left*) and the convergent hillslope profile (*right*). Results are integrating data during the following WY 2011, 2012, and 2013. The WY 2013 only includes data from the snowmelt period.

Figure 2 REY depletion and soil organic carbon (*top*) and extractability patterns (*bottom*) as a function of depth in planar (*left*, Pedon 1) and convergent (*right*, Pedon 5) hillslope profiles. Mass fractions are labeled with the names of the target phases, and are associated with the following chemical extractions: 1.0 M CH_3COONa (pH 5.5), 0.1M $\text{NH}_2\text{OH}\cdot\text{HCl}$ (pH 2), 0.1 M $\text{Na}_4\text{P}_2\text{O}_7$ (pH 10), 0.25 M $\text{NH}_2\text{OH}\cdot\text{HCl}$ (pH 1.5), and 1.0 M $\text{NH}_2\text{O HCl}$ (pH 1).

Figure 3 REY fractionation patterns normalized to the each genetic horizon in the planar (*left*, Pedon 1) and convergent (*right*, Pedon 5) hillslope profiles for the following fractions: exchangeable, Mn oxide (i.e., birnessite), and organo-metal colloids. The REY concentrations for each fraction were based on the results from the sequential extractions. Error bars were calculated from triplicate samples.

Figure 4 REY fractionation patterns normalized to the each genetic horizon in the planar (*left*, Pedon 1) and convergent (*right*, Pedon 5) hillslope profiles for the following fractions: short range order Fe-oxides (i.e., ferrihydrite), and long range order Fe-oxides (i.e., goethite), and residual (mainly silicates).

Figure 5 Eu/Eu^* values normalized to the each genetic horizon in the planar (Pedon 1) and convergent (Pedon 5) hillslope profiles for the following fractions: (A) exchangeable, (B) Mn oxide (i.e., birnessite), (C) organo-metal colloids, (D) short range order Fe-oxides (i.e., ferrihydrite), (E) long range order Fe-oxides (i.e., goethite), and (F) residual (mainly silicates). The Eu/Eu^* values for each fraction were based on the results from the sequential extractions. Error bars were calculated from triplicate samples. Eu/Eu^* higher than 1 represent positive anomalies (enrichment) and values lower than 1 represent negative anomalies (depletion) with respect to the genetic horizon.

Figure 6 Ce/Ce^* values normalized to the each genetic horizon in the planar (Pedon 1) and convergent (Pedon 5) hillslope profiles for the following fractions: (A) exchangeable, (B) Mn oxide (i.e., birnessite), (C) organo-metal colloids, (D) short range order Fe-oxides (i.e., ferrihydrite), (E) long range order Fe-oxides (i.e., goethite), and (F) residual (mainly silicates).

Figure 7 Y/Ho ratios normalized to the each genetic horizon in the planar (Pedon 1) and convergent (Pedon 5) hillslope profiles for the following fractions: (A) exchangeable, (B) Mn oxide (i.e., birnessite), (C) organo-metal colloids, (D) short range order Fe-oxides (i.e., ferrihydrite), (E) long range order Fe-oxides (i.e., goethite), and (F) residual (mainly silicates).

silicates). The Y/Ho ratios for each fraction were based on the results from the sequential extractions. Error bars were calculated from triplicate samples.

Figure 8 Organic carbon (OC) associated with the (A) organo-metal colloids and (B) SRO Fe-oxides for all genetic horizons in the planar (pedon 1) and convergent (pedon 5) hillslope profiles.

Figure 9 Mass balance plots for Ce, Mn, and Fe as a function of depth for the planar and convergent sites. The immobile element is titanium. All values were normalized by a weighted average of ZOB bedrock concentrations, based on the abundances of rhyodacite (0.44) and Bandelier tuff (0.56). Tau values higher than 0 represent enrichment and Tau values lower than 0 represent depletion with respect to the parent materials.

Table 1 Sequential extraction scheme for soils at La Jara ZOB. Mass:volume ratio, shaking time, and extraction temperature are also included. Adapted from Laveuf et al. (2012) and Land et al. (1999).

Step	Phases	Procedure
1	Adsorbed, exchangeable, and carbonate bound	1.0M CH ₃ COONa with CH ₃ COOH 99-100% Adjust pH at 5.5 1:10 m/V 1 extractions, shake 6h, room temperature
2	Mn oxide e.g. Birnessite	0.1M NH ₂ OH·HCl in 0.1M HCl Adjust pH at 2 1:20 m/V 2 extractions, shake 0.5h, room temperature
3	Organo-metal colloids	0.1M Na ₄ P ₂ O ₇ Adjust pH at 10 1:10 m/V shake 1.5h, room temperature
4	Short range order (SRO) Fe-oxides e.g. Ferrihydrite	0.25M NH ₂ OH·HCl in 0.25M HCl Adjust pH at 1.5 1:20 m/V 2 extractions, 2h each, 60°C
5	Long range order (LRO) Fe-oxides e.g. Goethite	1.0M NH ₂ OH·HCl in 25% CH ₃ COOH 99-100% Adjust pH at 1 1:30 m/V 3h, 90°C

Table 2 Organic carbon (OC), Mn, and Fe concentrations (reported in g kg⁻¹) in the bulk soil for the planar (pedon 1) and convergent (pedon 5) soils located in the ZOB.

Location	Horizon	Depth (cm)	OC	P	Mn	Fe	Mn:Fe
			g kg ⁻¹	g kg ⁻¹	g kg ⁻¹	g kg ⁻¹	Ratio
Planar (pedon 1)	O	0-1	163.1	0.74	2.63	13.36	1:05
	A	1-20	14	0.17	0.79	12.8	1:16
	B1	20-40	3	0.09	0.46	12.8	1:28
	B2	40-52	2.7	0.09	0.22	15.04	1:67
	B3	52-100	2.2	0.13	0.36	20.63	1:57
Convergent (pedon 5)	O	0-1	233.5	1.35	0.94	15.74	1:17
	A	1-13	51.5	0.65	0.98	18.6	1:19
	B1	13-42	173.2	0.65	1.49	20.77	1:14
	B2	42-60	185.4	0.52	1.07	20	1:19
	B3	60-125	1.9	0.26	1.21	35.46	1:29

Table 3 Extractable concentrations for P, Al, Mn, and Fe as a function of depth for the planar (Pedon 1) hillslope profile. Concentrations associated with the target phases are associated with the following chemical extractions: 1.0 M CH₃COONa (pH 5.5), 0.1M NH₂OH·HCl (pH 2), 0.1 M Na₄P₂O₇ (pH 10), 0.25 M NH₂OH·HCl (pH 1.5), and 1.0 M NH₂O HCl (pH 1).

Pedon ID	Horizon	Step	P		Al		Mn		Fe	
			mg/kg soil		mg/kg soil		mg/kg soil		mg/kg soil	
			Ave	s.d.	Ave	s.d.	Ave	s.d.	Ave	s.d.
1	O	Step (Exchangeable)	82	16	14	3	286	28	4.8	0.9
	A		4.40	3.5	34	4	73	4	14	1.1
	B1		0.00	0	30	3	8.7	1.1	5.8	1.3
	B2		0.05	0.08	32	3	4.2	0.5	7.0	3.3
	B3		0.44	0.77	36	4	8.6	1.8	3.4	0.4
1	O	Step 2 (Mn-oxide)	97	13	129	16	3026	10	171	18
	A		4.59	0.6	317	12	855	18	343	8
	B1		1.00	1.0	211	2	226	54	145	12
	B2		1.74	1.5	170	16	108	102	87	12
	B3		1.94	0.7	150	8	131	37	96	10
1	O	Step 3 (Organo- metal)	n.d.	n.d.	1259	38	330	83	962	70
	A		n.d.	n.d.	689	49	109	38	841	17
	B1		n.d.	n.d.	575	155	68	29	494	63
	B2		n.d.	n.d.	1214	40	94	121	558	27
	B3		n.d.	n.d.	1893	307	82	33	685	165
1	O	Step 4 (SRO Fe-oxides)	n.d.	n.d.	1325	31	136	19	1414	61
	A		n.d.	n.d.	1435	72	179	149	1487	231
	B1		n.d.	n.d.	1241	25	82	17	1269	98
	B2		n.d.	n.d.	1839	82	170	193	1549	81
	B3		n.d.	n.d.	2887	12	91	34	2089	51
1	O	Step 5 (LRO Fe-oxides)	n.d.	n.d.	1400	29	34	3	3276	67
	A		n.d.	n.d.	1134	55	58	25	3090	257
	B1		n.d.	n.d.	964	62	34	3	3143	77
	B2		n.d.	n.d.	1474	117	33	4	3916	282
	B3		n.d.	n.d.	2292	183	45	3	5166	256
1	O	Residual	n.d.	n.d.	35566	94	0	127	7531	141
	A		n.d.	n.d.	46298	42	0	229	7025	402
	B1		n.d.	n.d.	44876	203	90	103	7742	175
	B2		n.d.	n.d.	47295	44	58	420	8921	390
	B3		n.d.	n.d.	59109	223	54	90	12594	333

Table 4 Extractable concentrations for P, Al, Mn, and Fe as a function of depth for the convergent (Pedin 5) hillslope profile. Concentrations associated with the target phases are associated with the following chemical extractions: 1.0 M CH₃COONa (pH 5.5), 0.1M NH₂OH·HCl (pH 2), 0.1 M Na₄P₂O₇ (pH 10), 0.25 M NH₂OH·HCl (pH 1.5), and 1.0 M NH₂O HCl (pH 1).

Pedin ID	Horizon	Step	P		Al		Mn		Fe	
			mg/kg soil		mg/kg soil		mg/kg soil		mg/kg soil	
			Ave	s.d.	Ave	s.d.	Ave	s.d.	Ave	s.d.
5	O	Step (Exchangeable)	116	5	24	0.3	198	4	11.1	0.7
	A		12	2	83	1	69	2	27.1	0.7
	B1		30	34	134	1	40.0	1.9	60	3
	B2		11	1	172	8	47.5	3.1	66	3
	B3		7	1	107	8	40.3	1.4	14.1	0.8
5	O	Step 2 (Mn-oxide)	86	3	59	4	1293	350	102	2
	A		14.2	0.2	389	13	1028	57	320	8
	B1		12	1	435	12	1105	89	403	23
	B2		20	1	402	7	853	56	336	12
	B3		79	7	163	3	704	52	241	8
5	O	Step 3 (Organo- metal)	n.d.	n.d.	1534	196	200	32	1645	216
	A		n.d.	n.d.	2121	91	187	50	2722	114
	B1		n.d.	n.d.	2740	119	228	34	2821	121
	B2		n.d.	n.d.	1885	53	173	15	2240	24
	B3		n.d.	n.d.	939	26	217	51	487	19
5	O	Step 4 (SRO Fe-oxides)	n.d.	n.d.	1002	6	169	5	2135	148
	A		n.d.	n.d.	1228	10	199	26	2510	31
	B1		n.d.	n.d.	1441	181	116	15	2531	343
	B2		n.d.	n.d.	1384	12	106	8	2381	97
	B3		n.d.	n.d.	1624	116	144	6	1846	93
5	O	Step 5 (LRO Fe-oxides)	n.d.	n.d.	2600	84	75	6	4952	188
	A		n.d.	n.d.	2256	83	103	27	4756	144
	B1		n.d.	n.d.	2150	157	76	12	4062	224
	B2		n.d.	n.d.	1551	69	44	5	3160	146
	B3		n.d.	n.d.	1492	288	35	5	4669	1328
5	O	Residual	n.d.	n.d.	34473	194	699	322	4514	217
	A		n.d.	n.d.	43830	156	0	0	2466	160
	B1		n.d.	n.d.	40997	235	0	0	2923	257
	B2		n.d.	n.d.	46630	119	0	0	6854	132
	B3		n.d.	n.d.	62042	412	0	0	13377	1423

FIGURES

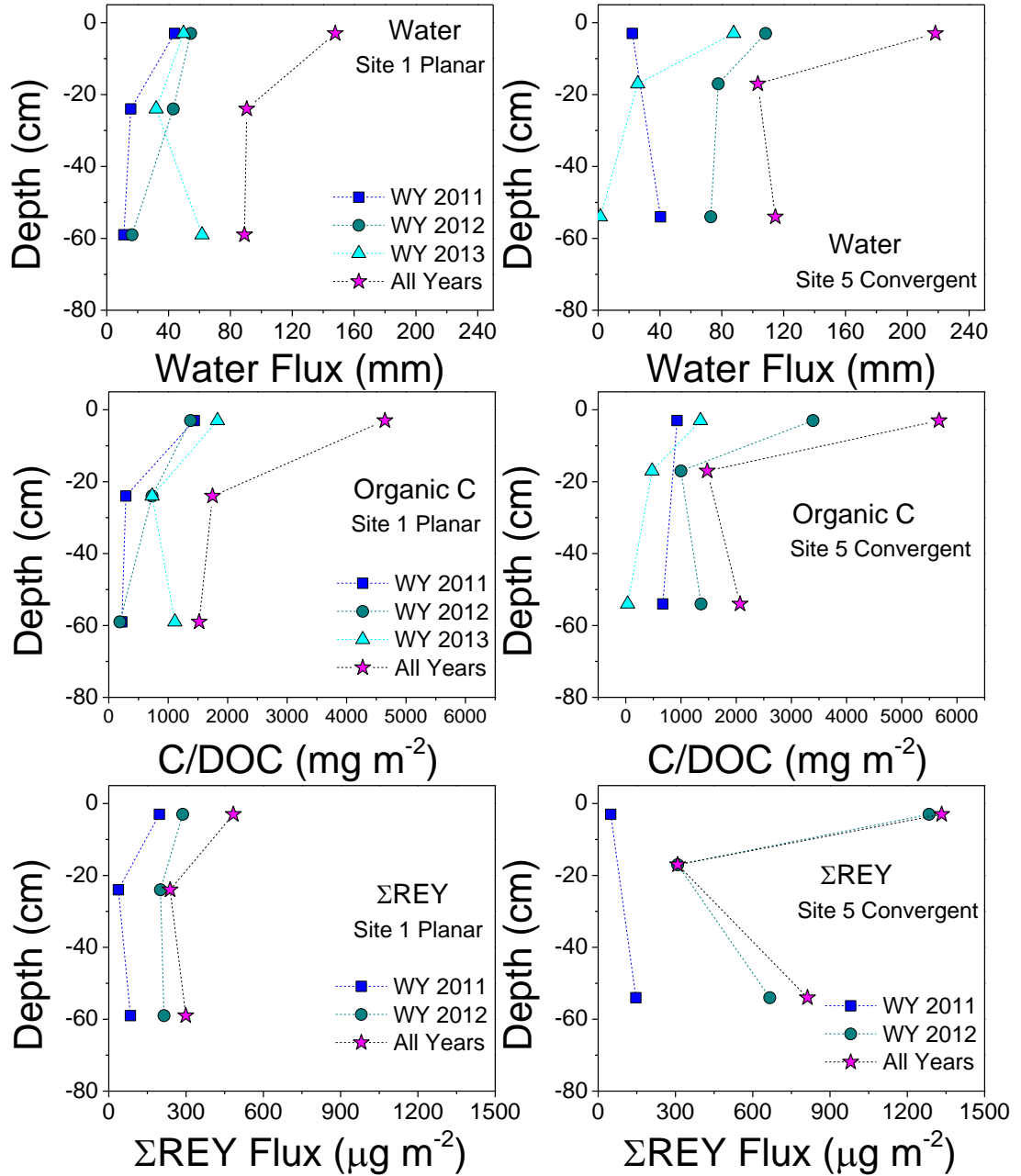


Figure 1 Water (*top*), dissolved organic carbon (*middle*), and Σ REY (*bottom*) fluxes through depth increments of the planar hillslope profile (*left*) and the convergent hillslope profile (*right*). Results are integrating data during the following WY 2011, 2012, and 2013. The WY 2013 only includes data from the snowmelt period.

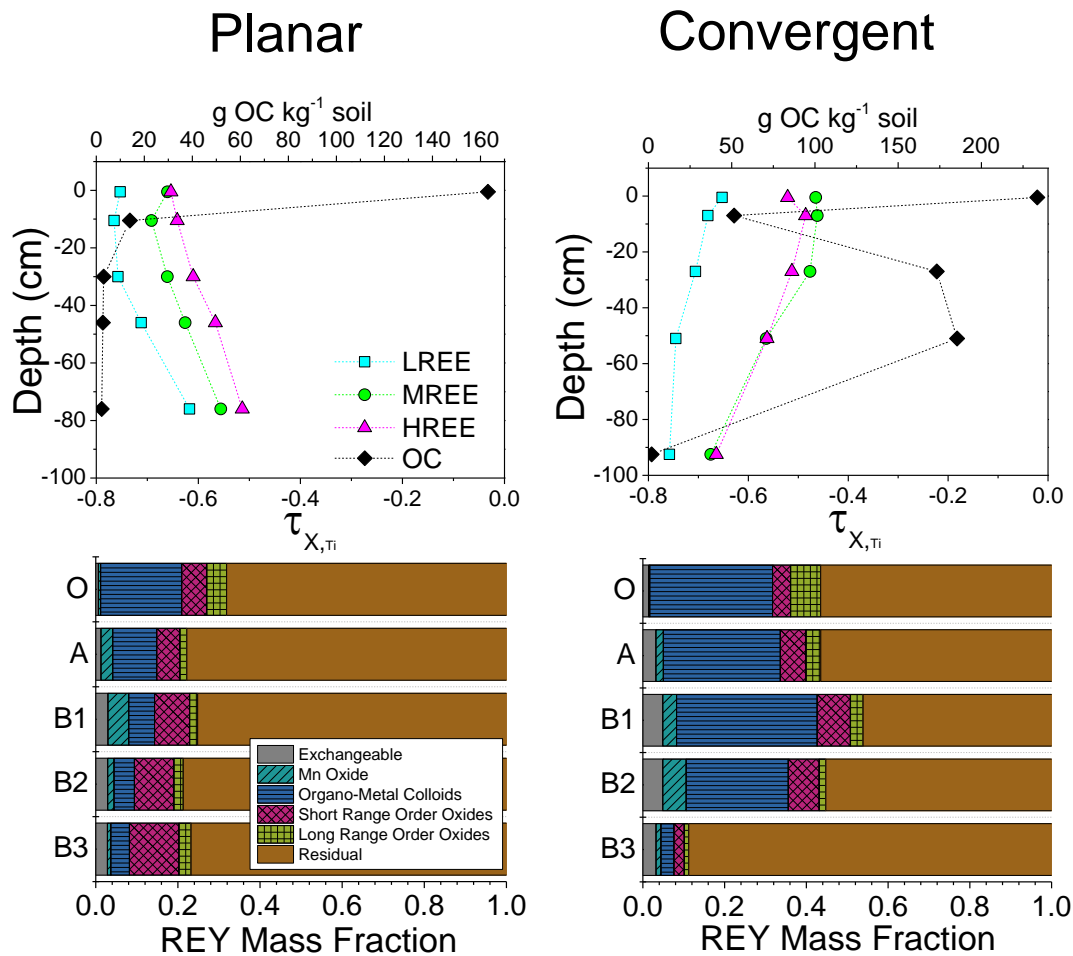


Figure 2 REY depletion and soil organic carbon (*top*) and extractability patterns (*bottom*) as a function of depth in planar (*left*, Pedon 1) and convergent (*right*, Pedon 5) hillslope profiles. Mass fractions are labeled with the names of the target phases, and are associated with the following chemical extractions: 1.0 M CH₃COONa (pH 5.5), 0.1M NH₂OH·HCl (pH 2), 0.1 M Na₄P₂O₇ (pH 10), 0.25 M NH₂OH·HCl (pH 1.5), and 1.0 M NH₂O HCl (pH 1).

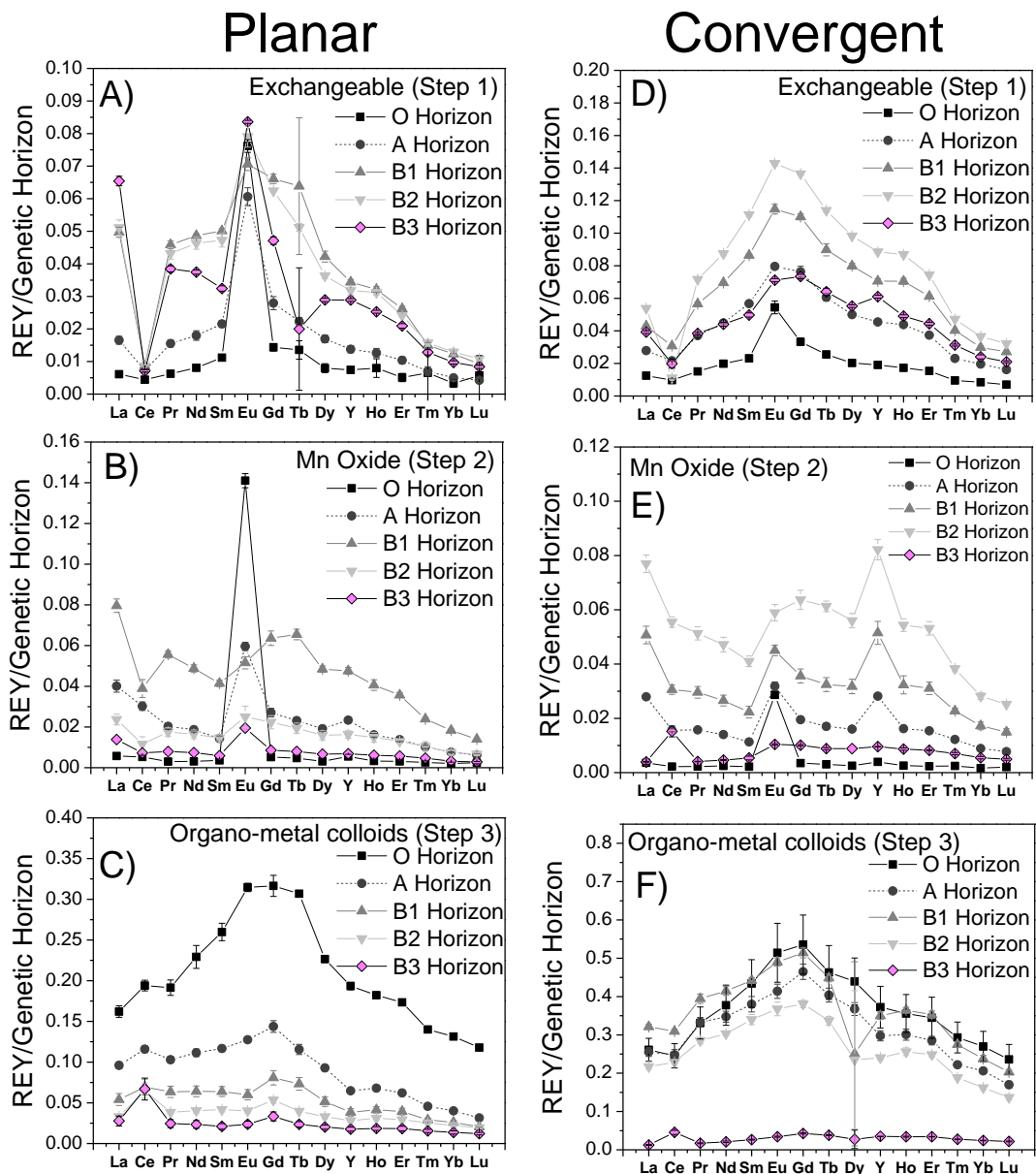


Figure 3 REY fractionation patterns normalized to the each genetic horizon in the planar (*left*, Pedon 1) and convergent (*right*, Pedon 5) hillslope profiles for the following fractions: exchangeable, Mn oxide (i.e., birnessite), and organo-metal colloids. The REY concentrations for each fraction were based on the results from the sequential extractions. Error bars were calculated from triplicate samples.

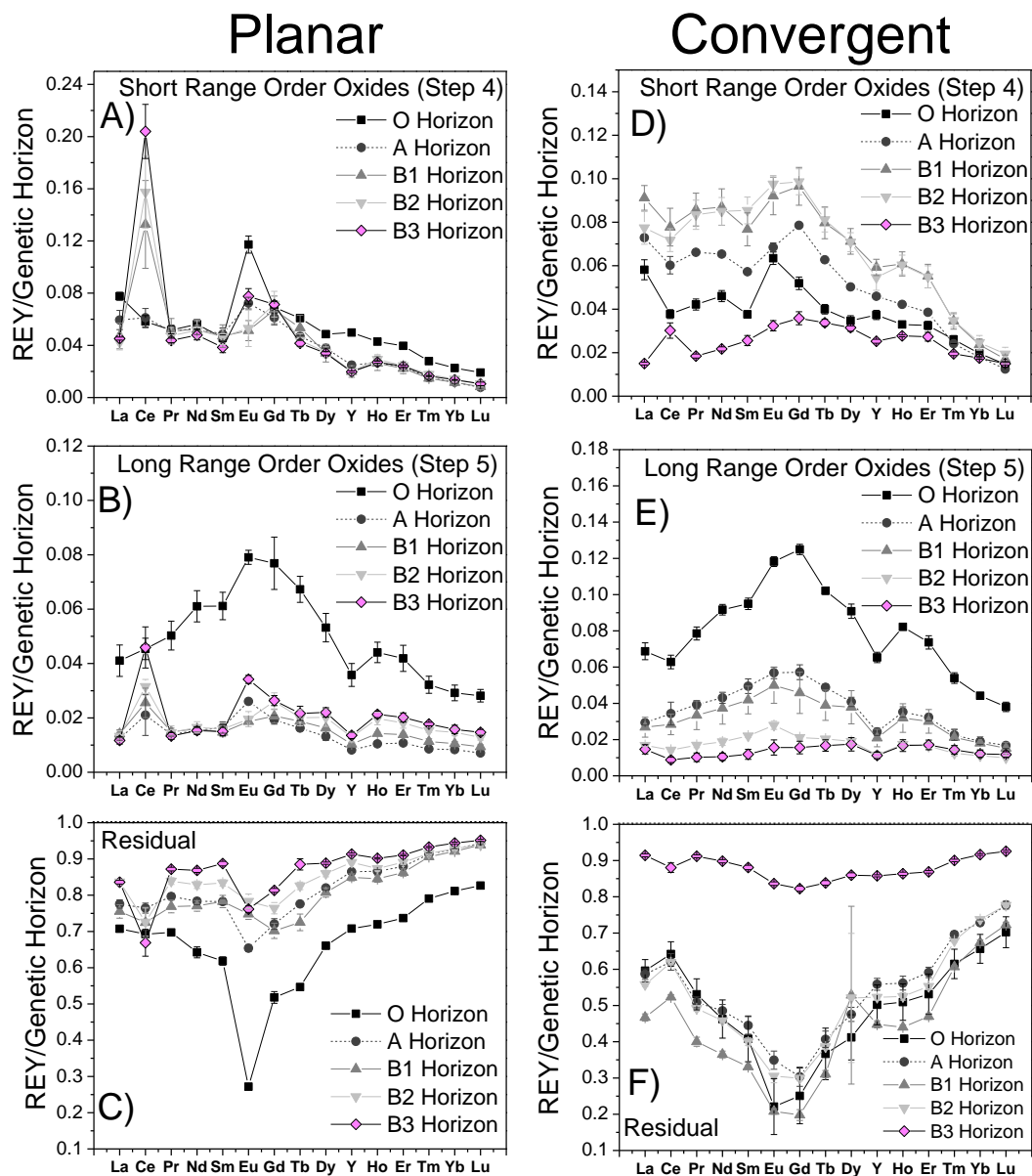


Figure 4 REY fractionation patterns normalized to the each genetic horizon in the planar (*left*, Pedon 1) and convergent (*right*, Pedon 5) hillslope profiles for the following fractions: short range order Fe-oxides (i.e., ferrihydrite), and long range order Fe-oxides (i.e., goethite), and residual (mainly silicates).

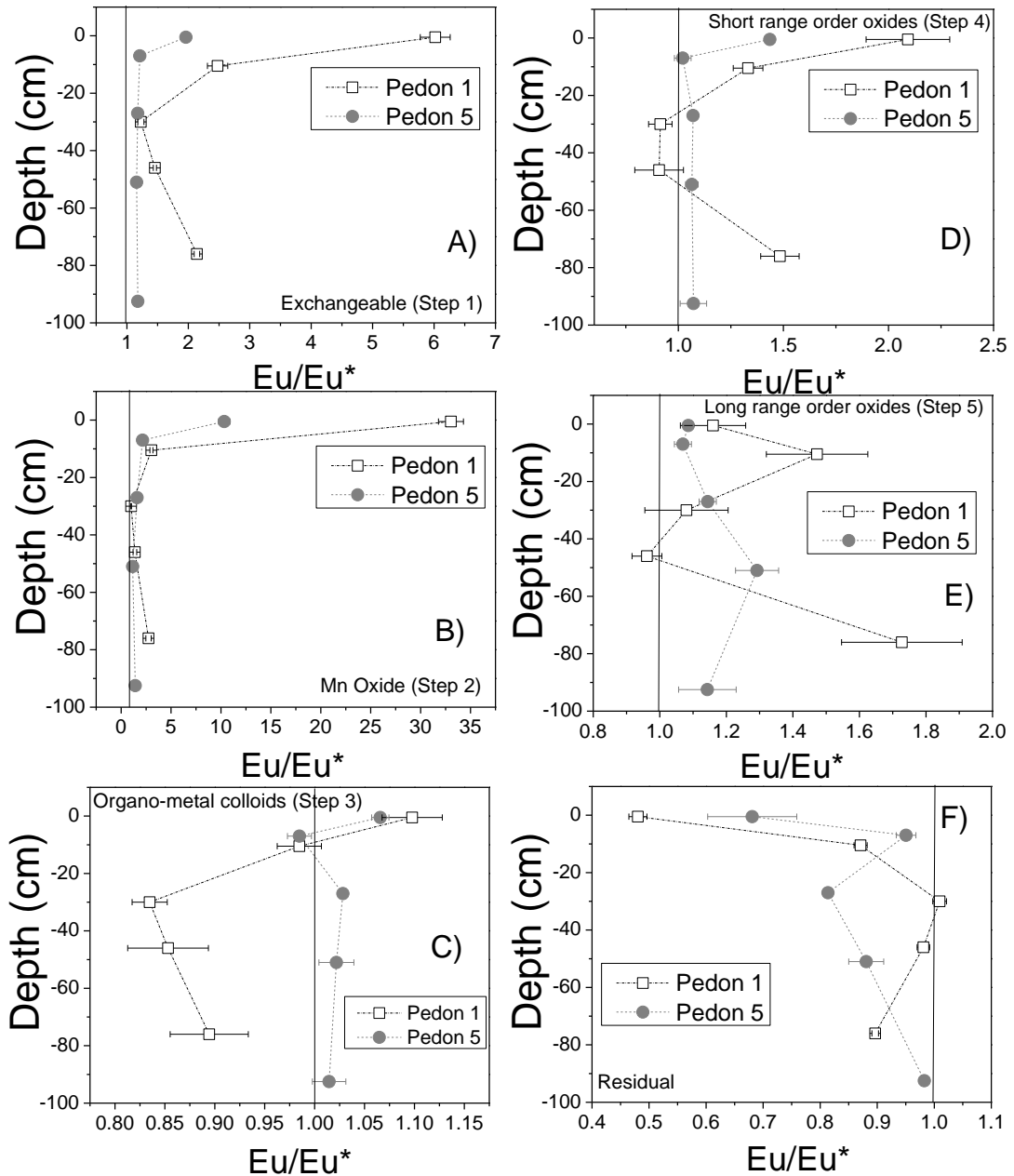


Figure 5 Eu/Eu* values normalized to the each genetic horizon in the planar (Pedon 1) and convergent (Pedon 5) hillslope profiles for the following fractions: (A) exchangeable, (B) Mn oxide (i.e., birnessite), (C) organo-metal colloids, (D) short range order Fe-oxides (i.e., ferrihydrite), (E) long range order Fe-oxides (i.e., goethite), and (F) residual (mainly silicates). The Eu/Eu* values for each fraction were based on the results from the sequential extractions. Error bars were calculated from triplicate samples. Eu/Eu* higher than 1 represent positive anomalies (enrichment) and values lower than 1 represent negative anomalies (depletion) with respect to the genetic horizon.

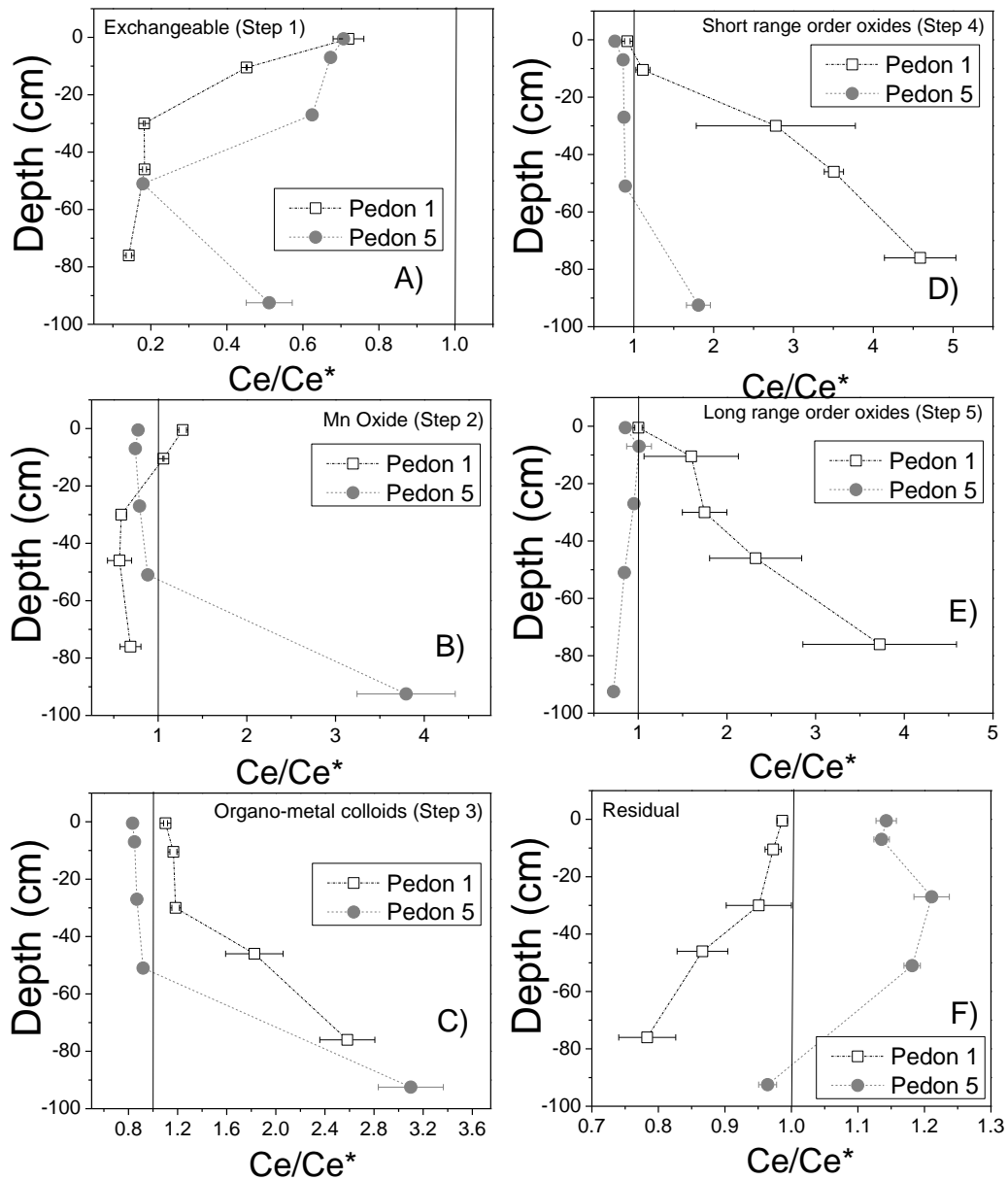


Figure 6 Ce/Ce^* values normalized to the each genetic horizon in the planar (Pedon 1) and convergent (Pedon 5) hillslope profiles for the following fractions: (A) exchangeable, (B) Mn oxide (i.e., birnessite), (C) organo-metal colloids, (D) short range order Fe-oxides (i.e., ferrihydrite), (E) long range order Fe-oxides (i.e., goethite), and (F) residual (mainly silicates).

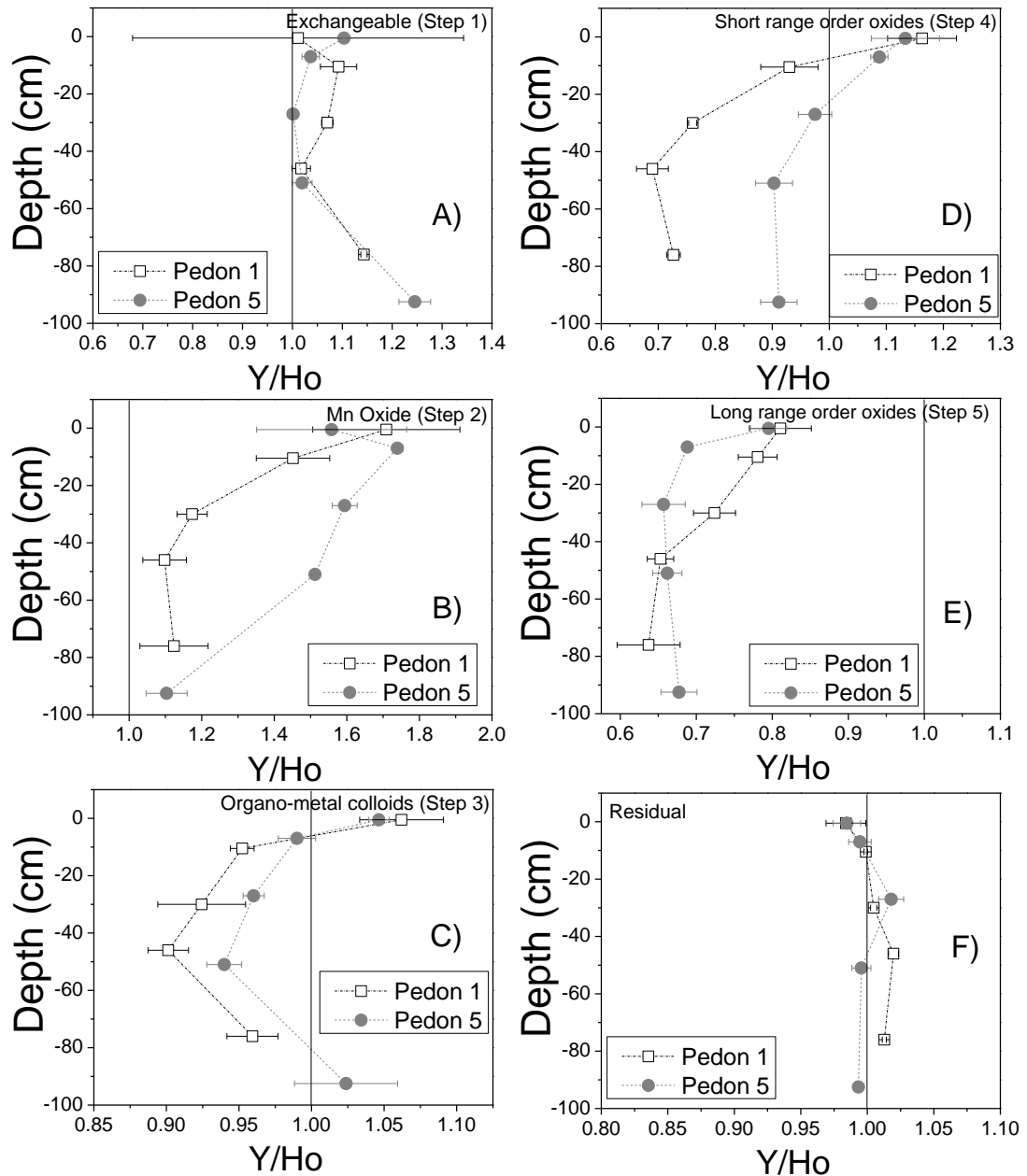


Figure 7 Y/Ho ratios normalized to the each genetic horizon in the planar (Pedon 1) and convergent (Pedon 5) hillslope profiles for the following fractions: (A) exchangeable, (B) Mn oxide (i.e., birnessite), (C) organo-metal colloids, (D) short range order Fe-oxides (i.e., ferrihydrite), (E) long range order Fe-oxides (i.e., goethite), and (F) residual (mainly silicates). The Y/Ho ratios for each fraction were based on the results from the sequential extractions. Error bars were calculated from triplicate samples.

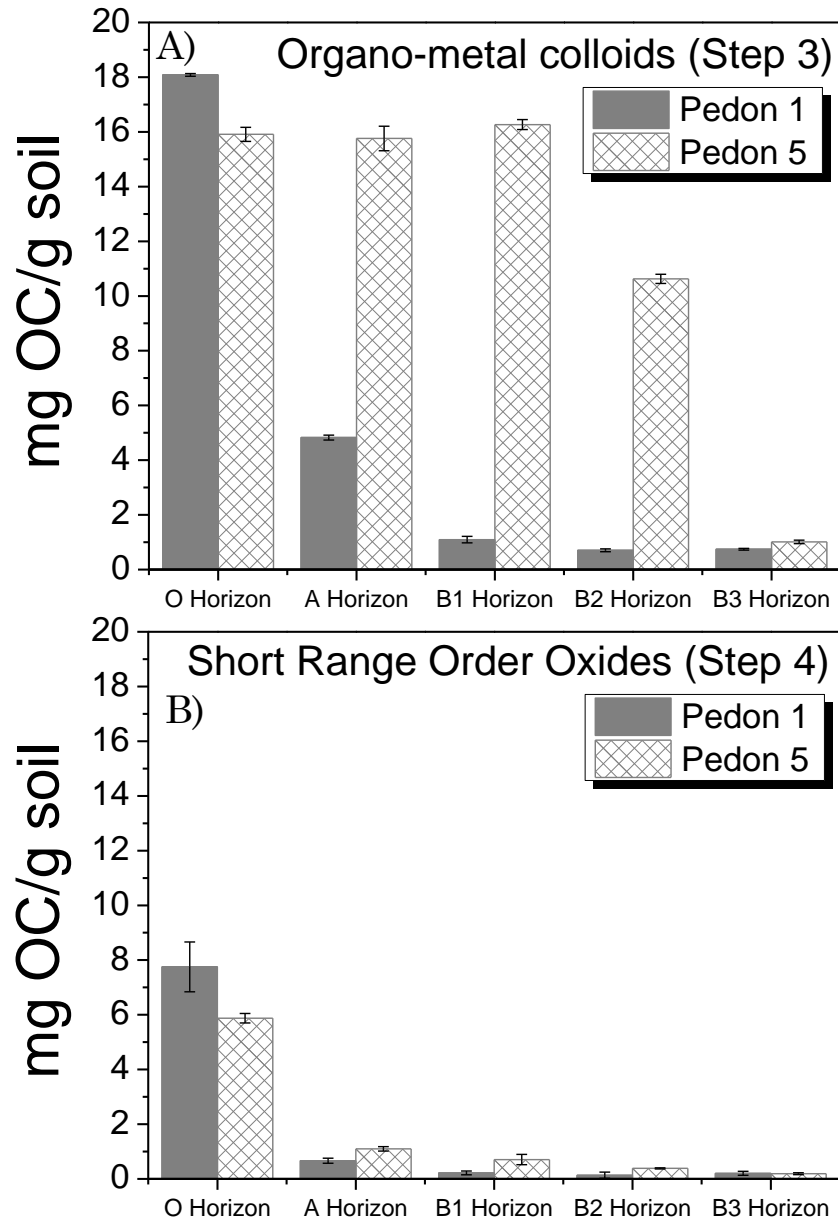


Figure 8 Organic carbon (OC) associated with the (A) organo-metal colloids and (B) SRO Fe-oxides for all genetic horizons in the planar (pedon 1) and convergent (pedon 5) hillslope profiles.

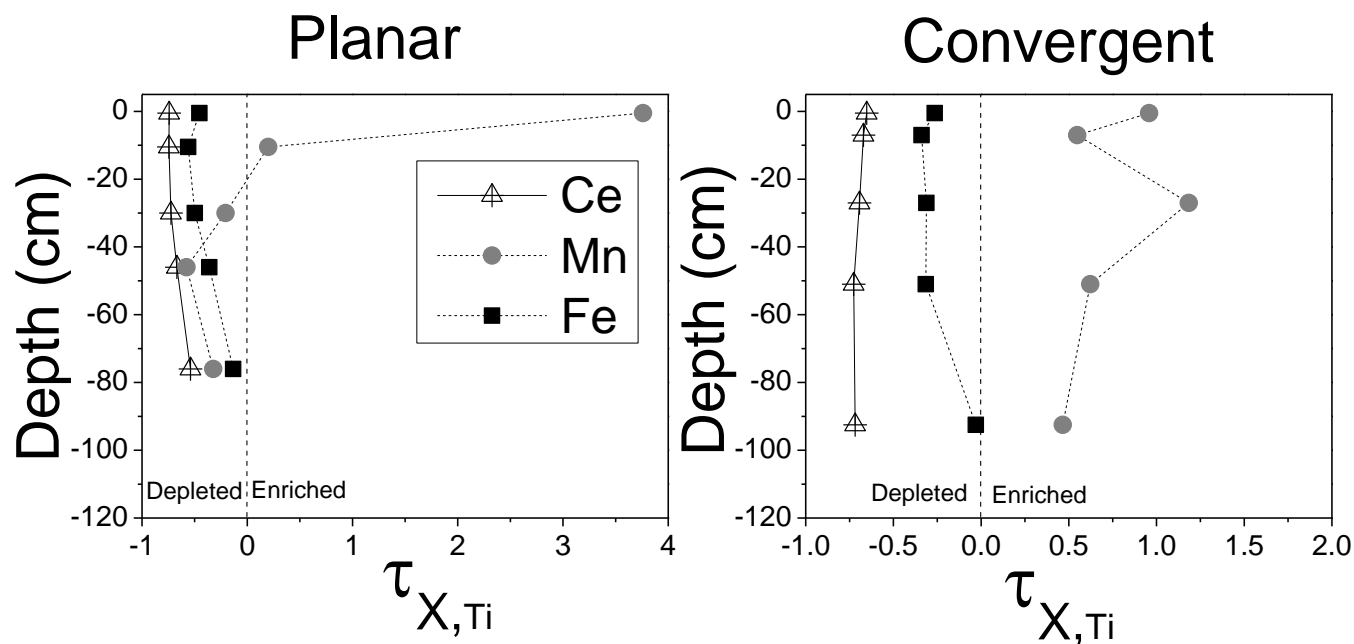


Figure 9 Mass balance plots for Ce, Mn, and Fe as a function of depth for the planar and convergent sites. The immobile element is titanium. All values were normalized by a weighted average of ZOB bedrock concentrations, based on the abundances of rhyodacite (0.44) and Bandelier tuff (0.56). Tau values higher than 0 represent enrichment and Tau values lower than 0 represent depletion with respect to the parent materials.

APPENDIX D: *ELECTRONIC ANNEX FOR*
FRACTIONATION OF DISSOLVED ORGANIC MATTER BY
(OXY)HYDROXIDE-COATED QUARTZ SANDS: COMPETITIVE SORBATE
DISPLACEMENT DURING REACTIVE TRANSPORT

Vadose Zone Journal

Angélica Vázquez-Ortega^{a*}, Selene Hernandez-Ruiz^a, Mary Kay Amistadi^a, Craig Rasmussen^a, Jon Chorover^a

^aDepartment of Soil, Water & Environmental Science, University of Arizona, 1177 East Fourth Street, Tucson, Arizona 85721-0038, USA

*Corresponding author: avazquez@email.arizona.edu

SECTION 1: FIGURES

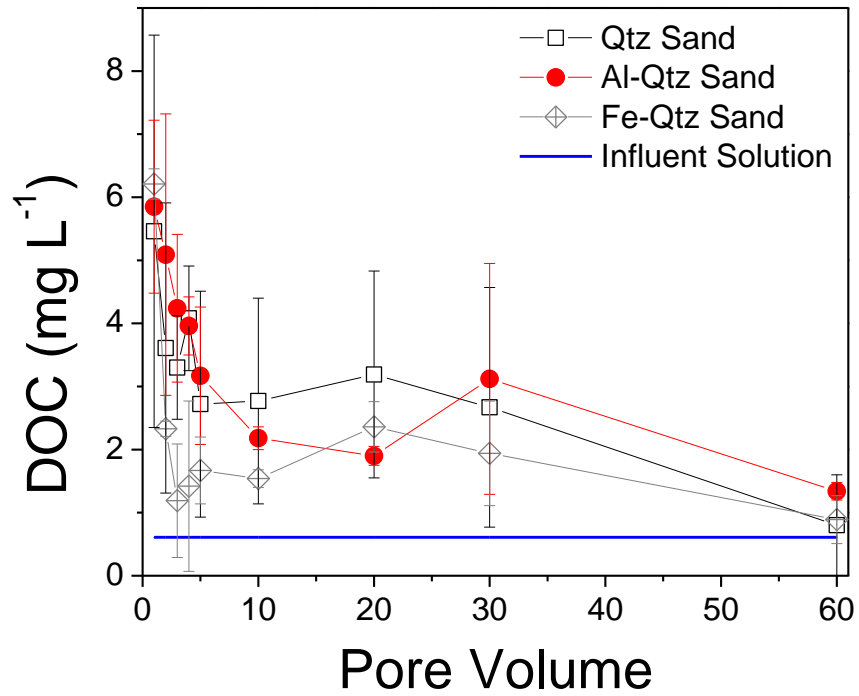


Figure E.1 DOC for all treatments during a control experiment with no-DOM using 0.01M NaCl. Solid blue line represents DOC concentrations in the influent solution. Small amounts of DOC were associated and mobilized from the mineral phases and determined in the effluent solution.

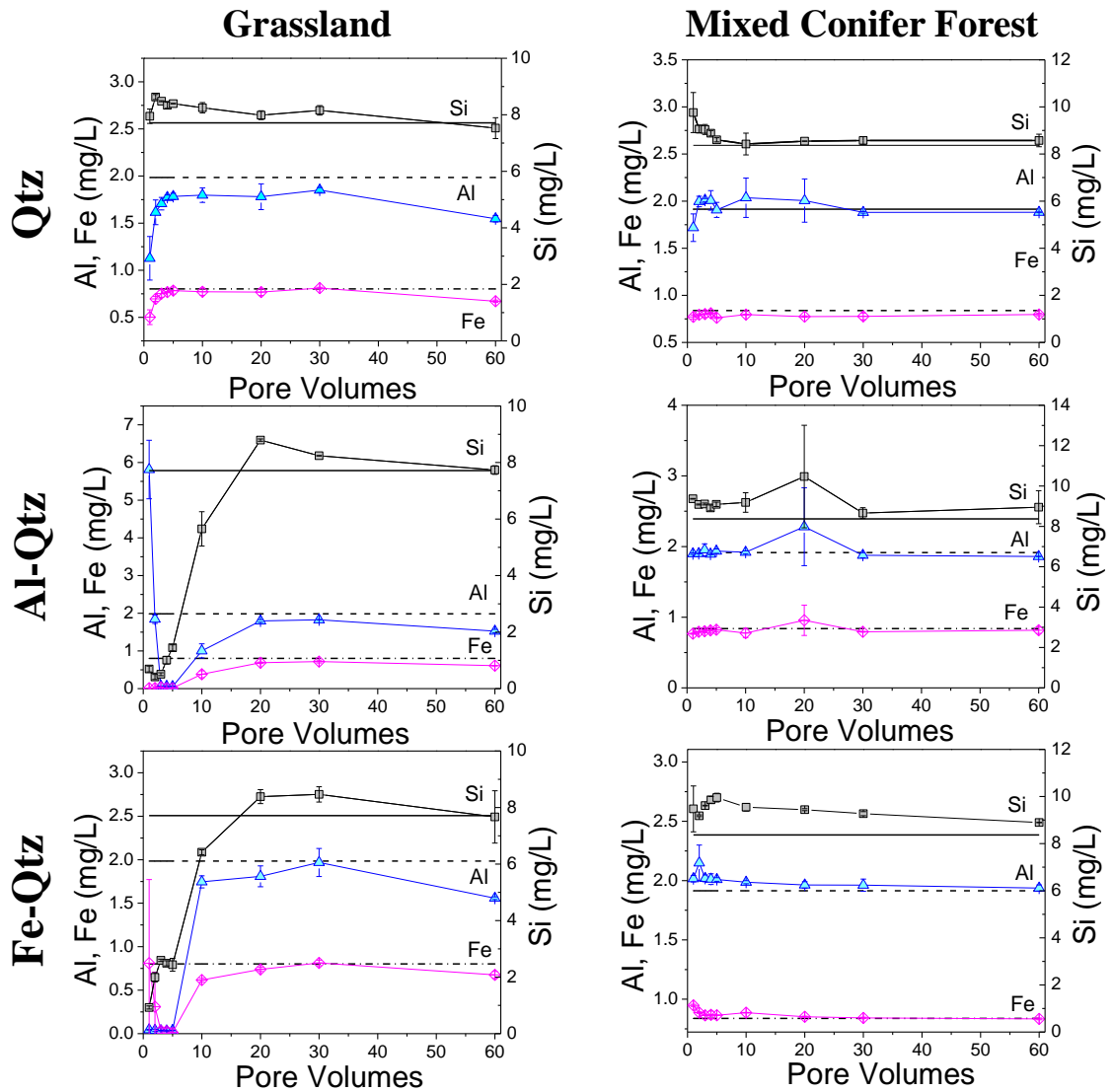


Figure E.2 Si, Al, and Fe concentrations for all treatments during grassland (left) and mixed conifer forest (right) DOM irrigation. Solid, dash, and dash and point black lines represent Si, Al, and Fe respectively in the influent solution. Small amounts of Si (square symbol), Al (triangle symbol), and Fe (diamond symbol) were mobilized from the mineral phases, indicating minimal coating dissolution.

APPENDIX E: *ELECTRONIC ANNEX FOR*
RARE EARTH ELEMENTS AS REACTIVE TRACERS OF
BIOGEOCHEMICAL WEATHERING IN FORESTED RHYOLITIC
TERRAIN

Geochimica et Cosmochimica Acta

Angélica Vázquez-Ortega^{a*}, Julia Perdrial^a, Adrian Harpold^{b1}, Xavier Zapata-Rios^b, Craig Rasmussen^a, Jennifer McIntosh^b, Marcel Schaap^a, Jon D. Pelletier^c, Mary Kay Amistadi^a,
Jon Chorover^a

^aDepartment of Soil, Water & Environmental Science, University of Arizona, 1177 East Fourth Street, Tucson, Arizona 85721-0038, USA

^bDepartment of Hydrology and Water Resources, University of Arizona, 1133 East James E. Rogers Way, Tucson, Arizona 85721-0011, USA

^cDepartment of Geosciences, University of Arizona, 1040 East Fourth Street, Tucson, Arizona 85721-0077, USA

¹Institute of Arctic and Alpine Research, University of Colorado, 1560 30th Street, Boulder, Colorado 80303-0450, USA

*Corresponding author: avazquez@email.arizona.edu; 520-626-8190

SECTION 1: FIGURES AND TABLES

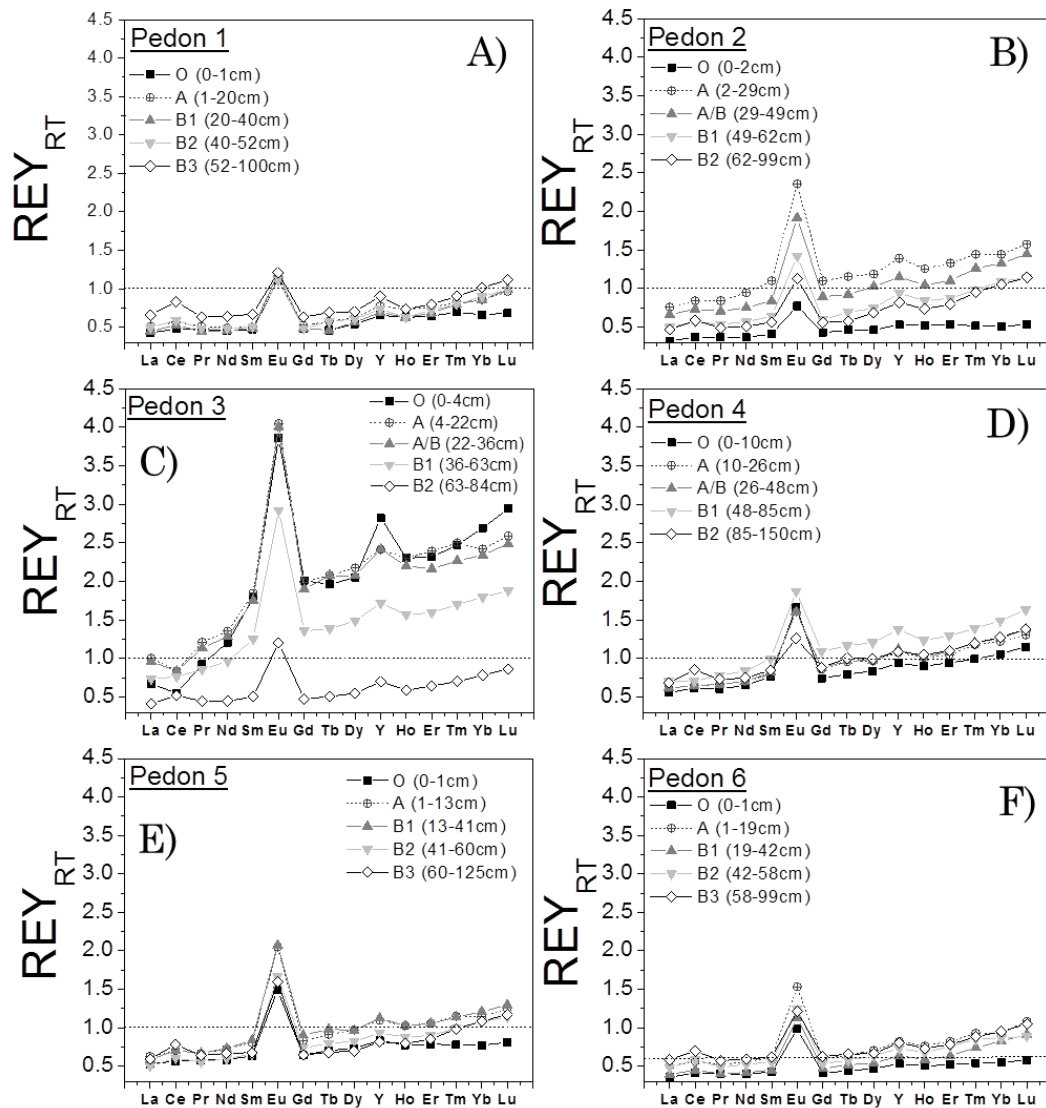


Figure E.1 REY fractionation patterns for all pedons excavated in La Jara ZOB. All values were normalized by WA La Jara ZOB. REY_{RT} values higher than 1 represent enrichment and REY_{RT} values lower than 1 represent depletion with respect to the parent materials. The generic horizon designation is followed by the depth boundaries of the horizon.

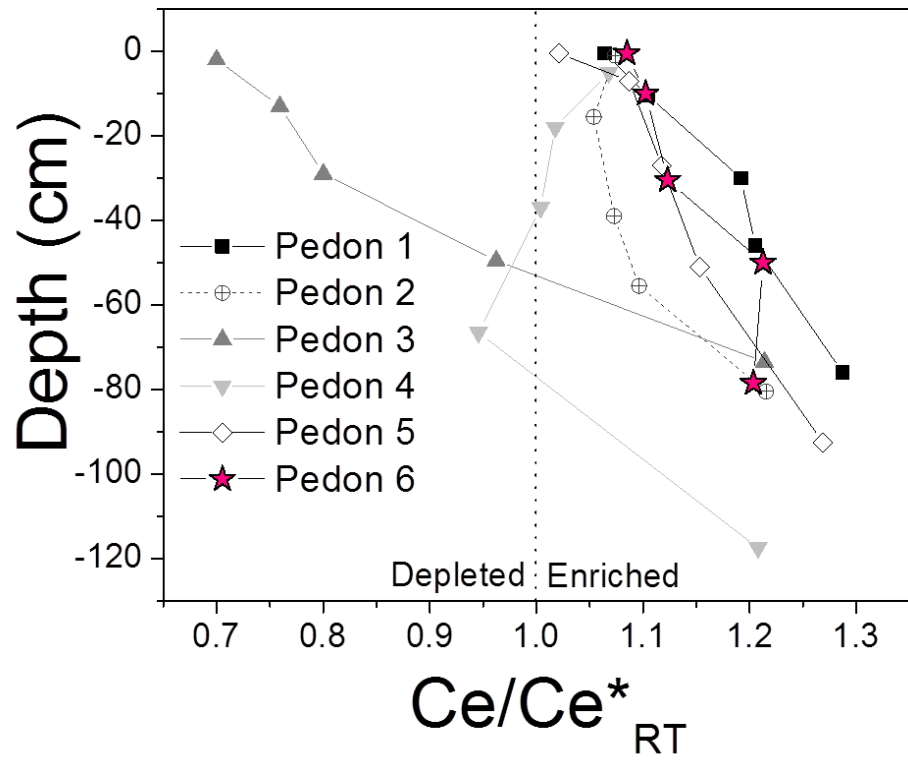


Figure E.2 Ce anomalies for all pedons (all horizons) excavated in La Jara ZOB. All values were normalized by WA LJ ZOB.

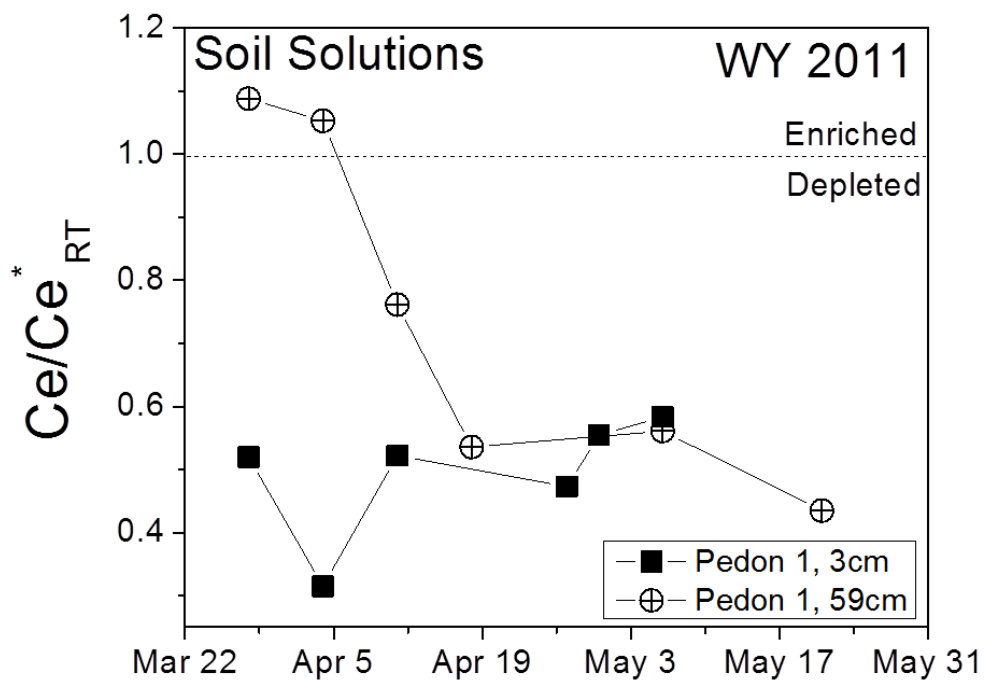


Figure E.3 Ce anomalies in soil solutions for pedon 1 during the snow melt WY 2011.

Table E.1 Mineral composition of Rhyodacite and Bandelier tuff determined by powder X-ray diffraction.

Rhyodacite		Bandelier tuff	
Mineral Phase	%	Mineral Phase	%
Albite	35	Clinoptilolite	45
Quartz	28	Sanidine	21
Sanidine	27	Cristobalite	16
Oligoclase	9	Mordenite	12
		Quartz	5
		Albite	0.4

Table E.2 Particle sized composition for all excavated pedons located in the ZOB.

Pedon	Depth	Horizon	% Clay	% Silt	% Sand	Textural Class
1	0-1	O-Horizon	21	47	32	Loam
	1-20	A-Horizon	15	38	46	Loam
	20-40	B1-Horizon	16	32	52	Sandy Loam
	40-52	B2-Horizon	29	24	47	Sandy Clay Loam
	52-100	B3-Horizon	34	25	41	Clay Loam
2	0-2	O-Horizon	23	39	38	Loam
	2-29	A-Horizon	38	31	32	Clay Loam
	29-49	A/B-Horizon	29	30	41	Clay Loam
	49-62	B1-Horizon	18	29	53	Sandy Loam
	62-99	B2-Horizon	20	28	52	Sandy Clay Loam
3	0-4	O-Horizon	36	33	31	Clay Loam
	4-22	A-Horizon	34	31	35	Clay Loam
	22-36	A/B-Horizon	29	33	39	Clay Loam
	36-63	B1-Horizon	21	33	46	Loam
	63-84	B2-Horizon	29	21	50	Sandy Clay Loam
4	0-10	O-Horizon	25	36	39	Loam
	10-26	A-Horizon	23	35	42	Loam
	26-48	A/B-Horizon	22	34	44	Loam
	48-85	B-Horizon	20	36	44	Loam
	85-120	C-Horizon	20	32	48	Loam
5	0-1	O-Horizon	31	41	28	Clay Loam
	1-13	A-Horizon	30	33	37	Clay Loam
	13-42	B1-Horizon	32	33	35	Clay Loam
	42-60	B2-Horizon	31	30	39	Clay Loam
	60-125	B3-Horizon	39	41	20	Clay Loam

6	0-1	O-Horizon	19	50	31	Silt Loam
	1-19	A-Horizon	17	36	47	Loam
	19-42	B1-Horizon	15	30	56	Sandy Loam
	42-58	B2-Horizon	36	19	45	Sandy Clay
	58-99	B3-Horizon	35	23	41	Clay Loam

Table E.3 Chemical properties and saturation indices for some pore solutions and stream waters during water years 2010 and 2011 in the study site.

Scale	Date	pH	DOC	Al	Fe	Log Ω	Log Ω
			(mg L ⁻¹)	(mg L ⁻¹)	(mg L ⁻¹)	Gibbsite	Goethite
Pedon 1, 3cm	3/28/11	7.0	24.0	0.14	0.18	2.1	5.6
Pedon 1, 3cm	4/11/11	7.0	44.2	0.27	0.31	2.3	5.8
ZOB 2011	3/25/11	6.8	11.2	0.13	0.20	2.2	5.4
ZOB 2011	3/28/11	7.3	11.5	0.14	0.17	1.8	5.8
LJC 2010	4/15/10	6.5	5.2	0.28	0.10	2.7	4.9
LJC 2010	4/25/10	6.6	3.4	0.12	0.04	2.3	4.6

LJC 2011	3/28/11	7.01	1.9	0.04	0.01	1.4	4.5
LJC 2011	4/4/11	7.3	2.2	0.06	0.02	1.4	4.9
EFJW 2010	4/18/10	6.3	14.1	0.64	0.36	3.0	5.2
EFJW 2010	4/25/10	6.6	9.3	0.65	0.27	3.0	5.4
EFJW 2011	3/28/11	7.5	3.0	0.17	0.10	1.7	5.7
EFJW 2011	4/4/11	7.8	2.8	0.34	0.14	1.7	6.1

APPENDIX F: *ELECTRONIC ANNEX FOR*
REDISTRIBUTION OF RARE EARTH ELEMENTS AND YTTRIUM (REY) IN
TOPOGRAPHICALLY DISTINCT, RHYOLITE-DERIVED PEDONS

Geoderma

Angélica Vázquez-Ortega^{a*}, Julia Perdrial^a, David Huckle^b, Craig Rasmussen^a, Mary Kay Amistadi^a, Jennifer McIntosh^b, and Jon Chorover^a

^aDepartment of Soil, Water & Environmental Science, University of Arizona, 1177 East Fourth Street, Tucson, Arizona 85721-0038, USA

^bDepartment of Hydrology and Water Resources, University of Arizona, 1133 East James E. Rogers Way, Tucson, Arizona 85721-0011, USA

*Corresponding author: avazquez@email.arizona.edu

SECTION 1: FIGURES

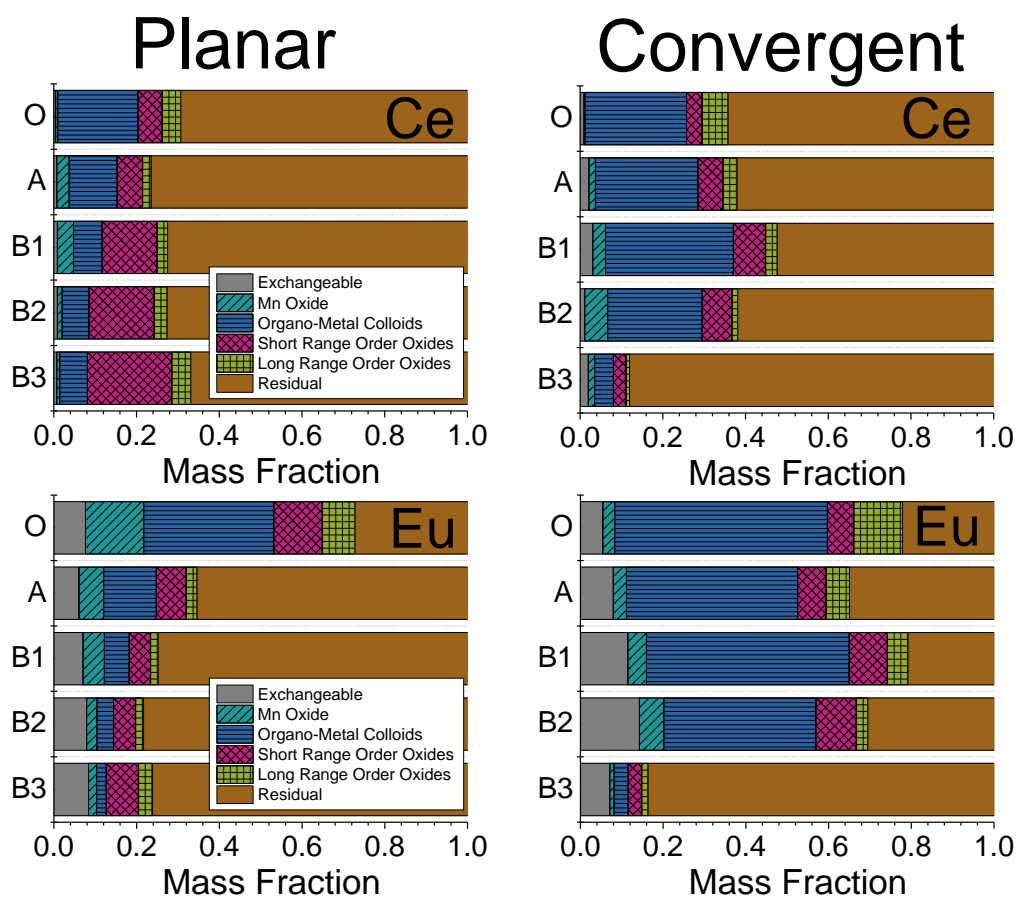


Figure E.1 Extractability patterns for Ce (*top*) and Eu (*bottom*) as a function of depth in planar (*left*, Pedon 1) and convergent (*right*, Pedon 5) hillslope profiles. Mass fractions are labeled with the names of the target phases, and are associated with the following chemical extractions: 1.0 M CH₃COONa (pH 5.5), 0.1M NH₂OH·HCl (pH 2), 0.1 M Na₄P₂O₇ (pH 10), 0.25 M NH₂OH·HCl (pH 1.5), and 1.0 M NH₂O HCl (pH 1).

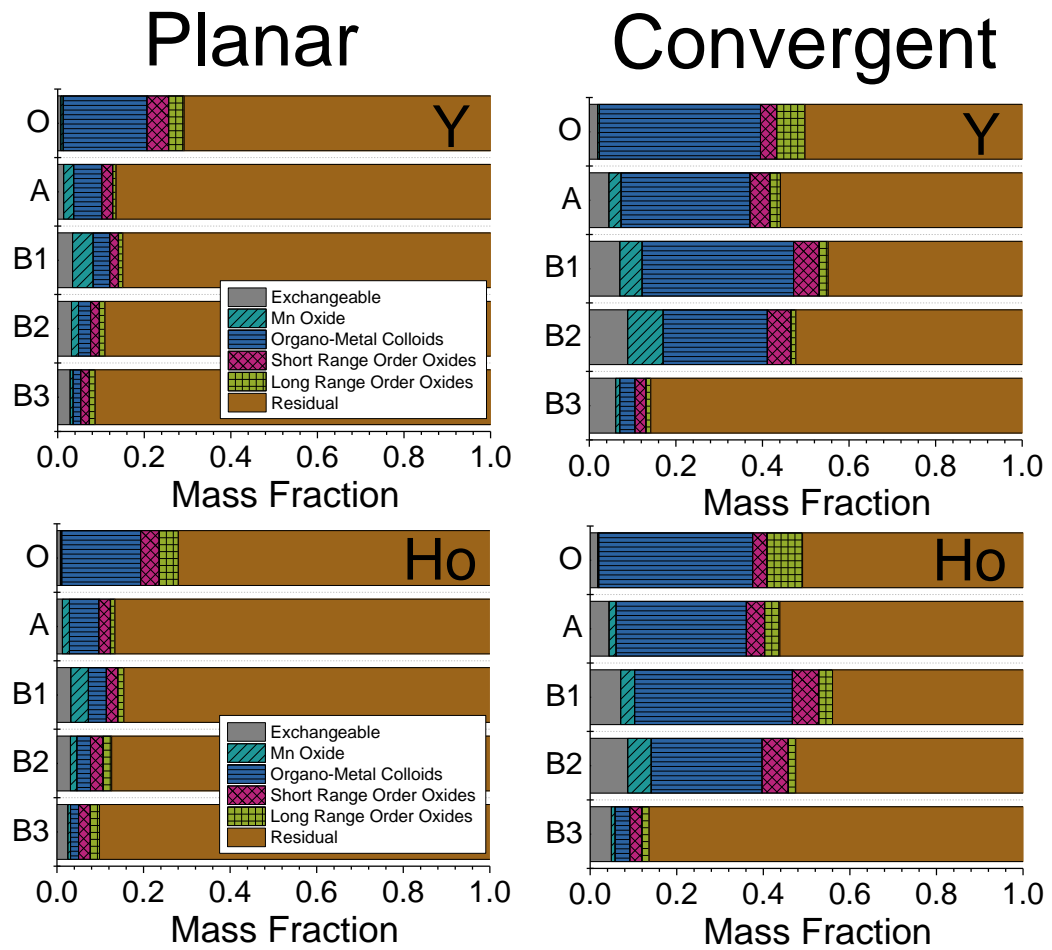


Figure E.2 Extractability patterns for Y (*top*) and Ho (*bottom*) as a function of depth in planar (*left*, Pedon 1) and convergent (*right*, Pedon 5) hillslope profiles. Mass fractions are labeled with the names of the target phases, and are associated with the following chemical extractions: 1.0 M CH_3COONa (pH 5.5), 0.1M $\text{NH}_2\text{OH}\cdot\text{HCl}$ (pH 2), 0.1 M $\text{Na}_4\text{P}_2\text{O}_7$ (pH 10), 0.25 M $\text{NH}_2\text{OH}\cdot\text{HCl}$ (pH 1.5), and 1.0 M $\text{NH}_2\text{O HCl}$ (pH 1).